Studies on enzymes and reaction conditions in recombinase polymerase amplification

KEVIN MAAFU JUMA

2024

Contents

Abbreviations

BSA	bovine serum albumin
Bst-Pol	*Bacillus stearothermophilus* strand-displacing DNA polymerase
C1-Pol	*Geobacillus zalihae* strand-displacing DNA polymerase
DMSO	dimethyl sulfoxide
dsDNA	double-stranded DNA
DTT	dithiothreitol
E. coli	*Escherichia coli*
EDTA	ethylenediaminetetraacetic acid
H1-Pol	*Aeribacillus pallidus* strand-displacing DNA polymerase
IPTG	isopropyl β-D-1-thiogalactopyranoside
MMLV	Moloney murine leukemia virus
NA	nucleic acid
ORF	open reading frame
PCR	polymerase chain reaction
PMSF	phenylmethylsulfonyl fluoride
RPA	recombinase polymerase amplification
RYMV	rice yellow mottle virus
SARS-CoV-2	severe acute respiratory syndrome coronavirus 2
SDS-PAGE	sodium dodecyl sulfate polyacrylamide gel electrophoresis
SSB	single-stranded DNA binding protein
ssDNA	single-stranded DNA
T_m	melting temperature
μTGGE	micro temperature gradient gel electrophoresis

General introduction

Since the discovery of polymerase chain reaction (PCR) in 1985 [1], various methods have been developed for nucleic acid (NA) amplification. These methods are currently used in several fields including clinical diagnosis. In pulmonary tuberculosis, such tests can rapidly and accurately identify *Mycobacterium* species in clinical respiratory samples than in sputum specimen examinations and culture-based methods. This advantage is key to appropriate treatment, prevention, and control of tuberculosis transmission [2]. Similarly, in the case of severe acute respiratory syndrome coronavirus 2 (SARS-CoV-2) detection, the NA amplification test is considered to be more effective since it is highly sensitive and quantitative compared to other methods based on SARS-CoV-2-specific antibody or viral antigens. It has a great advantage in detecting SARS-CoV-2 at the initial stage of infection and helps monitor disease progression [3].

Various techniques are available for NA amplification, but PCR is the most commonly used method. In basic research, most researchers use PCR primarily for amplification, possibly because primer design is convenient and the enzymes are available at a reasonable price. In clinical diagnosis on the other hand, isothermal NA amplification methods such as NA sequence-based amplification (NASBA) [4], strand displacement amplification (SDA) [5], rolling circle amplification (RCA) [6], helicase-dependent isothermal DNA amplification (HDA) [7], and loop-mediated isothermal amplification (LAMP) [8] are also used. The advantage of isothermal amplifications over PCR is that they do not require a complex device such as a thermal cycler, improving throughput in situations when large numbers of clinical samples must be processed, as well as facilitating point-of-care diagnosis [9].

The performance of each NA amplification test largely depends on the characteristics of the individual enzymes involved. Thermostable DNA polymerase, first identified in *Thermus aquaticus* (*Taq*) in 1976 [10], has become widely used since the discovery of PCR. Concerning performances of *Taq* polymerase, it was initially reported that the activity decreased to 50% at incubation at 95ºC for 1.6 h; the extension rate was 60–150 nucleotides/second; and the error rate was 0.38–1.32 × 10^4 errors/base [11]. Since then, the performance of *Taq* polymerase has been improved by genetic engineering. For example, the mutation of Phe667 into Tyr increased its efficiency of incorporation with ddNTP by 1,000-fold [12], and fusion of the helix-hairpin-helix motifs of DNA topoisomerase V to *Taq* polymerase increased the enzyme's stability and processivity [13]. The performances of DNA polymerases from the hyperthermophilic archaeon *Thermococcus kodakaraensis* (KOD) or *Pyrococcus furiosus* (*Pfu*) and that from hyperthermophilic bacteria *Thermus thermophilus* (*Tth*) have also been improved by genetic engineering. Today, they are widely used in PCR along with *Taq* polymerase.

Recombinase polymerase amplification (RPA) is an isothermal NA amplification technique that operates at a constant temperature (37–42ºC). It uses recombinase (Rec), single-stranded DNA binding protein (SSB), strand-displacing DNA polymerase (Pol), and an ATP-regenerating enzyme (Fig. 0-1) [14–17]. In RPA, Rec binds to the primers in the presence of ATP, forming a recombinase-primer complex. The complex scans dsDNA and binds to the homologous sequences. Pol extends the primers while SSB binds to the unwound strand. The presence of forward and reverse primers enables strand synthesis to occur in both directions simultaneously, resulting in the exponential accumulation of amplified duplex DNA. The ATP-regenerating enzyme supplies ATP, making ATP concentration constant. When a target NA is RNA, reverse transcription is required before

RPA.

Since the first report of RPA in 2006 [14], T4 phage uvsX and uvsY have been used as Rec, T4 phage gp32 as SSB, and *Bst*-Pol strand-displacing DNA polymerase, which is derived from *Geobacillus stearothermophilus* formally named *Bacillus stearothermophilus* as Pol. Rabbit muscle creatine kinase has been used as an ATP-regenerating enzyme. UvsX is the Rec that possesses pairing and strand-transfer activity and is crucial in a number of genetic processes, including recombination, DNA repair, and replication. UvsY is the Rec loading factor that is classified as a recombination-mediator protein. It stimulates the ssDNA-dependent ATPase activity of uvsX and lowers the critical concentration of uvsX required for activity. Gp32 is the SSB protein involved in DNA replication, repair, and recombination. UvsX, uvsY, and gp32 proteins work co-operatively to initiate the RPA reaction *via* unwinding and stabilization of the DNA template. Pol synthesizes new DNA templates by extending nucleotide building blocks from the bound primers. Creatine kinase is involved in ATP regeneration by converting phosphocreatine and ADP to creatine and ATP (Fig. 0-2).

Compared to PCR, RPA offers attractive advantages. One major advantage is its simplicity. RPA does not require sophisticated equipment such as a thermal cycler [18]. Instead, affordable and easy-to-operate apparatus such as incubators, heating blocks, and chemical heaters can be employed. Additionally, RPA can operate at ambient temperature in warm areas (above 30°C), a significant advantage in resource-limited settings. Another advantage of RPA is its rapidness. RPA can amplify target DNA or RNA in as little as 20 min. Amplification in 3–4 min has been reported. In contrast, typical PCR reactions are performed around 1–2 h. RPA is also tolerant to inhibitors, it has been demonstrated that RPA can be carried out directly in serum and in the presence of known PCR inhibitors

such as hemoglobin, ethanol, and heparin. Lastly, some studies have reported RPA to be more sensitive than PCR. Despite these attractive advantages, the adoption of RPA has been relatively gradual. This can be attributed to the following factors associated with the technology: 1) lack of special primer design software necessitating trial and error during primer design; 2) high reagent prices and limited availability of RPA kits in the market; 3) suitability for relatively short DNA sequences (ideally 100–300-bp) and not for longer sequences [19].

In the recent past, a myriad of published papers on RPA have highlighted the significance of RPA for point-of-care use with many targets being pathogenic organisms of economic importance such as SARS-CoV-2 [20–23], *Mycobacterium tuberculosis* [24–26], monkeypox virus [27–29], *Plasmodium falciparum* [30, 31], *Leishmania donovani* [32–34], *Streptococcus pneumoniae* [35, 36], *Yersinia pestis* [37], and *Vibrio cholerae* [38, 39]. To improve portability and achieve point-of-care use, several technologies for DNA extraction and amplicon detection have been combined with RPA. These advances include FTA cards [40–42] for DNA extraction, flocculation assay [43–45], electrochemical assay [46–48], chemiluminescence microarray assay [49], silicon microring resonator (SMR)-based photonic assay [50, 51], surface-enhanced Raman scattering (SERS) assay [52, 53], enzyme-linked oligonucleotide assay [54], and lateral flow assay [37–39] for amplicon detection.

Various factors, including enzyme performance and reaction conditions such as pH, ionic strength, temperature, and different additives, affect the efficiency of nucleic NA amplification. While numerous studies have been reported on optimizing these parameters for PCR [55–57], there is a relative scarcity of similar investigations concerning RPA. This disparity can be attributed to the nature of commercially available

pre-prepared RPA kits, previously sold by TwistDx and now owned by Abbott (San Diego, CA, USA), which are not designed for customization. Consequently, there is limited knowledge of enzymes and reaction conditions in RPA due to the constraints imposed by commercial kits.

The aim of this study is to develop recombinant enzymes and optimize reaction conditions in RPA. In Chapter 1, we established assays for detecting rice yellow mottle virus (RYMV) using PCR, RPA, and RNA-specific amplification. RYMV is a highly infectious plant virus that causes rice yellow mottle disease (RYMD), a severe threat to rice cultivation in sub-Saharan Africa [58–60]. To overcome the constraints of the pre-prepared nature of commercially available kits, to gain research flexibility to perform studies with various formulations and concentrations, and to establish a cost-efficient method to obtain large amounts of RPA enzymes that suited our unique research needs, we prepared recombinant RPA enzymes (uvsX, uvsY, and gp32) and examined the effects of reaction conditions and additives on the efficiency of RPA in Chapter 2. In Chapter 3, we optimized the reaction condition of RPA using a statistical method. In Chapter 4, we examined the effects of the N- and/or C-terminal hexahistidine tags of uvsY on its function in RPA. In Chapter 5, we isolated two novel thermostable strand-displacing DNA polymerases from *Aeribacillus pallidus* (H1) and *Geobacillus zalihae* (C1) and evaluated their performances in RPA reaction. Lastly, in Chapter 6, we established an assay to detect the D614G mutation in the SARS-CoV-2 spike protein using μTGGE. Micro temperature gradient gel electrophoresis (μTGGE) is one of the techniques used to detect DNA sequence differences. This technique can be used to screen for point mutations or other forms of mutations, eliminating or reducing the need for conventional sequencing methods [61, 62]. The separation of dsDNA molecules during TGGE relies

on temperature-dependent melting of the dsDNA into two ssDNA molecules. Based on the specific melting temperature (T_m), two DNA fragments of the same size but of different sequences will denature at different points within the gradient. T_m refers to the temperature at which half of the dsDNA separates into ssDNA. The differential melting profiles created by variations in T_m allow researchers to precisely identify mutations by analyzing the migration profiles of DNA on the gel. Generally, A-T-rich sequences will denature at a lower T_m than G-C-rich sequences.

The present study significantly contributes to our understanding of the RPA technique, its adaptability, and the optimal conditions for enzyme activity. We firmly believe that this research will serve as a crucial foundation for the advancements of RPA in disease diagnosis.

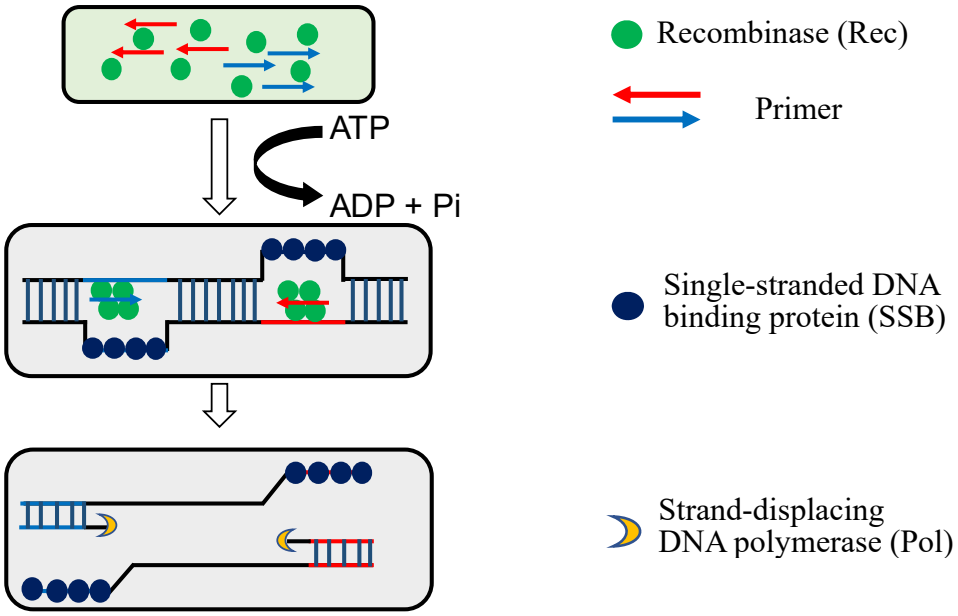

Figure 0-1. Schematic illustration of the RPA process. Rec binds to the primers in the presence of ATP. SSB binds to the unwound strand and prevents oligonucleotide primers from forming secondary structures. The synthesis of a new DNA strand occurs by Pol.

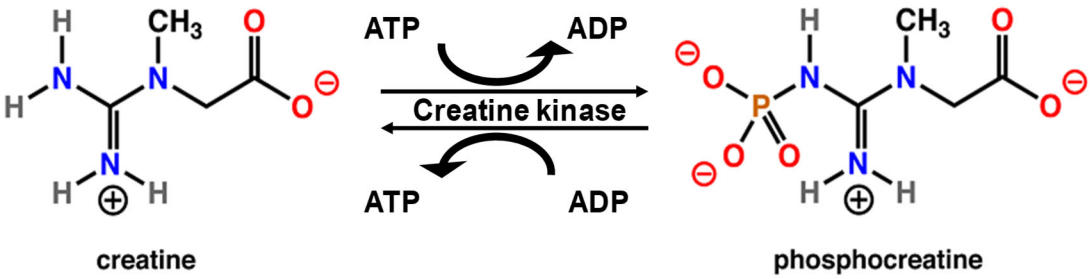

Figure 0-2. ATP regeneration. Creatine kinase catalyzes the conversion of phosphocreatine and ADP to creatine and ATP.

Chapter 1

Establishment of PCR, recombinase polymerase amplification, and RNA-specific assays for detection of rice yellow mottle virus*

Introduction

Rice yellow mottle virus (RYMV) is a highly infectious plant virus that causes rice yellow mottle disease (RYMD), a severe threat to rice cultivation in sub-Saharan Africa. First discovered in Kenya in 1966 [58], this pathogenic virus has rapidly disseminated, causing widespread devastation across virtually all rice-producing regions throughout the African continent (Fig. 1-1 A). The disease is characterized by yellow or orange leaf discoloration, stunting, sterility, and empty spikelets (Fig. 1-1 B). RYMV is transmitted through coleopterans (beetles), which act as vectors carrying the virus from wild rice (natural host) to healthy rice plants and occur in the rice field soon after rice planting. Secondary transmission occurs through mechanical contact between infected and healthy leaves (Fig. 1-1 C) [63]. RYMV belongs to *Sobemovirus* genus. The genome of RYMV is a single-stranded, positive sense RNA of 4,450 nucleotides (nt) (Fig. 1-2) [60]. It contains four open reading frames (ORF1 to ORF4). ORF1 encodes a 157 amino-acid protein whose function is unknown. ORF2 encodes a 999 amino-acid polyprotein

*The content described in this Chapter was originally published in *Journal of Biological Macromolecules.* Kevin Maafu Juma, Kenji Kojima, Teisuke Takita, Keiko T. Natsuaki, and Kiyoshi Yasukawa (2021). Comparison of sensitivity and rapidness of PCR, recombinase polymerase amplification, and RNA-specific amplification for detection of Rice yellow mottle virus. *J. Biol. Macromol*., **21**, 27–32.

comprised of the genome-linked protein, the viral protease, the helicase, the reverse transcriptase, and RNA-dependent RNA polymerase. ORF3 encodes a 126 amino-acid protein whose function is unknown. ORF4 encodes a 239 amino-acid coat protein (Fig. 1-2). Early detection and intervention of RYMD are crucial for preventing further transmission and minimizing its impact. Various methods have been developed for this purpose, including visual inspection [64], serological assays [65], and enzyme-linked immunosorbent assays. The introduction of PCR assays has significantly transformed the field and is now widely used [66, 67]. However, in settings where advanced laboratories are not easily accessible, such as farms, utilizing an isothermal NA amplification-based system is more advantageous than a PCR-based system. The primary advantage of the isothermal NA amplification approach is its independence from a thermal cycler, which makes it more practical and feasible in resource-limited environments.

RPA and RNA-specific amplification assays are isothermal reactions. RPA specifically amplifies a target DNA sequence at around 37–42ºC with Rec, SSB, and Pol [14–17]. RNA-specific amplification specifically amplifies a target RNA sequence at around 40–43ºC with reverse transcriptase and RNA polymerase [68, 69]. Various reports have revealed that both isothermal reactions are useful for pathogen detection.

In this Chapter, we developed highly efficient and specific detection methods for RYMV using PCR, RPA, and RNA-specific amplification assays. We evaluated their sensitivities and rapidness using standardized *in vitro* synthesized NAs. Additionally, we examined the effects of leaf extracts on the reaction efficiency.

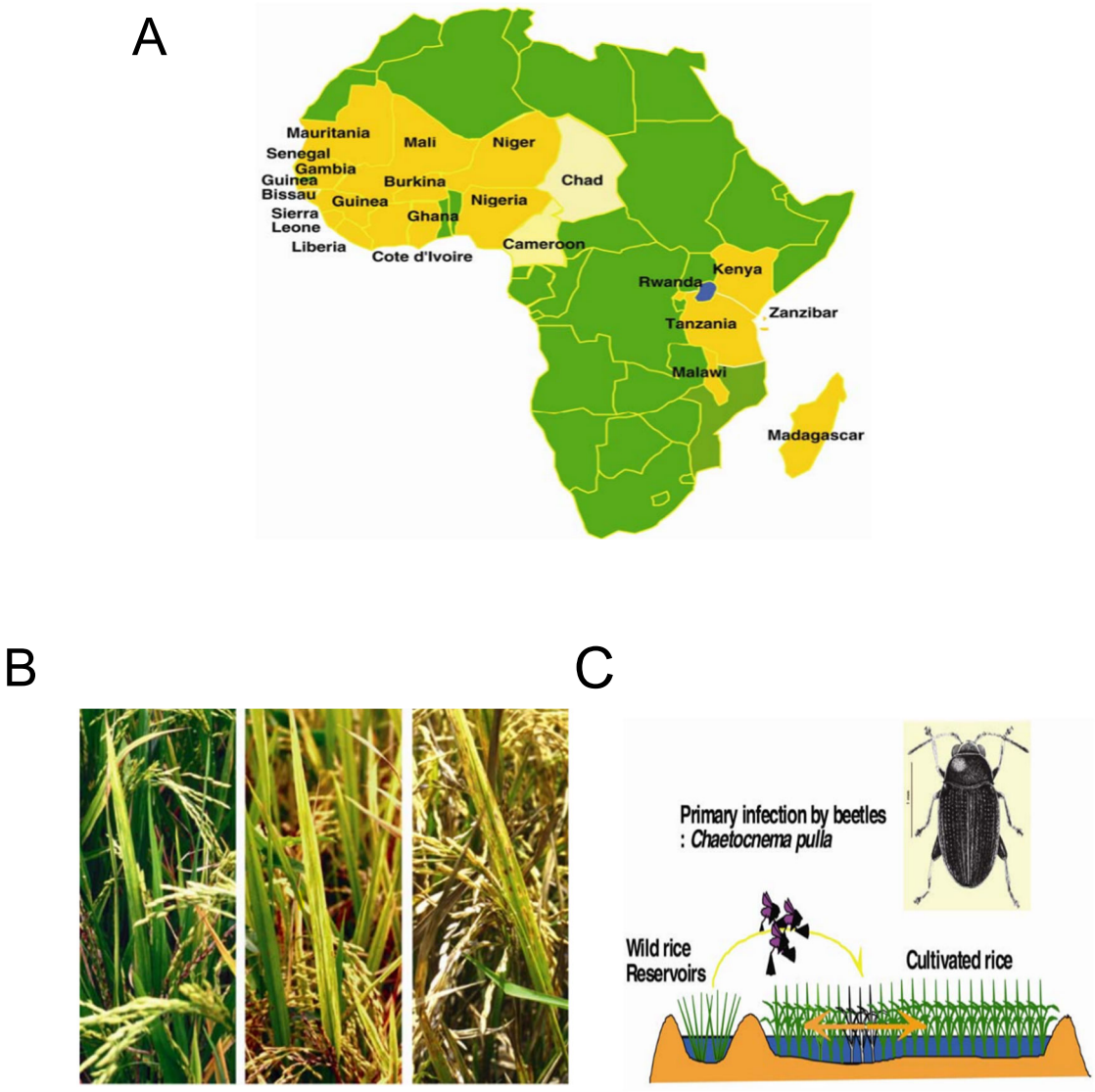

Figure 1-1. Rice yellow mottle disease. (A) Distribution of RYMV in Africa. The countries where the RYMV has been isolated are highlighted in yellow. (B) Symptoms of RYMV in infected rice fields. The infected rice plants exhibit distinct symptoms, including yellowing and mottling of leaves, stunted growth, reduced tillers, sterile spikelets, and ultimately death. (C) RYMV epidemiology. The transmission of RYMV involves coleopterans (beetles) that carry the virus from wild rice (natural host) to healthy rice plants. This transmission occurs at various locations in the field immediately after rice planting. Secondary spread occurs by mechanical contact between infected and healthy leaves.

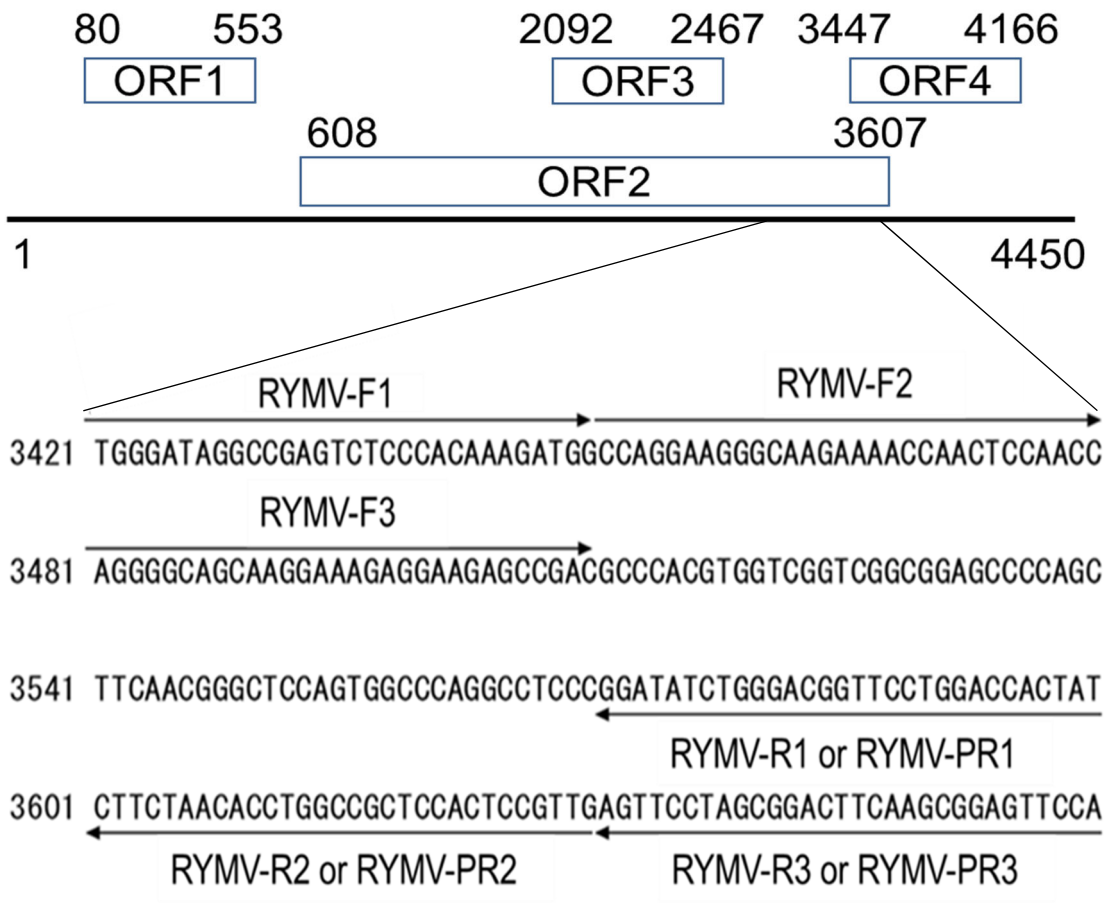

Figure 1-2. Genome organization and RYMV nucleotide sequence of the regions targeted by the primers in PCR, RPA, and RNA-specific amplification. Arrows indicate the sequences to which primers bind. The base position corresponds to that described in the sequences deposited in GenBank (L20893.1).

Materials and methods

Materials

The 240-nt single-stranded DNA (ssDNA) fragment of the RYMV gene, corresponding to DNA sequence 3421–3660 deposited in GenBank (L20893.1) and target primers, were purchased from Eurofins Genomics (Tokyo, Japan).

Preparation of standard DNA

The 240-bp DNA was amplified by PCR using primers RYMV-F1 and RYMV-R3 (Table 1-1) and *Taq* polymerase (Toyobo, Osaka, Japan) under 35 cycles of 30 s at 95ºC, 30 s at 55ºC, and 30 s at 72ºC, and purified using MagExtractor (Toyobo). The concentration of purified DNA was determined spectrophotometrically at 260 nm and stored at –20ºC for subsequent use.

Preparation of standard RNA

In vitro transcription was carried out with 0.024 μg/mL standard DNA mentioned above as a template using RiboMAX Large Scale RNA Production System (Promega, Madison, WI) at 37ºC for 3 h. The resultant RNA was purified by NICK Columns (GE Healthcare, Buckinghamshire, UK) and then extracted by ethanol precipitation. The concentration of purified RNA was determined spectrophotometrically at 260 nm and stored at –80ºC for subsequent use.

Detection of RYMV DNA by PCR

The reaction mixture (15 μL) was prepared by mixing 9.2 μL of water, 1.5 μL of 10 × PCR buffer [100 mM Tris-HCl buffer (pH 8.3), 500 mM KCl, 15 mM $MgCl_2$], 1 μL of

10 μM forward primer, 1 μL of 10 μM reverse primer, 1.2 μL of dNTPs (2 mM each), 1 μL of DNA, and 0.2 μL of 1 U/μL *Taq* polymerase. The cycling parameters were 95ºC for 30 s, followed by 5–35 cycles at 95ºC for 30 s, 60ºC for 30 s, and 72ºC for 30 s with a final extension at 72ºC for 2 min. The amplified products were separated on 2.0% agarose gels and stained with ethidium bromide (1 μg/mL).

Detection of RYMV DNA by RPA

The reaction was carried out with TwistAmp Liquid Basic (TwistDx, Cambridge, MA). The reaction mixture was prepared by mixing 7.5 μL of 2 × reaction buffer, 2.46 μL of dNTPs (2 mM each), 0.3 μL water, 1.5 μL of Basic E-Mix, 0.72 μL of 10 μM forward primer, 0.72 μL of 10 μM reverse primer, 0.75 μL of 20 × Core Reaction Mix, 0.75 μL of 280 mM $Mg(CH_3COO)_2$, and 0.3 μL of DNA in a PCR tube, and incubated at 41ºC for 1–40 min. The amplified products were separated on 2.0% agarose gels and stained with ethidium bromide (1 μg/mL).

Detection of RYMV RNA by RNA-specific amplification

The reaction mixture was prepared by mixing 2.5 μL of RNA and 10 μL of substrate primer solution [175 mM Tris-HCl buffer (pH 8.6), 195 mM KCl, 26 mM $MgCl_2$, 1.5 dithiothreitol (DTT), dNTPs (0.38 mM each), 2.8 mM each NTP, 5.4 mM inositol triphosphate, 0.32 U/μL RNase inhibitor, 1.5 μM forward primer, 1.5 μM promoter-bearing reverse primer, and 19.5% v/v dimethyl sulfoxide (DMSO)] in a PCR tube and incubated at 65ºC for 5 min and then at 41ºC for 5 min. The reaction was started by adding 2.5 μL of enzyme solution [0.72 mg/mL bovine serum albumin (BSA), 12% v/v sorbitol, 1.6 U/μL avian myeloblastosis virus (AMV) reverse transcriptase (Life Sciences Inc,

Petersburg, FL), 28.4 U/μL T7 RNA polymerase (Toyobo)] and continued at 41ºC for 1–40 min. The amplified products were separated on 2.0% agarose gel and stained with ethidium bromide (1 μg/mL).

Table 1-1. Primer sequences used in PCR, RPA, and RNA-specific amplification. The promoter sequence is shown in italics.

Primer type	Sequence (5′→3′)
RYMV-F1	TGGGATAGGCCGAGTCTCCCACAAAGATGG
RYMV-F2	CCAGGAAGGGCAAGAAAACCAACTCCAACC
RYMV-F3	AGGGGCAGCAAGGAAAGAGGAAGAGCCGAC
RYMV-R1	ATAGTGGTCCAGGAACCGTCCCAGATATCC
RYMV-R2	CAACGGAGTGGAGCGGCCAGGTGTTAGAAG
RYMV-R3	TGGAACTCCGCTTGAAGTCCGCTAGGAACT
RYMV-PR1	*AATTCTAATACGACTCACTATAGGGAGA*ATAGTGGTCCAGGAACCGTCCCAGATATCC
RYMV-PR2	*AATTCTAATACGACTCACTATAGGGAGA*CAACGGAGTGGAGCGGCCAGGTGTTAGAAG
RYMV-PR3	*AATTCTAATACGACTCACTATAGGGAGA*TGGAACTCCGCTTGAAGTCCGCTAGGAACT

Results and discussion

Establishment of PCR, RPA, and RNA-specific amplification assays for the detection of RYMV

Figure 1-2 shows the genomic organization of RYMV and the nucleotide sequence targeted by primers. A part of ORF2 (nt: 3,421–3,660) was selected as a target sequence because the divergences of ORF2 and ORF4 are comparatively lower than other ORFs [70]. The following factors are important in designing primers for RPA and RNA-specific amplification: (i) GC content does not exceed 60%; (ii) the length of the primer region that binds to a target DNA or RNA is about 30 nt; and (iii) the size of amplified DNA is 100–300-bp, and that of amplified RNA is 100–300-nt. However, unlike PCR, no method for the rational design of primers has yet been developed for RPA and RNA-specific amplification, necessitating trial and error.

We designed three forward primers (RYMV-F1, RYMV-F2, and RYMV-F3), three reverse primers (RYMV-R1, RYMV-R2, and RYMV-R3), and three promoter-bearing reverse primers (RYMV-PR1, RYMV-PR2, and RYMV-PR3). The primer sequences are shown in Table 1-1, while the expected sizes of the amplified DNA and RNA of each combination are shown in Tables 1-2 and 1-3, respectively. We evaluated the effects of primer combination on the amplification efficiency of the three assays: PCR, RPA, and RNA-specific amplification. These assays were carried out with primer combinations No. 1–9 with the initial copy number of 10^9 copies. The target bands were observed on agarose gel with primer combinations No. 1–9 in PCR, No. 1–6 and 8 in RPA, and No. 1–4 and 6–9 in RNA-specific amplification, but did not for No. 7 and 9 in RPA and No. 5 in RNA-specific amplification (Fig. 1-3). Primer combination No. 6 gave the best performance and was thus selected for use in subsequent studies.

Table 1-2. PCR and RPA primer combinations and expected size of amplicons.

No.	Primer combination		Expected size of amplified DNA (bp)
	Forward primer	Reverse primer	
1	RYMV-F1	RYMV-R1	180
2	RYMV-F1	RYMV-R2	210
3	RYMV-F1	RYMV-R3	240
4	RYMV-F2	RYMV-R1	150
5	RYMV-F2	RYMV-R2	180
6	RYMV-F2	RYMV-R3	210
7	RYMV-F3	RYMV-R1	120
8	RYMV-F3	RYMV-R2	150
9	RYMV-F3	RYMV-R3	180

Table 1-3. RNA-specific amplification primer combinations and expected size of amplicons.

No.	Primer combination		Expected size of amplified RNA (nt)
	Forward primer	Reverse primer	
1	RYMV-F1	RYMV-PR1	186
2	RYMV-F1	RYMV-PR2	216
3	RYMV-F1	RYMV-PR3	246
4	RYMV-F2	RYMV-PR1	156
5	RYMV-F2	RYMV-PR2	186
6	RYMV-F2	RYMV-PR3	216
7	RYMV-F3	RYMV-PR1	126
8	RYMV-F3	RYMV-PR2	156
9	RYMV-F3	RYMV-PR3	186

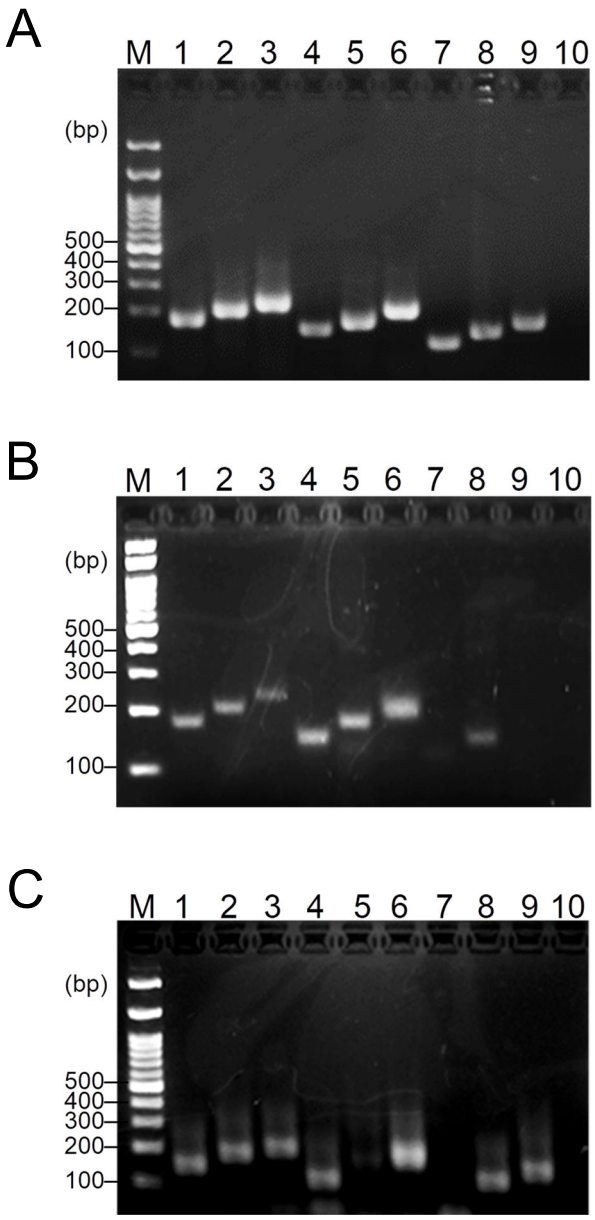

Figure 1-3. Comparison of primer performance. PCR (A), RPA (B), and RNA-specific amplification (C) were carried out from 10^9 copies of standard DNA (A, B) or 10^9 copies of standard RNA (C). The cycle number of PCR was 35, and RPA and RNA-specific amplification reaction time was 20 min. Lanes: M, DNA marker; 1–9, reaction solution with primer combinations No. 1–9 (Tables 1-2 and 1-3), respectively; and 10 corresponds to the reaction without primers.

Comparison of the sensitivity and rapidness of the PCR, RPA, and RNA-specific amplification assays

We compared the sensitivity of the three assays. When the PCR cycle number was set at 35, and the reaction time was set at 20 min for RPA and RNA-specific amplification, the intensities of the target bands on agarose gel decreased with a decrease in the initial copy numbers. PCR and RPA detected 1 DNA copy while RNA-specific amplification detected 10 RNA copies (Fig. 1-4). Additionally, in RNA-specific amplification, smaller-sized bands corresponding to non-specific primer-derived amplified products were also observed (Fig. 1-4 C). Considering the dilution error, the results indicated that the sensitivities of the assays ranged from several copies of the target DNA for PCR and RPA to dozens of copies of the target RNA for RNA-specific amplification.

Next, we compared the rapidness of the three assays. When the initial copy numbers of the target DNA or RNA were set at 10^9, the target band was observed on agarose gel after 15 cycles for PCR and 5 min for RPA, and 10 min for RNA-specific amplification (Fig. 1-5). Considering that 15 cycles take 27 min in PCR, these results suggested that RPA and RNA-specific amplification are more rapid than PCR.

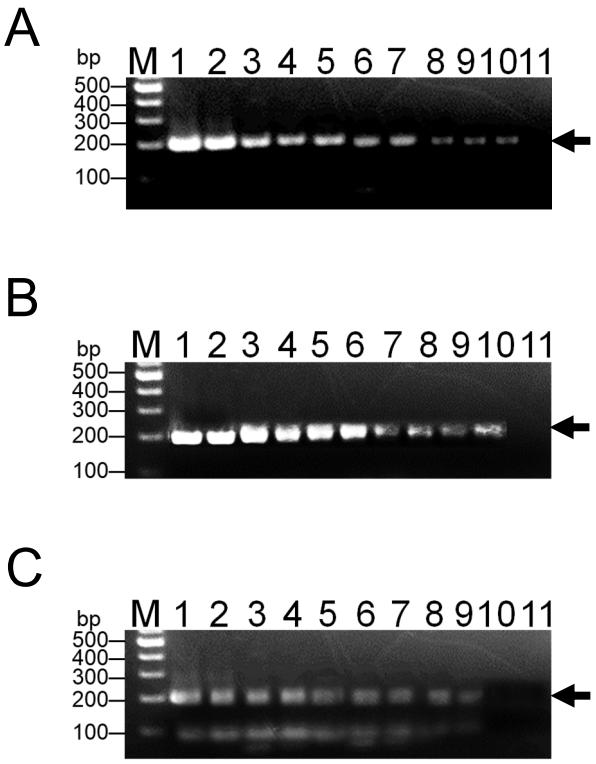

Figure 1-4. Effects of initial copies on the amplification. PCR (A), RPA (B), and RNA-specific amplification (C) were carried out with primer combination No. 6 (Tables 1-2 and 1-3). The cycle number of PCR was 35 (A), and the reaction time of RPA (B) and RNA-specific amplification (C) were 20 min. Lanes: M, DNA marker; 1–9, reaction solutions from 10^9 (lane 1), 10^8 (lane 2), 10^7 (lane 3), 10^6 (lane 4), 10^5 (lane 5), 10^4 (lane 6), 10^3 (lane 7), 10^2 (lane 8), 10 (lane 9), 1 (lane 10), and 0 (lane 11) copies of standard DNA (A, B) or standard RNA (C). The arrow indicates the amplified target band.

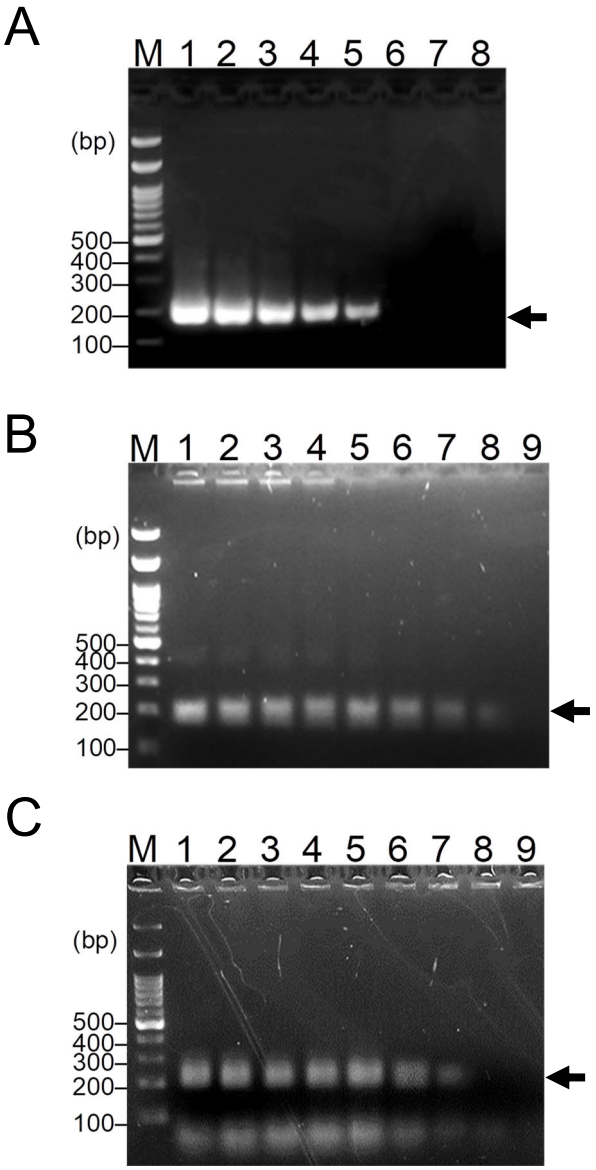

Figure 1-5. Effects of cycle number or reaction time on the amplification. PCR (A), RPA (B), and RNA-specific amplification (C) were carried out with primer combination No. 6 from 10^9 copies of standard DNA (A, B) or standard RNA (C). Lanes: M, DNA marker; 1–8 in (A), reaction solutions at 35 (lane 1), 30 (lane 2), 25 (lane 3), 20 (lane 4), 15 (lane 5), 10 (lane 6), 5 (lane 7), and 1 (lane 8) cycles; 1–9 in (B and C), reaction solutions at 40 (lane 1), 35 (lane 2), 30 (lane 3), 25 (lane 4), 20 (lane 5), 15 (lane 6), 10 (lane 7), 5 (lane 8), and 1 (lane 9) min. The arrow indicates the amplified target band.

Effects of plant extracts on the RPA, and RNA-specific amplification assays

To investigate the potential presence of inhibitors in plant samples to RPA and/or RNA-specific amplification, we examined if plant extracts inhibited RPA and RNA-specific amplification. However, Japan's Ministry of Agriculture, Forestry, and Fisheries has prohibited the entry of rice plant materials from Kenya and other countries into the country due to the potential risk of disease. We thus used extracts of *Morus australis* leaf [71] and *Ficus carica* leaf [72] instead. Neither *M. australis* leaf nor *F. carica* leaf extract inhibited the reaction (Fig. 1-6). These results suggested that plant extracts will not much affect the performance of the RPA or RNA-specific amplification-based detection systems for RYMV.

One of the merits of RPA and RNA-specific amplification over PCR is that they are isothermal reactions, and thus have the potential to eliminate the use of specialized equipment to provide the complex temperature control. It should be noted that RPA reaction occurs even at the human body temperature (37ºC). Recently, a completely instrument-free, RPA-based system to detect *Leishmania* species was reported [42]. Thus, RPA might be the ideal NA amplification method for point-of-care diagnosis.

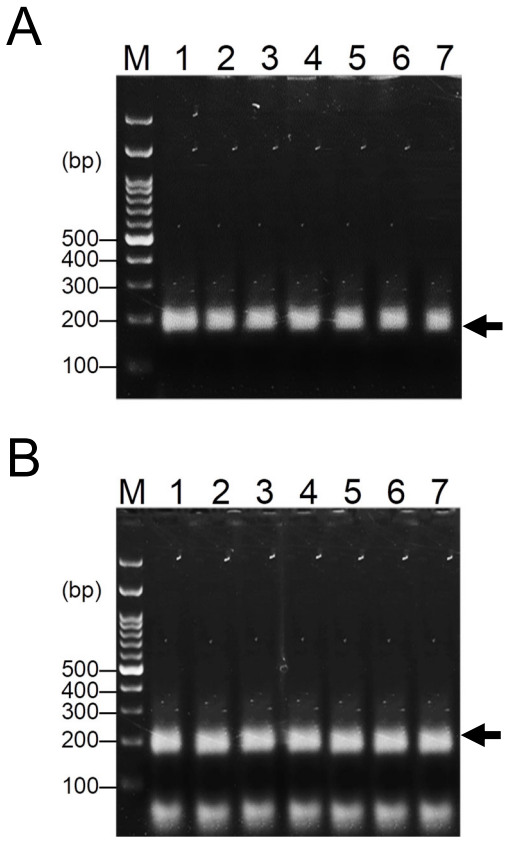

Figure 1-6. Effects of leaf extracts on the amplification. RPA (A) and RNA-specific amplification (B) were carried out from 10^9 copies of standard DNA (A) or RNA (B) for 20 min. Lanes: M, DNA marker; 1–7, reaction solutions without (1) or with *M. australis* (2–4) or *F. carica* (5–7) leaf extract. The protein concentrations of the extracts in the reaction solutions were 5 (lane 2), 0.5 (lane 3), 0.05 (lane 4), 45 (lane 5), 4.5 (lane 6), and 0.45 μg/mL (lane 7). The arrow indicates the amplified target band.

Conclusion

We developed PCR, RPA, and RNA-specific amplification assays for the detection of RYMV. RPA exhibited comparable while RNA-specific amplification exhibited slightly lower sensitivity to PCR in detecting RYMV. However, the rapidness of RPA and RNA-specific amplification was higher than that of PCR. These results suggested that isothermal RPA and RNA-specific amplification can potentially replace PCR in diagnostic applications, particularly in regions with limited resources, especially in Africa.

Chapter 2

Expression in *Escherichia coli* and characterization of recombinant recombinase and single-stranded DNA binding protein*

Introduction

Recombinase polymerase amplification (RPA) technology was first reported in 2006 using proteins involved in cellular DNA synthesis, recombination, and repair [14]. The RPA process begins when a Rec protein binds to the primers in the presence of ATP forming a recombinase-primer complex. The complex scans the dsDNA, searching for a homologous sequence, and promotes strand invasion by the primer at the cognate site. In order to prevent the ejection of the inserted primer by branch migration, the displaced DNA strand is stabilized by the SSB. Finally, Rec disassembles and Pol (e.g., *Bst*-Pol) binds to the 3′ end of the primer to elongate it in the presence of dNTPs. Cyclic repetition of this process results in exponential amplification [15–17]. The RPA process is performed around 37–42ºC.

The efficiency of NA amplification techniques including RPA is significantly influenced by various factors, including pH, ionic strength, temperature, and the presence of additives. While extensive studies have been reported in PCR [73–75], relatively limited information is available for RPA. This limitation can be attributed to the

*The content described in this Chapter was originally published in *Journal of Bioscience and Bioengineering.* Kenji Kojima, Kevin Maafu Juma, Shihomi Akagi, Kaichi Hayashi, Teisuke Takita, Ciara K. O'Sullivan, Shinsuke Fujiwara, Yukiko Nakura, Itaru Yanagihara, and Kiyoshi Yasukawa (2021). Solvent engineering studies on recombinase polymerase amplification. *J. Biosci. Bioeng.*, **131**, 219–224.

pre-prepared nature of the commercially available RPA kit, previously sold by TwistDX, now owned by Abbot (San Diego, USA), which restricts the ability to conduct detailed studies. Using a commercial kit for RPA in Chapter 1 limited our ability to carry out these specific investigations [76].

In this Chapter, we prepared recombinant Rec (uvsX and uvsY) and SSB (gp32) as N- and C-terminally $(His)_6$-tagged proteins from T4 phage and used them to examine the effects of reaction conditions and additives on the efficiency of RPA. We chose to use $(His)_6$ tags due to their strong affinity for metal ions, allowing for efficient and gentle purification. They are easily removed upon thrombin-treatment, compatible with *E. coli* expression systems, and readily available from various suppliers.

Materials and methods

Materials

Standard DNA was prepared as described in Chapter 1. *Bst* DNA polymerase (large fragment) was purchased from New England BioLabs (Ipswich, MA), and creatine kinase was obtained from Roche (Mannheim, Germany).

Construction of plasmids

The expression plasmids for uvsX, uvsY, and gp32, each containing hexahistidine ((His)6) tags at their N- and C-terminal sites and a thrombin cleavage site at its N-terminus, pET-uvsX-1, pET-uvsY-1, and pET-gp32-1, respectively (Fig. 2-1), were constructed as follows. The 1,173-bp DNA fragment encoding uvsX from T4 phage, corresponding to DNA sequence 22,375–23,547 deposited in GenBank (KJ477686.1), the 411-bp DNA fragment encoding uvsY from T4 phage, corresponding to DNA sequence

114,929–115,339 deposited in GenBank (KJ477686.1), and the 903-bp DNA fragment encoding gp32 from T4 phage, corresponding to DNA sequence 146,963–147,865 deposited in GenBank (KJ477686.1), were inserted into the *Nde*I and *Xho*I sites of pET-28a(+).

The expression plasmids for uvsX, uvsY, and gp32 each containing $(His)_6$ and a thrombin cleavage site at its N- and C-terminal sites, pET-uvsX-2, pET-uvsY-2, and pET-gp32-2, respectively (Fig. 2-2), were constructed as follows. The 6,490-bp DNA fragment was amplified from pET-uvsX-1 using primers thrombinF and uvsX-thrombinR (Table 2-1) with the cycling parameter of 35 cycles at 98ºC for 10 s and 68ºC for 5 min. The 5,728-bp DNA fragment was amplified from pET-uvsY-1 using primers thrombinF and uvsY-thrombinR with the same cycling parameter. The 6,217-bp DNA fragment was amplified from pET-gp32-1 using primers thrombinF and gp32-thrombinR (Table 2-1) with the same cycling parameter. Each amplified fragment was phosphorylated at its 5' terminus with T7 polynucleotide kinase, ligated, and then transfected into *Escherichia coli* BL21(DE3) [F^- *ompT hsdS*$_B$ (r_B^- m_B^-) *gal dcm* (DE3)].

Table 2-1. Primers used in PCR.

Primers	Sequences (5′→3′)
thrombinF	ACGCGGTAGTCTCGAGCACCACCACCACCACCACTGA
uvsX-thrombinR	GGCACCAGACCTTCATTAAATTCTTCCATATCACTTAGC
uvsY-thrombinR	GGCACCAGACCTTTTCCAGCCTCAAATGCTCGCATGTC
gp32-thrombinR	GGCACCAGACCTTTTCCAGCCTCAAATGCTCGCATGTC

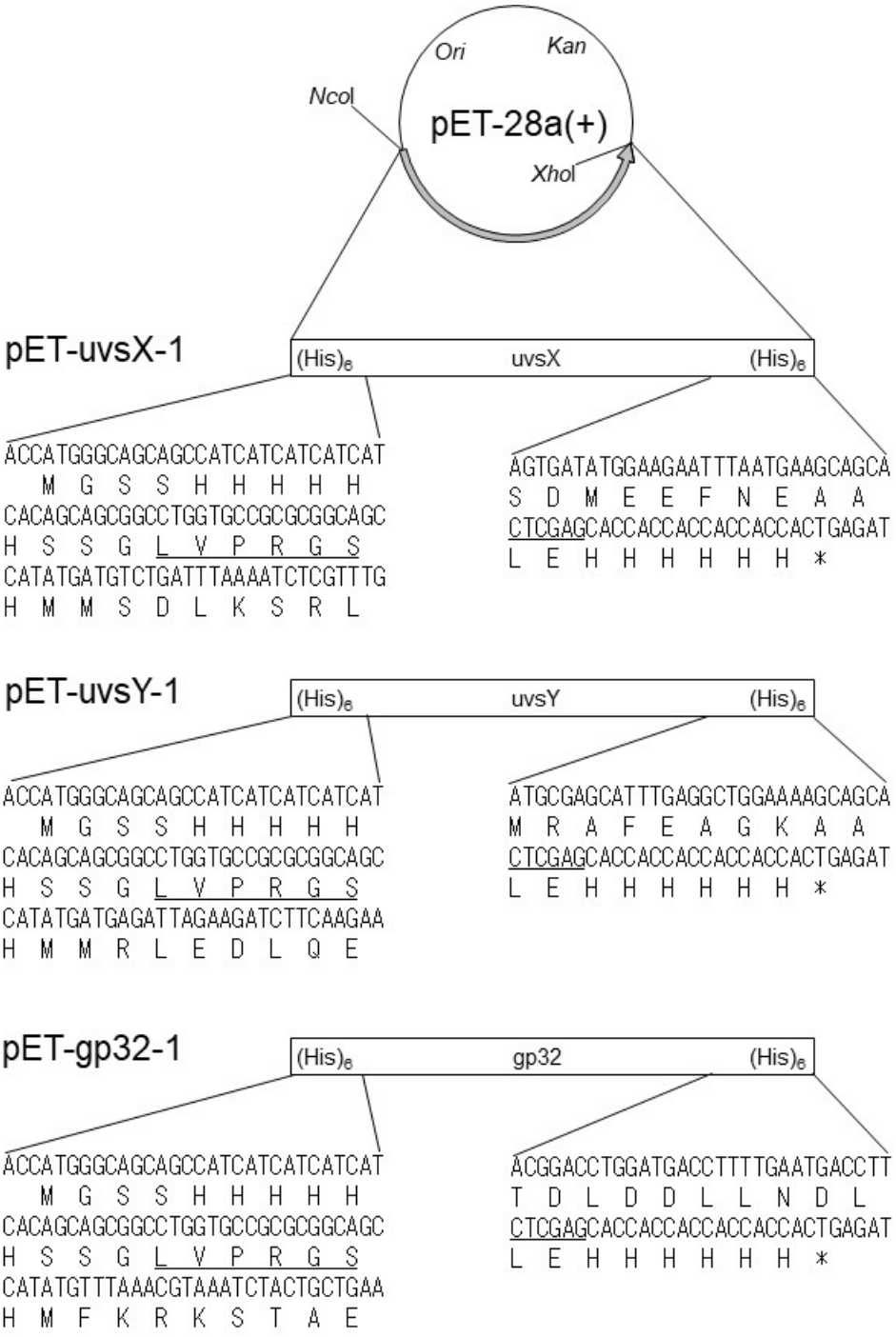

Figure 2-1. Expression plasmids. The structures of pET-uvsX-1, pET-uvsY-1, and pET-gp32-1 are shown. The asterisk indicates the termination codon. The *Xho*I site and thrombin recognition sequence are underlined.

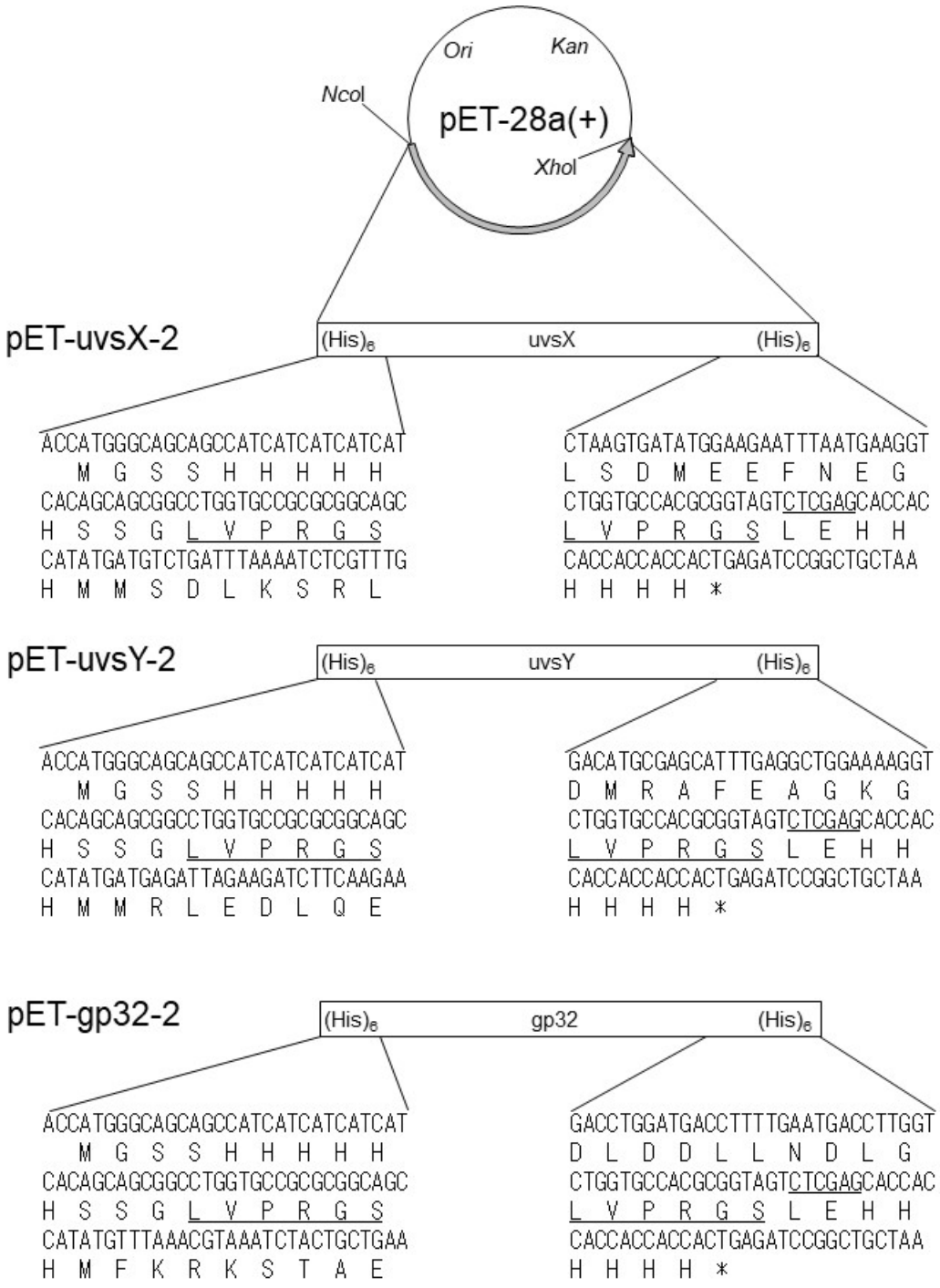

Figure 2-2. Expression plasmids. The structures of pET-uvsX-2, pET-uvsY-2, and pET-gp32-2 are shown. The asterisk indicates the termination codon. The *Xho*I site and thrombin recognition sequence are underlined.

Expression and purification of uvsX, uvsY, and gp32

Recombinant uvsX, uvsY, and gp32 were expressed and purified as follows. The overnight culture of the transformants (10 mL) was added to 1,000 mL of L broth containing 50 μg/mL kanamycin and incubated with shaking at 37ºC. When OD_{660} reached 0.6–0.8, 2.0 mL of 0.5 M isopropyl β-D-1-thiogalactopyranoside (IPTG) was added and growth was continued at 30ºC for 4 h. After centrifugation at 8,000 × *g* for 3 min, the cells were harvested, suspended with 30 mL of buffer A (50 mM phosphate buffer (pH 7.2), 500 mM NaCl, 2 mM phenylmethylsulfonyl fluoride (PMSF)), and disrupted by sonication. After centrifugation at 20,400 × *g* for 10 min, the supernatant was collected, to which 5 M NaCl and 15% w/v polyethyleneimine were added to a final concentration of 1 M and 0.15% w/v, respectively. After centrifugation at 20,400 × *g* for 10 min, the supernatant was collected, and solid ammonium sulfate ($(NH_4)_2SO_4$) was added to a final concentration of 80% saturation.

Following centrifugation at 20,400 × *g* for 10 min, the pellet was collected and dissolved in 20 mL of buffer B (50 mM phosphate buffer (pH 7.2), 500 mM NaCl) and applied to a HisTrap HP column (1 mL, GE Healthcare) equilibrated with buffer B. After washing with 100 mL of buffer B, the bound enzyme was eluted with each 2 mL of buffer B containing 30, 60, 90, 120, 150, 180, 210, or 500 mM imidazole. Each fraction was assessed for the presence of enzyme by sodium dodecyl sulfate polyacrylamide gel electrophoresis (SDS-PAGE). As for uvsY, active fractions with imidazole concentrations of 500 mM were collected and subjected to Amicon Ultra-15 MWCO 10 k (Merck Millipore, Burlington, MA) to remove imidazole using 10 mM sodium borate buffer (pH 9.3) at 4ºC. The solution was finally concentrated to 0.8 mL and stored at –30ºC before use.

In the case of uvsX and gp32, active fractions with imidazole concentrations of 180–500 and 150–180 mM, respectively, were collected and incubated with 20 units/mL thrombin (Nacalai tesque, Kyoto, Japan) at 4ºC for 13 h. The reaction solution was applied to a column [10 mm (inner diameter) × 13 mm] packed with Toyopearl DEAE-650M gel (Tosoh, Tokyo, Japan) and equilibrated with 20 mM Tris-HCl buffer (pH 8.0). The bound enzyme was eluted with each 10 mL of 20 mM Tris-HCl buffer (pH 8.0) containing 50, 100, 150, 200, 250, 300, 400, 450, 500, or 700 mM NaCl. Each fraction was assessed by SDS-PAGE for the presence of enzyme. Active fractions with NaCl concentrations of 150–250 mM for uvsX and 150–200 mM for gp32 were collected, desalted, concentrated, and stored as described above for uvsY.

RPA reaction

The RPA reaction (30 μL) was carried out in a 0.2 mL PCR tube using RYMV-F2 and RYMV-R3 (Table 2-2) at various conditions as described in the legends to the figures. PCR Thermal Cycler Dice (Takara Bio, Kusatsu, Japan) was used to warm the reaction tube. The amplified products were separated on 2% agarose gels and stained with ethidium bromide (1 μg/mL).

Table 2-2. Primers used in RPA.

Primers	Sequences (5′→3′)
RYMV-F2	CCAGGAAGGGCAAGAAAA CCAACTCCAACC
RYMV-R3	TGGAACTCCGCTTGAAGTC CGCTAGGAACT

Results and discussion

Expression and purification of recombinant uvsX, uvsY, and gp32

We constructed three plasmids pET-uvsX-2, pET-uvsY-2, and pET-gp32-2 for expression of uvsX, uvsY, and gp32, respectively, as an N- and C-terminally $(His)_6$-tagged protein with a thrombin site (Fig. 2-2). The uvsX, uvsY, and gp32 genes were expressed in *E. coli* BL21(DE3) cells and purified. Polyethyleneimine treatment was conducted to remove NA, followed by ammonium sulfate fractionation and Ni^{2+} affinity column chromatography. Figure 2-3 shows the results of SDS-PAGE analysis of purification of uvsX, uvsY, and gp32 using Ni^{2+} affinity column chromatography. UvsX, uvsY, and gp32 were eluted at 180–500, 500, and 150–180 mM imidazole, respectively.

The active fractions of uvsX, uvsY, and gp32 were treated by thrombin to cleave the $(His)_6$ tag. Figure 2-4 shows the results of SDS-PAGE analysis of treatment of uvsX, uvsY, and gp32 with thrombin. After subjecting uvsX, uvsY, and gp32 to thrombin-treatment, their respective molecular masses decreased, indicating that thrombin effectively cleaved the $(His)_6$ tag from these proteins. Thrombin-treated uvsX, uvsY, and gp32 were then subjected to anion exchange chromatography to remove thrombin and the $(His)_6$ tag. Figure 2-5 shows the results of SDS-PAGE analysis of purification of thrombin-treated uvsX, uvsY, and gp32 using anion exchange chromatography. UvsX and gp32 were eluted at 150–250 mM NaCl. However, uvsY was not purified using anion exchange chromatography because the active fraction did not bind to the column and was observed in the flow-through fraction (Fig. 2-5 B). Subsequently, uvsY was not treated with thrombin because the treatment resulted in precipitation. Next, the active fractions of uvsX and gp32 were collected and subjected to Amicon Ultra-15 MWCO 10 k to remove NaCl and concentrate the enzymes.

In order to quantify the concentration of uvsX and gp32, the active fraction of uvsX was diluted 40-fold and that of gp32 20-fold, and the absorbance was continuously measured using DU 800 spectrophotometer (Beckman Coulter) at 240–340 nm. Since uvsY precipitated during purification, it was not quantified using UV absorption at 280 nm but was quantified using Bradford method. Figure 2-6 shows the results of SDS-PAGE analysis of the active fractions at each purification stage and the purified enzyme preparations. The purified uvsX, uvsY, and gp32 preparations yielded a single band with molecular masses of 45, 22, and 34 kDa, respectively. From a one-liter culture, 1.3 mg of uvsX, 0.6 mg of uvsY, and 1.6 mg of gp32 were obtained.

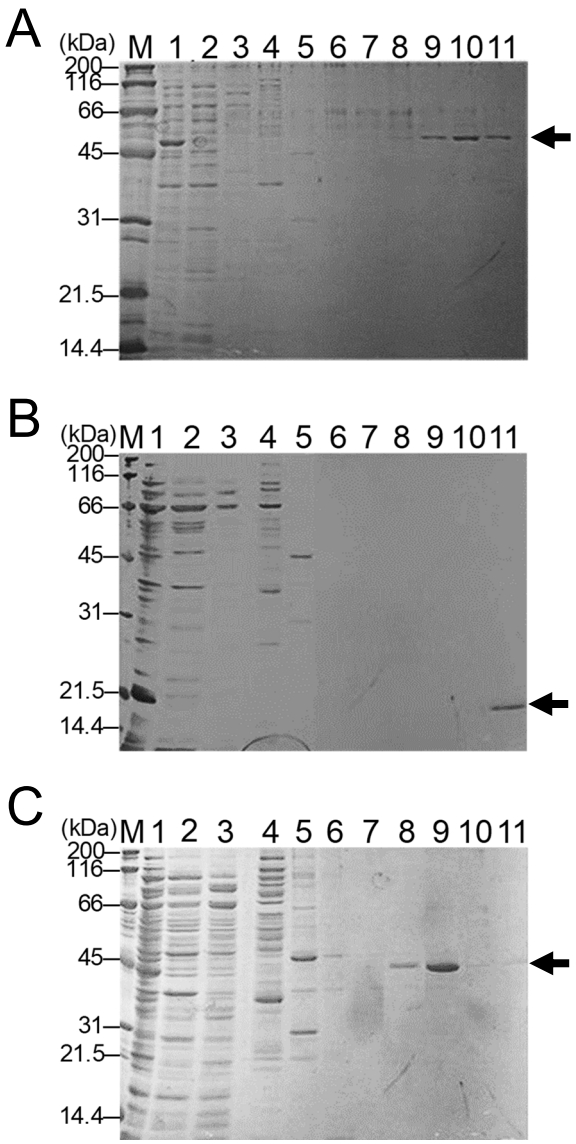

Figure 2-3. SDS-PAGE under reducing conditions. Coomassie Brilliant Blue-stained 12.5% SDS polyacrylamide gels are shown. (A) uvsX. (B) uvsY. (C) gp32. Ni^{2+} affinity chromatography fractions were applied. Marker proteins (M), the centrifuged pellets after fractionation by ammonium sulfate at 80% saturation (lane 1), flow-through fraction (lane 2), wash fraction (lane 3), elution fractions with imidazole at 30 mM (lane 4), 60 mM (lane 5), 90 mM (lane 6), 120 mM (lane 7), 150 mM (lane 8), 180 mM (lane 9), 210 mM (lane 10), and 500 mM (lane 11). The arrow indicates the band corresponding to uvsX, uvsY, or gp32.

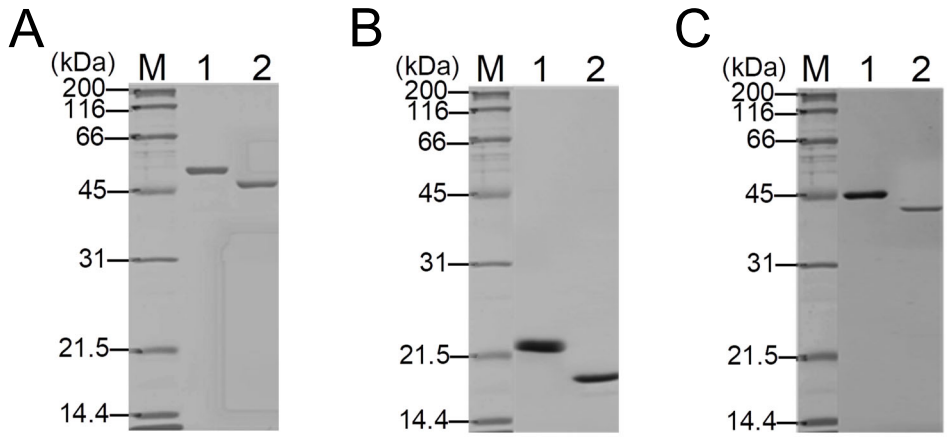

Figure 2-4. SDS-PAGE under reducing conditions. Coomassie Brilliant Blue-stained 12.5% SDS polyacrylamide gels are shown. (A) uvsX. (B) uvsY. (C) gp32. Marker proteins (M), active fraction before thrombin-treatment (lane 1), active fraction after thrombin-treatment (lane 2).

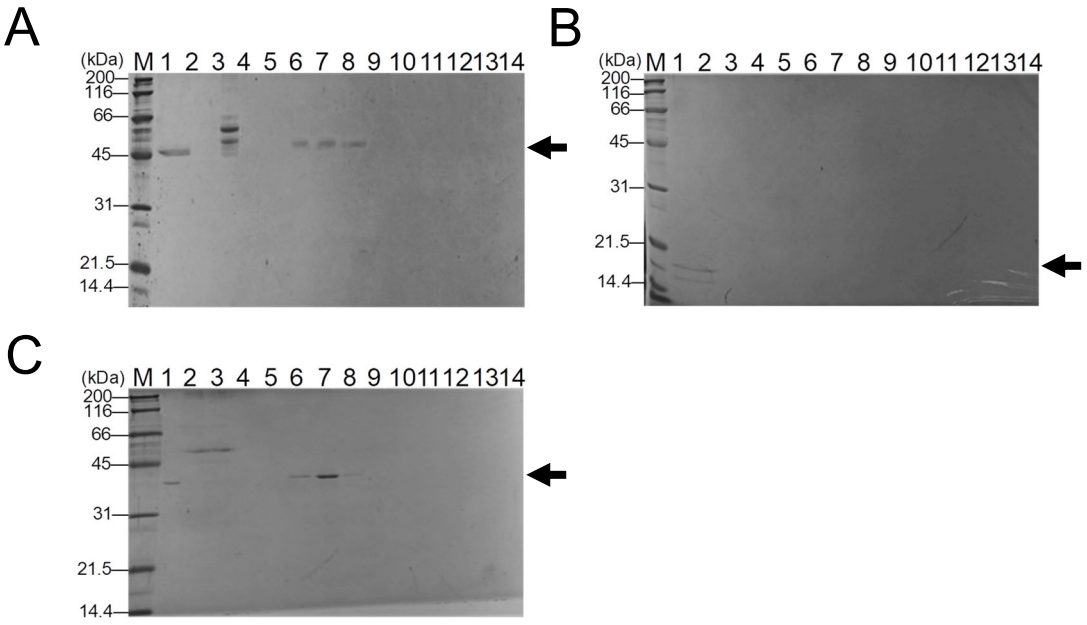

Figure 2-5. SDS-PAGE under reducing conditions. Coomassie Brilliant Blue-stained 12.5% SDS polyacrylamide gels are shown. Anion-exchange chromatography fractions were applied. (A) uvsX. (B) uvsY. (C) gp32. Marker proteins (lane M), active fraction after thrombin-treatment (lane 1), flow-through fraction (lane 2), wash fraction (lane 3), elution fractions with NaCl at 50 mM (lane 4), 100 mM (lane 5), 150 mM (lane 6), 200 mM (lane 7), 250 mM (lane 8), 300 mM (lane 9), 350 mM (lane 10), 400 mM (lane 11), 450 mM (lane 12), 500 mM (lane 13), and 700 mM (lane 14). The arrow indicates the band corresponding to uvsX, uvsY, or gp32.

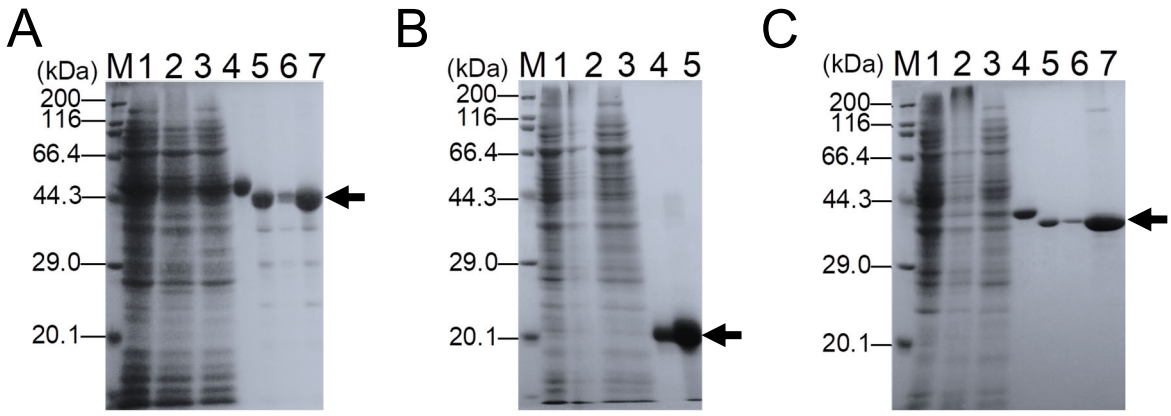

Figure 2-6. SDS-PAGE under reducing conditions. Coomassie Brilliant Blue-stained 12.5% SDS polyacrylamide gels are shown. Active fractions of each purification stage were applied. (A) uvsX. (B) uvsY. (C) gp32. Lanes 1–4 for uvsX, uvsY, and gp32: marker proteins (lane M), soluble fractions of the total extracts (lane 1), the centrifuged supernatants after polyethyleneimine treatment (lane 2), the centrifuged pellets after fractionation by ammonium sulfate at 80% saturation (lane 3), and active fractions of Ni^{2+} affinity chromatography (lane 4). Lanes 5-7 for uvsX and gp32: thrombin-treated fraction (lane 5), active fractions of anion-exchange chromatography (lane 6), and the purified uvsX or gp32 preparations after membrane concentration (lane 7). Lane 5 for uvsY: the purified uvsY preparation after membrane concentration. The arrow indicates the band corresponding to uvsX, uvsY, or gp32.

RPA reaction with uvsX, uvsY, and gp32 preparations

We performed the RPA reaction using uvsX, uvsY, and gp32 preparations. The structure of RYMV and the target sequence were as reported in Chapter 1 [76] and the reaction conditions used were as previously described [14]. When the reaction was performed in the presence of standard DNA, uvsX, uvsY, gp32, *Bst* DNA polymerase, creatine kinase, and DTT, the 210-bp band was observed clearly. When the reaction was performed in the absence of standard DNA, uvsX, gp32, or *Bst* DNA polymerase, the band was not observed, indicating that these four components were indispensable. When the reaction was performed in the absence of uvsY, creatine kinase, or DTT, the 210-bp band was observed although it was less clear (Fig. 2-7). This indicated that these three components were not indispensable but contributed to an enhanced reaction efficiency. We speculated that uvsX binds to the primers even without the assistance of uvsY or ATP regeneration system to some extent.

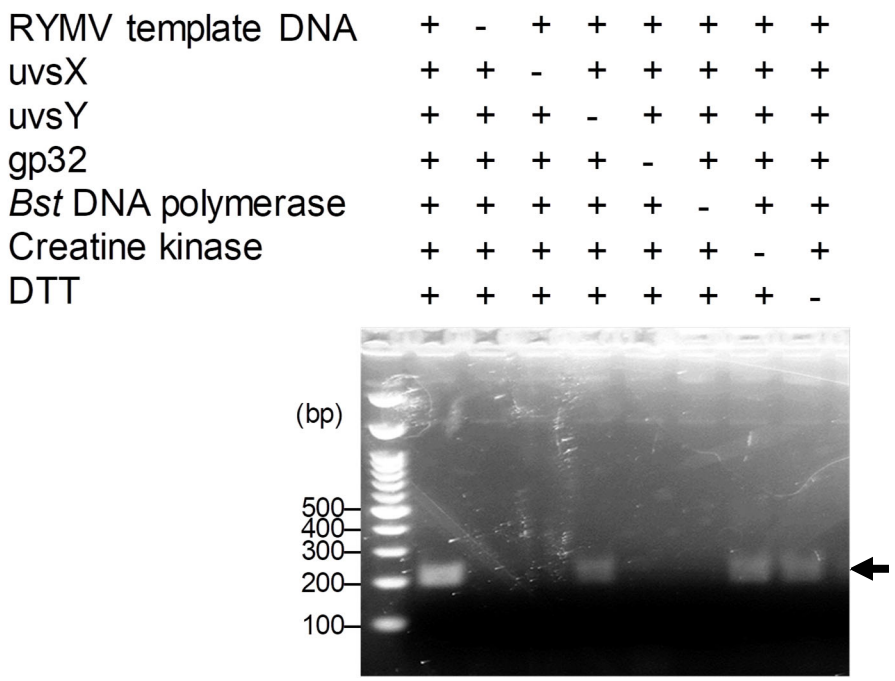

Figure 2-7. Effects of the absence of one RPA reaction component on RPA. RPA reaction was carried out in 30 mM Tris-HCl buffer (pH 8.6), 90 mM CH_3COOK, dNTPs (450 μM each), 50 mM phosphocreatine, 0.48 μM RYMV-F2 primer, 0.48 μM RYMV-R3 primer, 5.5% w/v PEG35,000, 2.5 mM ATP, and 14 mM $Mg(CH_3COO)_2$ in the presence of 2×10^7 copies/μL standard DNA, 570 ng/μL uvsX, 480 ng/μL uvsY, 340 ng/μL gp32, 0.4 units/μL *Bst* DNA polymerase, 300 ng/μL creatine kinase, and 2 mM DTT or in the absence of standard DNA, uvsX, uvsY, gp32, *Bst* DNA polymerase, creatine kinase, or DTT at 41ºC for 1 h. The arrow indicates the amplified target band.

Effects of pH, CH_3COOK concentration, and temperature on RPA efficiency

The first RPA reaction reported in 2006 using T4 uvsX, uvsY, and gp32 was carried out with 50 mM Tris-HCl buffer (pH 7.9 or 8.4) and 80 mM CH_3COOK at pH 7.9–8.4, at 37ºC [14]. We examined the effects of pH, CH_3COOK concentration, and temperature on RPA efficiency (Fig. 2-8). Thirty mM Tris-HCl buffer (pH 8.6), 40 mM CH_3COOK, and 41ºC were used as standard conditions. The amplified DNA band was observed at pH 7.0–9.0, but not at pH 5.0–6.5 and pH 9.5–10.5, suggesting that pH 7.5–8.0 was optimal. (Fig. 2-8 A). The optimal pH values of recombinase and strand-displacing DNA polymerase are different. DNA binding and DNA exchange assays of recombinase are performed at pH 7.6 [77], while the reaction with strand-displacing DNA polymerase reaction is at pH 8.5–8.8. Our results suggested that it is more important for the reaction efficiency of RPA that recombinase rather than strand-displacing DNA polymerase exhibits the highest performance.

The effect of CH_3COOK concentration on the efficiency of RPA was examined. The amplified DNA band that was observed at 20 and 100–140 mM was less clear than that at 40–80 mM, suggesting that the optimal CH_3COOK concentration was 40–80 mM (Fig. 2-8 B). However, we presume that the optimal CH_3COOK concentration is to some extent dependent on the T_m of the primers. The effect of temperature on the efficiency of the RPA reaction was explored. The amplified DNA band was observed at 37–45ºC, with 41ºC appearing to be optimal for the specific target used as a model. The reactions carried out at 33–35ºC and at 47ºC did not result in successful amplification (Fig. 2-8 C). The former might be due to the strand-displacing DNA polymerase not being fully functional, whilst in the latter it can be assumed that the recombinase was inactivated.

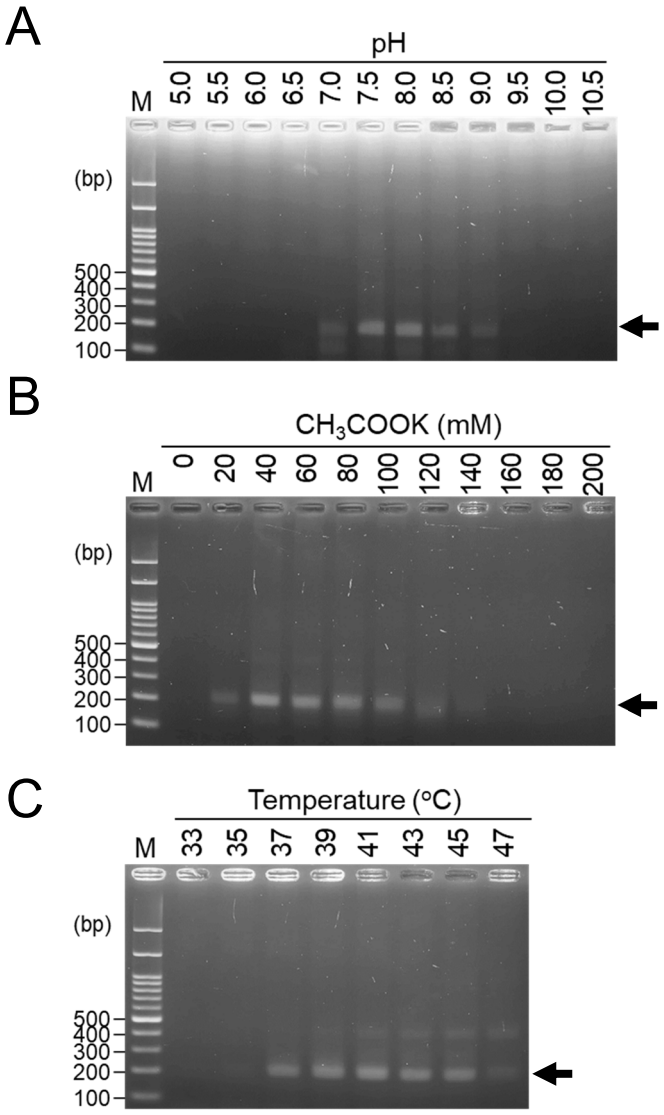

Figure 2-8. Effects of pH, CH_3COOK concentration, and temperature on RPA reaction efficiency. RPA was carried out in the following conditions: Buffer, 30 mM acetic acid-sodium acetate buffer (pH 5.0 or 5.5), 30 mM sodium phosphate buffer (pH 6.0, 6.5, or 7.0), 30 mM Tris-HCl buffer (pH 7.5, 8.0, 8.5, or 9.0), or 30 mM sodium carbonate bicarbonate buffer (pH 9.5, 10.0, or 10.5) (A) or 30 mM Tris-HCl buffer (pH 8.6) (B, C); CH_3COOK, 40 mM (A), 0–200 mM (B), or 20 mM (C); Other components (A–C), 2 mM DTT, dNTPs (450 μM each), 460 ng/μL uvsX, 80 ng/μL uvsY, 380 ng/μL gp32, 0.4 units/μL *Bst* DNA polymerase, 120 ng/μL creatine kinase, 20 mM phosphocreatine, 0.48 μM RYMV-F2 primer, 0.48 μM RYMV-R3 primer, 6.5% w/v PEG35,000, 2.5 mM ATP, 14 mM $Mg(CH_3COO)_2$, and 2×10^7 copies/μL standard DNA; Temperature, 41ºC (A, B) or 33–47ºC (C); Reaction time: 1 h. The arrow indicates the amplified target band.

Effects of additives on RPA efficiency

To increase the performance of a NA amplification reaction, it is important to optimize the reaction conditions. In the amplification techniques using multiple enzymes, such as RPA, this process is more complicated because each enzyme has its own optimal condition. In NA sequence-based amplification (NASBA), an isothermal reaction (41–43ºC) that specifically amplifies a target RNA sequence with reverse transcriptase, RNA polymerase, and ribonuclease H (RNase H) [4], this type of complex optimization has been reported [68, 69]. A recent study reported cDNA synthesis using Moloney murine leukemia virus (MMLV) reverse transcriptase, a thermostable DNA polymerase with reverse transcriptase activity, and DNA/RNA helicase. The researchers utilized Taguchi's method, a well-known statistical approach for optimizing multiple factors in a single reaction or process [73], to develop a highly sensitive one-step RT-PCR with these three enzymes [74]. However, in the case of RPA, the effect of additives on the reaction efficiency remains relatively unknown, making it challenging to apply statistical methods like Taguchi method.

We examined the effects of gelatin, bovine serum albumin (BSA), trehalose, sorbitol, glycerol, DMSO, formamide, Triton X-100, Tween 20, and ammonium sulfate on RPA reaction efficiency. In PCR, gelatin, BSA, trehalose, sorbitol, glycerol, Triton X-100, and Tween 20 are used as enzyme stabilizers, whilst DMSO, formamide, and ammonium sulfate are used to increase specificity. In this study, the concentrations of each additive were established according to a previous report on the optimization of PCR parameters [75, 78]. DMSO at 5% v/v, formamide at 5% v/v, and ammonium sulfate at 20 mM inhibited the reaction while other additives did not (Fig. 2-9). Our results are in contrast to the previous results for the synthesis of cDNA that showed that DMSO (12% v/v) and

formamide (6–8% v/v) improved the reaction efficiency [79] and PCR where DMSO (5% v/v) and formamide (5% v/v) improved the reaction efficiency [80]. We speculate that at least one of uvsX, uvsY, and gp32 are susceptible to DMSO, formamide, and ammonium sulfate. In PCR, DMSO, and formamide are frequently used for the reaction with a G+C-rich DNA to improve specificity.

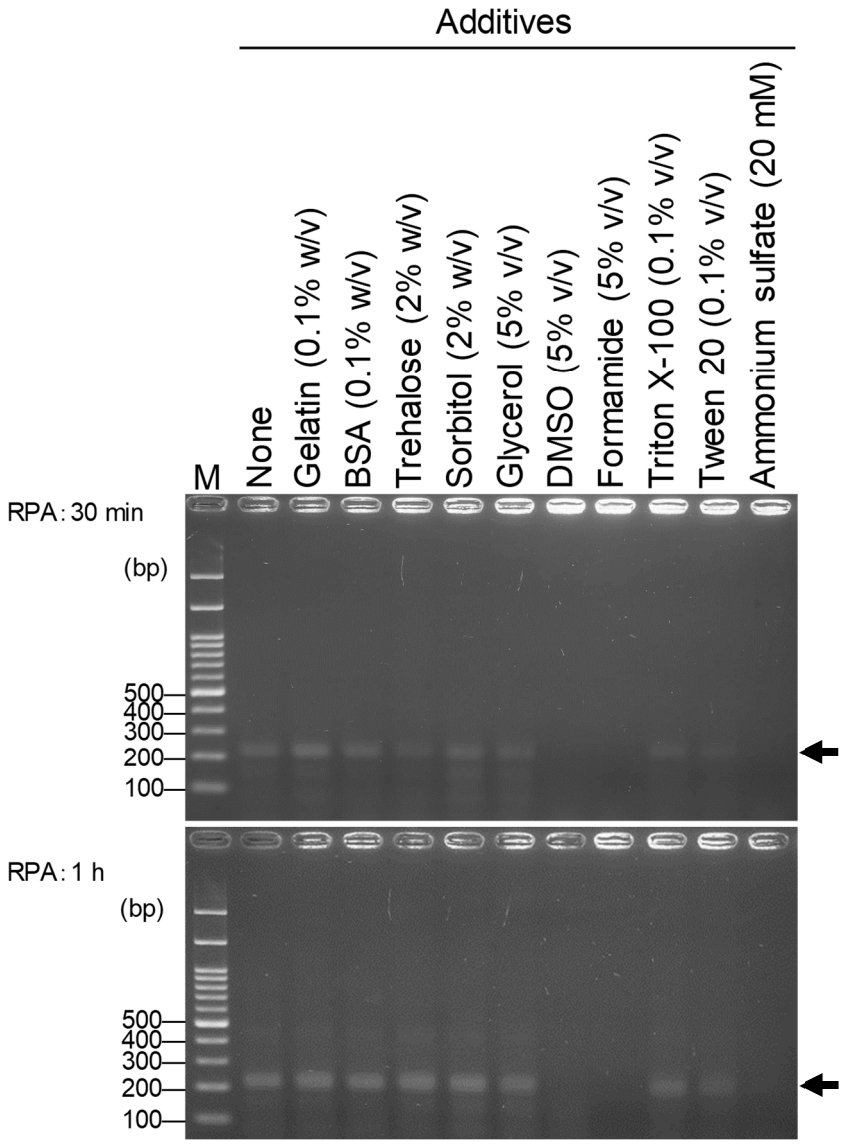

Figure 2-9. Effects of additives on RPA reaction efficiency. RPA reaction was carried out in 30 mM Tris-HCl buffer (pH 8.0), 40 mM CH_3COOK, 2 mM DTT, dNTPs (450 μM each), 460 ng/μL uvsX, 80 ng/μL uvsY, 380 ng/μL gp32, 0.4 units/μL *Bst* DNA polymerase, 120 ng/μL creatine kinase, 20 mM phosphocreatine, 0.48 μM RYMV-F2 primer, 0.48 μM RYMV-R3 primer, 7.5% w/v PEG35,000, 2.5 mM ATP, 14 mM $Mg(CH_3COO)_2$, and 2×10^7 copies/μL standard DNA in the presence of indicated concentration of each of additives at 41ºC for 30 min (upper panel) or 1 h (lower panel). The arrow indicates the amplified target band.

Conclusion

We prepared recombinant Rec and SSB proteins from T4 phage and used them to examine the effects of reaction conditions and additives on the efficiency of RPA. The results revealed that the optimal pH was 7.5–8.0, the optimal CH_3COOK was 40–80 mM, and the optimal reaction temperature was 37–45ºC. DMSO at 5% v/v and formamide at 5% v/v inhibited the reaction.

Chapter 3

Optimization of reaction condition of recombinase polymerase amplification using a statistical method*

Introduction

The artificial replication of genetic material (NA amplification), has extensively been used in life sciences and biotechnology for pathogen detection, sequencing, genetic engineering, cloning, drug discovery etc. PCR is considered the industry's 'gold standard' for NA amplification. However, its dependence on a thermocycler has limited its use in laboratory settings. To overcome this challenge, an isothermal method performed at 37–41ºC was developed in 2006 as a potential alternative to PCR, known as RPA [14]. In RPA, the T4 uvsX protein (Rec) and T4 uvsY protein (loading factor) bind to primers forming a nucleoprotein filament. The resulting complex searches for the homologous sequences within the dsDNA. After locating the target sequence, the complex infiltrates the dsDNA. The unwound complementary strand is stabilized through interaction with SSB protein, specifically the T4 gp32. The Rec disassembles from the nucleoprotein and DNA synthesis is initiated by Pol (*Bst*-Pol) [15–17]. The use of a constant temperature simplifies the experimental setup and eliminates the need for sophisticated equipment

*The content described in this Chapter was originally published in *Biochemical and Biophysical Research Communications*. Kevin Maafu Juma, Teisuke Takita, Kenji Ito, Masaya Yamagata, Shihomi Akagi, Emi Arikawa, Kenji Kojima, Manish Biyani, Shinsuke Fujiwara, Yukiko Nakura, Itaru Yanagihara, and Kiyoshi Yasukawa (2021). Optimization of reaction condition of recombinase polymerase amplification to detect SARS-CoV-2 DNA and RNA using a statistical method. *Biochem. Biophys. Res. Commun*., **567**, 195–200.

(like a thermal cycler), making RPA more accessible and cost-effective.

For successful deployment and implementation of RPA technology at the point-of-care use, it is important to maximize the optimization of RPA conditions. Numerous optimization studies in PCR conditions have been reported [56, 57, 75]. In NA sequence-based amplification (NASBA), an isothermal reaction performed at a specific temperature range (41–43ºC) to amplify target RNA sequences using reverse transcriptase, RNA polymerase, and ribonuclease H (RNase H), optimization of reaction conditions has been reported [4]. However, in RPA that involves multiple enzymes, substrates, and buffers, the optimization process becomes more complex because each reaction component has its optimal conditions. Unfortunately, there is limited knowledge regarding the optimization of RPA conditions due to the nature of pre-prepared RPA kits. This limitation restricts researchers' flexibility in exploring the effects of varying component concentrations on reaction efficiency. In Chapter 2, we prepared Rec and SSB and examined the effects of pH, temperature, and various additives on RPA reaction efficiency [81].

In this Chapter, we optimized the reaction conditions of RPA to detect SARS-CoV-2 DNA and RNA using a well-known statistical method, the Taguchi method (Fig. 3-1). This method balanced the effects of all factors and their associated levels by using an orthogonal array rather than a factorial array [73, 82].

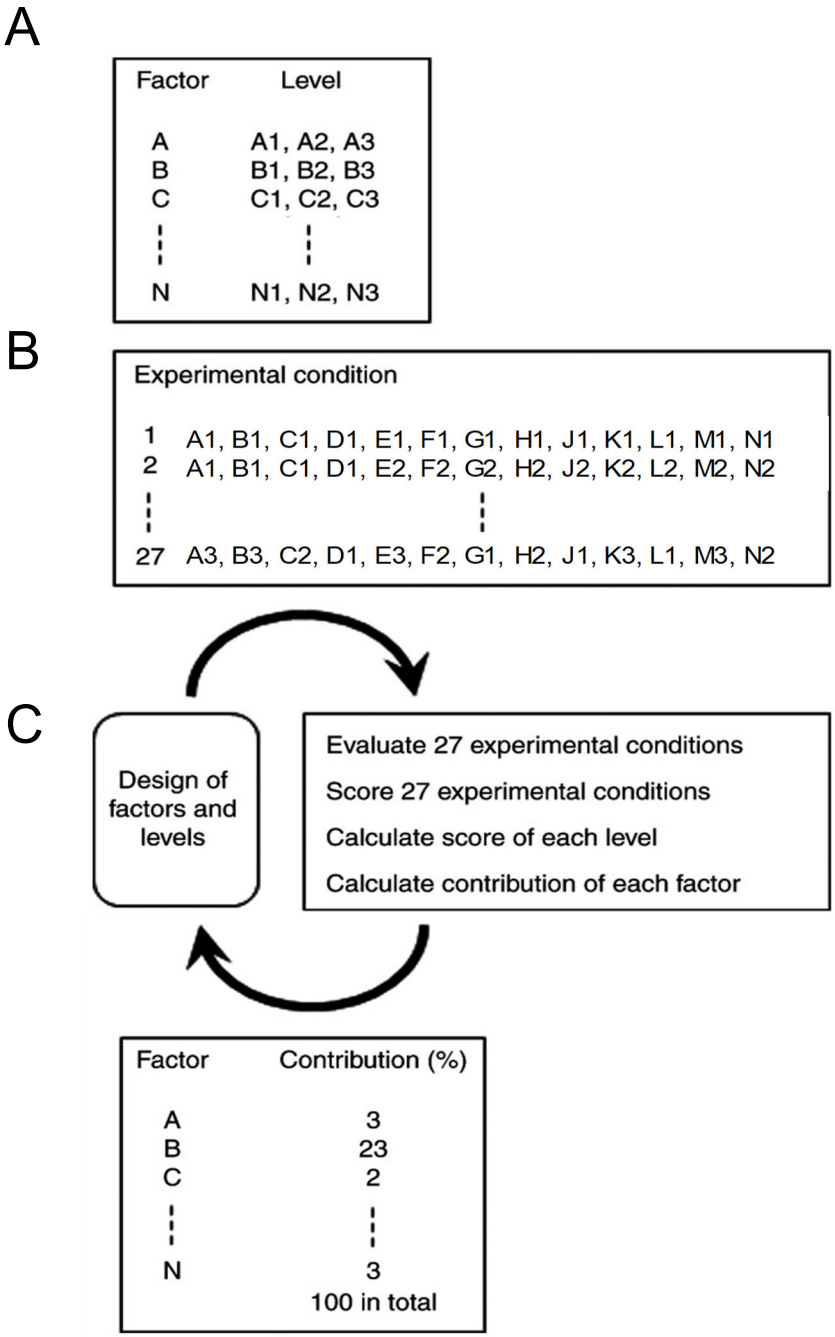

Figure 3-1. Optimization of reaction conditions. (A) Thirteen factors and three levels for each factor were set. (B) Twenty-seven reaction conditions were designed according to Taguchi's L27 orthogonal array. The performance of each condition is scored. (C) By repeating the cycle, the reaction condition gets optimized.

Materials and methods

Materials

Recombinant uvsX, uvsY, and gp32 were expressed and purified as described in Chapter 2. The recombinant thermostable quadruple variant (E286R/E302K/L345R/D524A) of MMLV reverse transcriptase was expressed in *E. coli* and purified from the cells as described previously [83].

Preparation of standard DNA and RNA

Standard DNA and RNA corresponding to sequences 28,571–28,970 (System 1 in Fig. 3-2 A) and 28,171–28,470 (System 2 in Fig. 3-2 B) of the SARS-CoV-2 gene deposited in GenBank (NC_045512.2) were prepared as follows. PCR was carried out using the oligonucleotides listed in Tables 3-1 and 3-2 and *Taq* polymerase (Toyobo) for 35 cycles of 30 s at 95ºC, 30 s at 55ºC, and 30 s at 72ºC. The amplified DNA was purified using a MagExtractor (Toyobo). *In vitro* transcription was carried out using RiboMAX Large Scale RNA Production System (Promega, Madison, WI) at 37ºC for 3 h. The synthesized RNA was purified by NICK Columns (GE Healthcare). The purified DNA and RNA concentrations were determined spectrophotometrically at 260 nm. The DNA and RNA were stored at –30ºC or –80ºC, respectively before use.

In System 1, the standard DNA was amplified by PCR using 400nt-F and 400nt-B as a pair of primers and the mixture of oligonucleotides 400nt-1, 400nt-2, and 400nt-3 as a template. The T7 promoter-bearing standard DNA was amplified by PCR using T7-400nt-F and 400nt-B as a pair of primers and the standard DNA as a template (Table 3-1). Standard RNA was synthesized by *in vitro* transcription using the T7 promoter-bearing standard DNA as a template. In System 2, the standard DNA was amplified by PCR using

300nt-F and 300nt-B as a pair of primes and the mixture of oligonucleotides 300nt-1 and 300nt-2 as a template. The T7 promoter-bearing standard DNA was amplified by PCR using T7-300nt-F and 300nt-B as a pair of primers and the standard DNA as a template (Table 3-2). Standard RNA was synthesized by *in vitro* transcription using the T7 promoter-bearing standard DNA as a template.

Table 3-1. Oligonucleotides used in System 1.

Primers	Sequences (5′→3′)
400nt-F	GGAGAATTATTGATCTCGAGGACAAGCTTGCGGCC
400nt-B	GGCCGCAAGCTTGTCCTCGAGATCAATAATTCTCC
T7-400nt-F	AATTCTAATACGACTCACTATAGGGAGA
	GGAGAATTATTGATCTCGAGGACAAGCTTGCGGCC
400nt-1	AAAATGAAAGATCTCAGTCCAAGATGGTATTTCTACTACC
	TAGGAACTGGGCCAGAAGCTGGACTTCCCTATGGTGCTAA
	CAAAGACGGCATCATATGGGTTGCAACTGAGGGAGCCTTG
400nt-2	TTGCAACTGAGGGAGCCTTGAATACACCAAAAGATCACAT
	TGGCACCCGCAATCCTGCTA ACAATGCTGCAATCGTGCTA
	CAACTTCCTCAAGGAACAAC ATTGCCAAAAGGCTTCTACG
	CAGAAGGGAGCAGAGGCGGCAGTCAAGCCTCTTCTCGTTC
	CTCATCACGTAGTCGCAACAGTTCAAGAAATTCAACTCCA
400nt-3	TGCTCTCAAGCTGGTTCAATCTGTCAAGCAGCAGCAAAGC
	AAGAGCAGCATCACCGCCATTGCCAGCCATTCTAGCAGGA
	GAAGTTCCCCTACTGCTGCCTGGAGTTGAATTTCTTGAAC
1F	CACATTGGCACCCGCAATC
1F+4	CACATTGGCACCCGCAATCCTGC
1F+8	CACATTGGCACCCGCAATCCTGCTAAC
1R	GAGGAACGAGAAGAGGCTTG
1R+4	GAGGAACGAGAAGAGGCTTGACTG
1R+8	GAGGAACGAGAAGAGGCTTGACTGCCGC

Table 3-2. Oligonucleotides used in System 2.

Primers	Sequences (5′→3′)
300nt-F	CTAAATTGGGTAGTCTTGTAGTGCG
300nt-B	AATTTAAGGTCTTCCTTGCCATGTT
T7-300nt-F	AATTCTAATACGACTCACTATAGGGAGA
	CTAAATTGGGTAGTCTTGTAGTGCG
300nt-1	CTAAATTGGGTAGTCTTGTAGTGCGTTGTTCGTTCTATGA
	AGACTTTTTAGAGTATCATGACGTTCGTGTTGTTTTAGAT
	TTCATCTAAACGAACAAACTAAAATGTCTGATAATGGACC
	CCAAAATCAGCGAAATGCACCCCGCATTACGTTTGGTGGA
300nt-2	AATTTAAGGTCTTCCTTGCCATGTTGAGTGAGAGCGGTGA
	ACCAAGACGCAGTATTATTGGGTAAACCTTGGGGCCGACG
	TTGTTTTGATCGCGCCCCACTGCGTTCTCCATTCTGGTTA
	CTGCCAGTTGAATCTGAGGGTCCACCAAACGTAATGCGGG
2F	GACCCCAAAATCAGCGAAAT
2F+4	GACCCCAAAATCAGCGAAATGCAC
2F+8	GACCCCAAAATCAGCGAAATGCACCCCG
2F-4	AATGGACCCCAAAATCAGCGAAAT
2F-8	TGATAATG GACCCCAAAATCAGCGAAAT
2F-12	TGTCTGATAATGGACCCCAAAATCAGCGAAAT
2F-13	ATGTCTGATAATGGACCCCAAAATCAGCGAAAT
2F-14	AATGTCTGATAATGGACCCCAAAATCAGCGAAAT
2F-15	AAATGTCTGATAATG GACCCCAAAATCAGCGAAAT
2R	TCTGGTTACTGCCAGTTGAATCTG
2R+4	TCTGGTTACTGCCAGTTGAATCTGAGGG
2R+8	TCTGGTTACTGCCAGTTGAATCTGAGGGTCCA
2R-4	CCAT TCTGGTTACTGCCAGTTGAATCTG
2R-8	TTCTCCAT TCTGGTTACTGCCAGTTGAATCTG
2R-11	GCGTTCTCCATTCTGGTTACTGCCAGTTGAATCTG
2R-11-1	TGCGTTCTCCATTCTGGTTACTGCCAGTTGAATCT
2R-11-2	CTGCGTTCTCCATTCTGGTTACTGCCAGTTGAATC

RPA reaction and statistical analysis

The reaction mixture (30 μL) for RPA was designed and prepared according to Taguchi's L27 orthogonal array consisting of 13 factors (Table 3-3). The reaction was performed in a 0.2 mL PCR tube at 41ºC in PCR Thermal Cycler Dice (Takara Bio). The amplified products were separated on 2.0% agarose gels and stained with ethidium bromide (1 μg/mL). Each reaction condition for cDNA synthesis was scored as 1, 2, or 3 according to the amplified products' intensity (no, faint, or clear, respectively). The data were analyzed by the following equation:

$$S/N_m = -10 \log (s_m^2) \quad (1)$$

where S/N_m is the signal-to-noise ratio of and s_m is the score of each reaction condition (m=1, 2, -----, 27). The $S/N_{x,i}$ of level i (= 1, 2, or 3) of factor x (= 1 to 13) was the total of nine out of 27 S/N_m values where the level of factor x is i. For example, the $S/N_{1,1}$ and $S/N_{2,1}$ were calculated as follows:

$$S/N_{1,1} = S/N_1 + S/N_2 + S/N_3 + S/N_4 + S/N_5 + S/N_6 + S/N_7 + S/N_8 + S/N_9$$

$$S/N_{2,1} = S/N_1 + S/N_2 + S/N_3 + S/N_{10} + S/N_{11} + S/N_{12} + S/N_{19} + S/N_{20} + S/N_{21}$$

Accordingly, the lowest $S/N_{x,i}$ value of the three $S/N_{x,i}$ values ($S/N_{x,1}$, $S/N_{x,2}$, $S/N_{x,3}$) indicates that level i is the most appropriate. Variation (V_x; x = 1 to 13) and percentage contribution (P_x) for factor x were calculated using the following equations:

$$V_x = (S/N_{x,1}^2 + S/N_{x,2}^2 + S/N_{x,3}^2)/9 - (S/N_1 + S/N_2 + \text{-------} + S/N_{27})^2/27 \quad (2)$$

$$P_x = V_x / (V_1 + V_2 + \text{-------} + V_{13}) \times 100 \quad (3)$$

Accordingly, high V_x and P_x values indicate that the effect of the difference in the three levels in factor x is high on the reaction efficiency.

Table 3-3. Taguchi's L27 orthogonal array.

Reaction Condition	Factor[a]												
	1	2	3	4	5	6	7	8	9	10	11	12	13
	Level[a]												
1	1	1	1	1	1	1	1	1	1	1	1	1	1
2	1	1	1	1	2	2	2	2	2	2	2	2	2
3	1	1	1	1	3	3	3	3	3	3	3	3	3
4	1	2	2	2	1	1	1	2	2	2	3	3	3
5	1	2	2	2	2	2	2	3	3	3	1	1	1
6	1	2	2	2	3	3	3	1	1	1	2	2	2
7	1	3	3	3	1	1	1	3	3	3	2	2	2
8	1	3	3	3	2	2	2	1	1	1	3	3	3
9	1	3	3	3	3	3	3	2	2	2	1	1	1
10	2	1	2	3	1	2	3	1	2	3	1	2	3
11	2	1	2	3	2	3	1	2	3	1	2	3	1
12	2	1	2	3	3	1	2	3	1	2	3	1	2
13	2	2	3	1	1	2	3	2	3	1	3	1	2
14	2	2	3	1	2	3	1	3	1	2	1	2	3
15	2	2	3	1	3	1	2	1	2	3	2	3	1
16	2	3	1	2	1	2	3	3	1	2	2	3	1
17	2	3	1	2	2	3	1	1	2	3	3	1	2
18	2	3	1	2	3	1	2	2	3	1	1	2	3
19	3	1	3	2	1	3	2	1	3	2	1	3	2
20	3	1	3	2	2	1	3	2	1	3	2	1	3
21	3	1	3	2	3	2	1	3	2	1	3	2	1
22	3	2	1	3	1	3	2	2	1	3	3	2	1
23	3	2	1	3	2	1	3	3	2	1	1	3	2
24	3	2	1	3	3	2	1	1	3	2	2	1	3
25	3	3	2	1	1	3	2	3	2	1	2	1	3
26	3	3	2	1	2	1	3	1	3	2	3	2	1
27	3	3	2	1	3	2	1	2	1	3	1	3	2

[a] Factors and levels of each factor in the Round 1–3 analyses are described in Tables 3-4, 3-5, and 3-6.

Results and discussion

Establishment of the RPA detection systems of SARS-CoV-2 DNA

For use as the assay in the optimization of RPA reaction conditions, we established two detection systems (Systems 1 and 2) of SARS-CoV-2 DNA (Fig. 3-2). In System 1, the nucleocapsid phosphoprotein gene was selected as a target according to the previous report [84]. We designed three forward and three reverse primers (Table 3-1) and selected one combination (1F+4 and 1R+8) that exhibited the best performance in sensitivity. The size of the amplified product by the primer combination was 128-bp. In System 2, the ORF8 protein gene was used as a target because Centers for Disease Control and Prevention (CDC), USA reported the PCR primers targeting this region, and these primers are widely used in approved diagnostics of SARS-CoV-2 RNA. We designed nine forward and eight reverse primers (Table 3-2) and selected one combination (2F-15 and 2R-11) that exhibited the best performance in sensitivity. The size of the amplified product by the primer combination was 99-bp.

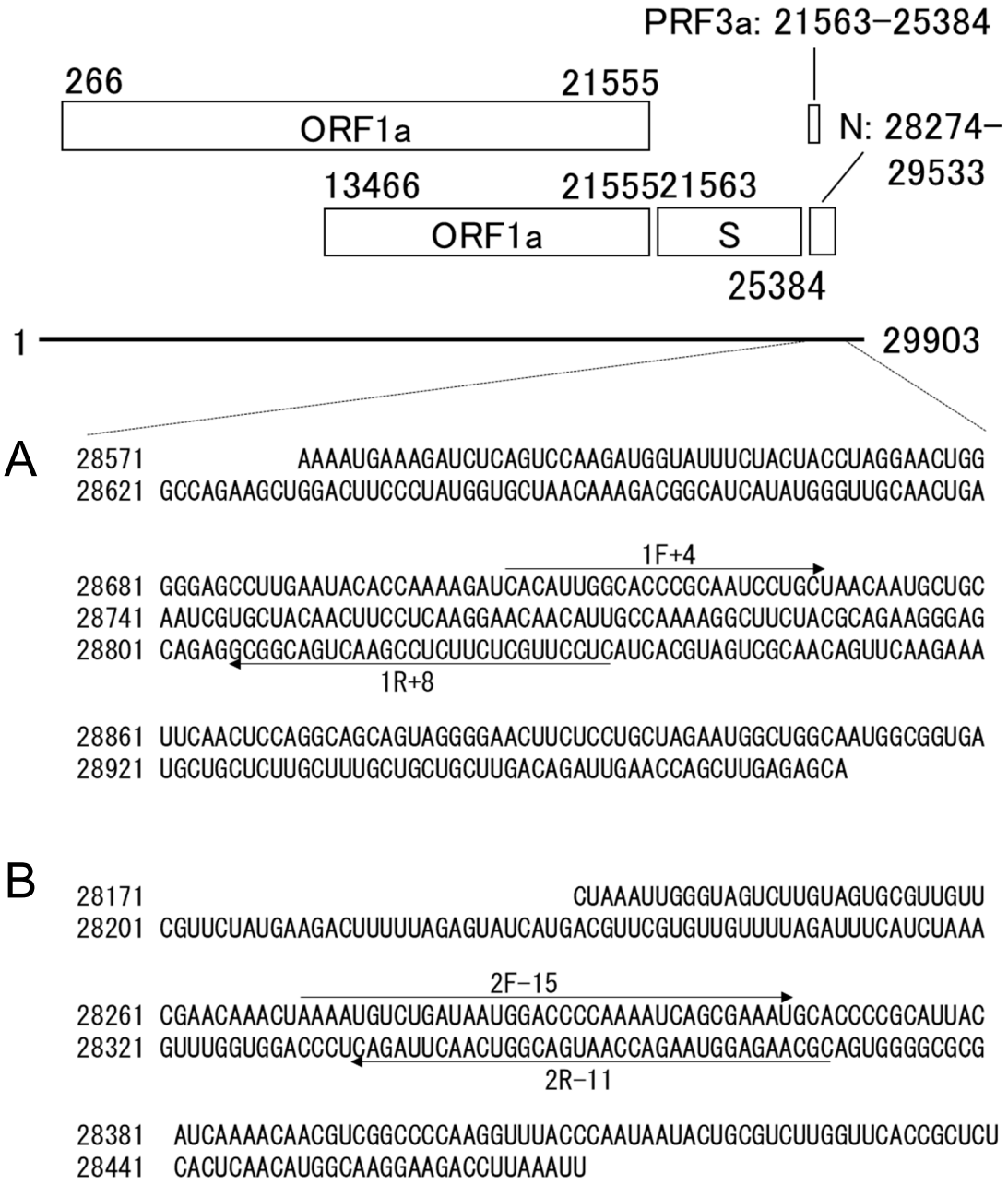

Figure 3-2. Structure of SARS-CoV-2 and a target sequence for RPA amplification. Arrows indicate the sequences to which primers bind. (A) System 1. (B) System 2.

Round 1 of optimization of RPA reaction condition

We designed 13 factors and three concentrations (levels 1–3) for each factor (Table 3-4). Level 2 was set as the concentration used in the standard condition in Chapter 2 [81]. Levels 1 and 3 were set as 25–50% and 200–400%, respectively, of level 2. According to Taguchi's L27 orthogonal array (Table 3-3), the RPA reaction was carried out with 6×10^8 copies (2×10^7 copies/μL) of standard DNA and primers in System 1. The reaction product was analyzed by agarose gel electrophoresis (Fig. 3-3). Of the 27 reaction conditions, six (2, 3, 7, 17, 24, and 25) exhibited clear, four (5, 12, 13, and 18) exhibited faint, and the other 17 exhibited no 128-bp band corresponding to the amplified product. The signal-to-noise ratios for each reaction condition (S/N_m; m = 1 to 27), those for each level of each factor ($S/N_{x,i}$; x = 1 to 13, i = 1, 2, or 3), and variations (V) and percentage contributions (P) for each factor were calculated (Table 3-4). The results indicated that the $Mg(CH_3COO)_2$ concentration exhibited the highest V (142) and P (39.7%) values with the optimal concentration of 7 mM (level 1).

It is known that the optimal concentration of $Mg(CH_3COO)_2$ depends on primer and target sequences. Indeed, in the RPA kit sold by TwistDx, $Mg(CH_3COO)_2$ is not premixed but is added by users. High V and P values in our results suggested that the optimal range of $Mg(CH_3COO)_2$ concentration is relatively narrow.

Table 3-4. Signal-to-noise ratio for levels 1–3 of each factor and variation (V) and percentage contribution (P) for each factor in RPA in Round 1.

Factor		Level			V	P (%)
		1	2	3		
1	uvsX (ng/μL)	226 (–18)	452 (–31)	904 (–21)	10.8	3.0
2	uvsY (ng/μL)	35 (–18)	70 (–27)	140 (–25)	5.8	1.6
3	gp32 (ng/μL)	100 (–20)	200 (–27)	400 (–22)	2.7	0.8
4	*Bst* DNA pol (units/μL)	0.2 (–26)	0.4 (–22)	0.8 (–23)	1.0	0.3
5	Creatine kinase (ng/μL)	60 (–28)	120 (–26)	240 (–17)	7.8	2.2
6	DTT (mM)	0.5 (–16)	2 (–27)	8 (–27)	9.9	2.8
7	PEG35,000 (% w/v)	4 (–27)	6.5 (–35)	10 (–8)	42.4	11.9
8	dNTPs (μM)	225 (–21)	450 (–12)	900 (–37)	36.3	10.2
9	ATP (mM)	1.25 (–14)	2.5 (–23)	5 (–33)	21.6	6.1
10	CH_3COOK (mM)	20 (–18)	40 (–28)	60 (–24)	6.5	1.8
11	Tris-HCl buffer (pH 8.2) (mM)	15 (–16)	30 (–27)	60 (–27)	8.6	2.4
12	$Mg(CH_3COO)_2$ (mM)	7 (–52)	14 (–14)	28 (–4.0)	142	39.7
13	Primer (μM)	0.24 (–8.1)	0.48 (–41)	0.96 (–21)	62.0	17.4
	Total					100

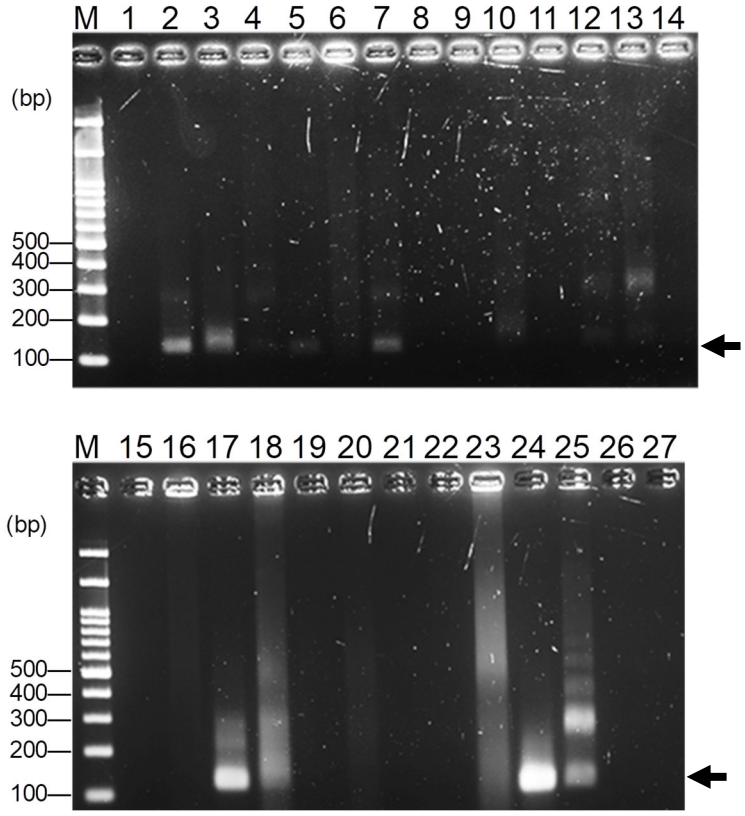

Figure 3-3. Results of 27 reaction conditions of Round 1. M, DNA marker; lane number, experimental number. The pattern of 2.0% agarose gel electrophoresis is shown. The arrow indicates the amplified target band.

Rounds 2 and 3 of optimization of RPA reaction condition

The 13 factors and each three levels in Round 2 are shown in Table 3-5. Based on the results of Round 1 where the $Mg(CH_3COO)_2$ concentrations were set as 7, 14, and 28, for levels 1, 2, and 3, respectively, they were set as 5, 8, and 11 mM in Round 2. The concentrations of PEG35,000, dNTPs, ATP, and primers were also altered. Tris-HCl buffer (pH 8.2) was replaced with phosphocreatine. Twenty-seven RPA reactions were carried out with 6×10^8 copies (2×10^7 copies/μL) of standard DNA and primers in System 1. Results are shown in Table 3-5, indicating that the optimal uvsY, gp32, and ATP concentrations were not level 2 but level 1 (35 ng/μL) for uvsY, level 3 (400 ng/μL) for gp32, and level 1 (3 mM) for ATP concentrations. In addition, the uvsX, uvsY, gp32, and ATP concentrations exhibited relatively high V (21.1, 35.3, 130.4, and 28.6, respectively) and P values (4.2%, 6.9%, 25.7%, and 5.6%, respectively). These results suggested that these concentrations were rate-determining factors.

In the RPA process, the balance of binding and dissociation between uvsX and DNA primer is important. In the presence of ATP, uvsX binds to the DNA primer to form the nucleoprotein with the aid of uvsY. Upon hydrolysis of ATP, uvsX dissociates from DNA primer and is replaced by gp32. Thus, uvsX, uvsY, and ATP shift the balance to the binding, while gp32 shifts it to the dissociation. If this binding affinity is not high enough, the nucleoprotein cannot invade dsDNA, thereby preventing DNA primer from binding to the target sequence. On the other hand, if the binding affinity is too high, uvsX remains occupied even after the elongation starts, preventing another nucleoprotein from binding to the target sequence and starting the elongation. Therefore, it was thought that the binding affinity of the reaction condition with the 13 factors' concentrations of level 2 was a little too high.

Based on the results of Round 2, we attempted to lower the binding affinity by increasing the concentration of gp32 and decreasing the concentrations of uvsY and ATP. Thirteen factors and each three levels in Round 3 were determined (Table 3-6). Twenty-seven RPA reactions were carried out with 6×10^4 copies (2×10^3 copies/μL) of standard DNA and primers using System 1. Results are shown in Table 3-6. Level 2 was optimal for the uvsX and gp32 concentrations. The uvsY concentration exhibited low V (12.6) and P (3.9%) values. These results suggested that the balance between the binding and dissociation of uvsX and DNA primer was adequately adjusted.

Table 3-5. Signal-to-noise ratio for levels 1–3 of each factor and variation (V) and percentage contribution (P) for each factor in RPA in Round 2.

Factor		Level			V	P (%)
		1	2	3		
1	uvsX (ng/μL)	226 (–44)	452 (–50)	904 (–31)	21.1	4.2
2	uvsY (ng/μL)	35 (–54)	70 (–29)	140 (–43)	35.3	6.9
3	gp32 (ng/μL)	100 (–16)	200 (–47)	400 (–63)	130.4	25.7
4	*Bst* DNA pol (units/μL)	0.2 (–41)	0.4 (–35)	0.8 (–50)	13.7	2.7
5	Creatine kinase (ng/μL)	60 (–34)	120 (–54)	240 (–38)	24.7	4.9
6	DTT (mM)	0.5 (–41)	2 (–31)	8 (–54)	28.6	5.6
7	PEG35,000 (% w/v)	5 (–25)	6 (–54)	7 (–47)	49.4	9.7
8	dNTPs (μM)	550 (–50)	650 (–38)	750 (–37)	11.7	2.3
9	ATP (mM)	3.0 (–54)	3.5 (–41)	4.0 (–31)	28.6	5.6
10	CH_3COOK (mM)	20 (–35)	40 (–60)	60 (–31)	54.1	10.7
11	Phosphocreatine (mM)	15 (–35)	30 (–66)	60 (–25)	100.5	19.8
12	$Mg(CH_3COO)_2$ (mM)	5 (–35)	8 (–47)	11 (–44)	9.0	1.8
13	Primer (μM)	0.4 (–41)	0.6 (–44)	0.8 (–41)	0.9	0.2
	Total					100

Table 3-6. Signal-to-noise ratio for levels 1–3 of each factor and variation (V) and percentage contribution (P) for each factor in RPA in Round 3.

Factor		Level			V	P (%)
		1	2	3		
1	uvsX (ng/μL)	226 (–16)	452 (–29)	904 (0)	45.6	13.9
2	uvsY (ng/μL)	20 (–19)	35 (–6.0)	50 (–19)	12.6	3.9
3	gp32 (ng/μL)	300 (–9.5)	450 (–25)	600 (–9.5)	17.9	5.5
4	*Bst* DNA pol (units/μL)	0.2 (0)	0.4 (–16)	0.8 (–29)	45.7	13.9
5	Creatine kinase (ng/μL)	60 (–9.5)	120 (–19)	240 (–16)	5.2	1.6
6	DTT (mM)	0.5 (–9.5)	2 (–19)	8 (–16)	5.2	1.6
7	PEG35,000 (% w/v)	5.5 (–9.5)	6.0 (–19)	6.5 (–16)	5.2	1.6
8	dNTPs (μM)	550 (–25)	650 (–19)	750 (0)	38.2	11.6
9	ATP (mM)	3.0 (–16)	3.5 (–9.5)	4.0 (–19)	5.2	1.6
10	CH_3COOK (mM)	30 (–35)	40 (0)	50 (–9.5)	71.2	21.7
11	Phosphocreatine (mM)	15 (–19)	20 (–16)	25 (–9.5)	5.2	1.6
12	$Mg(CH_3COO)_2$ (mM)	5 (0)	8 (–25)	11 (–19)	38.2	11.6
13	Primer (μM)	0.4 (–9.5)	0.6 (–6.0)	0.8 (–29)	32.9	10.0
	Total					100

Performance of the optimized reaction condition

We examined the sensitivities of the optimized RPA and reverse transcription-RPA (RT-RPA) conditions. Using System 2, RPA was carried out with 60−6 × 10^7 copies of standard DNA, and RT-RPA was carried out with 60−6 × 10^7 copies of standard RNA, both at 41ºC for 1 h. In the analysis of the RPA or RT-RPA products in the subsequent electrophoresis, the optimized conditions detected 60 copies of standard DNA (Fig. 3-4 A) or RNA (Fig. 3-4 B).

Finally, we compared the sensitivities of RPA before and after optimization. Using System 2, RPA was carried out with 60−6 × 10^7 copies of standard DNA (Fig. 3-5). The condition after optimization detected 60 copies of standard DNA while that before optimization did not detect 600 copies. These results indicated that by optimizing the reaction conditions for three enzymes, 100 to 1,000-fold higher sensitivity was achieved.

Generally, the performance of a NA amplification test depends largely on the performance of the enzymes involved. Indeed, DNA polymerases and reverse transcriptases whose activity and/or stability have been improved by genetic engineering techniques are currently used in PCR and RT-PCR [85, 86]. However, such improvement has not been done for Rec and SSB. It is worth mentioning that the optimal concentrations of uvsX, uvsY, and gp32 in the RPA reaction solution fall within the range of 1–10 μM, which is 1,000 times higher than the concentrations typically used for reverse transcriptase and thermostable DNA polymerase in cDNA synthesis and PCR. Such high protein concentration makes RPA reagents less flexible in fabrication. To solve this problem, an increase in activity and/or binding ability of Rec and SSB is required. On the other hand, considering the field use of RPA, it is anticipated that storage of the reagents at room temperature is possible. To address this issue, the use of thermostable Rec and

SSB from thermophilic organisms might be useful.

In PCR, various additives that increase the reaction efficiency have been reported: bovine serum albumin, trehalose, sorbitol, glycerol, Triton X-100, and Tween 20 are used as enzyme stabilizers, and DMSO, formamide, and ammonium sulfate increase specificity [75, 78]. Helicase increases specificity by decreasing non-specific binding [87]. Spermidine suppresses reaction inhibition problems encountered while analyzing clinical stool samples [88, 89]. In RPA, little is known about such additives except for the recent report that betaine increases specificity [90]. Our results in this study might make the evaluation of the effects of various additives on the RPA reaction efficiency easier.

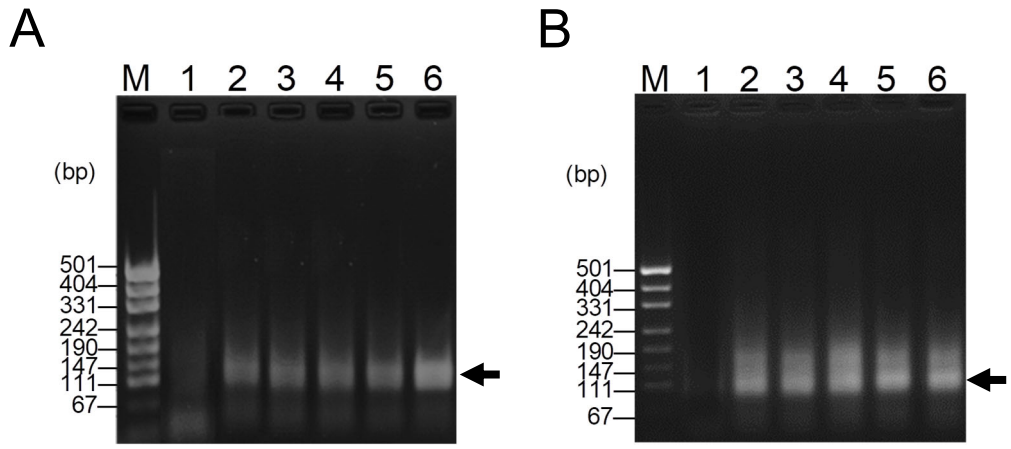

Figure 3-4. Comparison of the sensitivities of RPA and RT-RPA. (A) RPA. (B) RT-RPA. The reactions (30 μL) were carried out with 400 ng/μL uvsX, 40 ng/μL uvsY, 400 ng/μL gp32, 0.4 units/μL *Bst* DNA polymerase, 120 ng/μL creatine kinase, 2 mM DTT, 6% w/v PEG35,000, 3.5 mM ATP, dNTPs (650 μM each), 3.5 mM ATP, 50 mM Tris-HCl buffer (pH 8.6), 40 mM CH_3COOK, 20 mM phosphocreatine, 8 mM $Mg(CH_3COO)_2$, 1 μM 2F-15 primer, and 1 μM 2R-11 primer in the absence (A) or presence (B) of 100 nM MMLV reverse transcriptase, at 41ºC for 30 min. Initial copies of standard DNA (A) and RNA (B): 0 (lane 1), 60 (lane 2), 600 (lane 3), 6×10^3 (lane 4), 6×10^5 (lane 5), and 6×10^7 (lane 6). The arrow indicates the amplified target band.

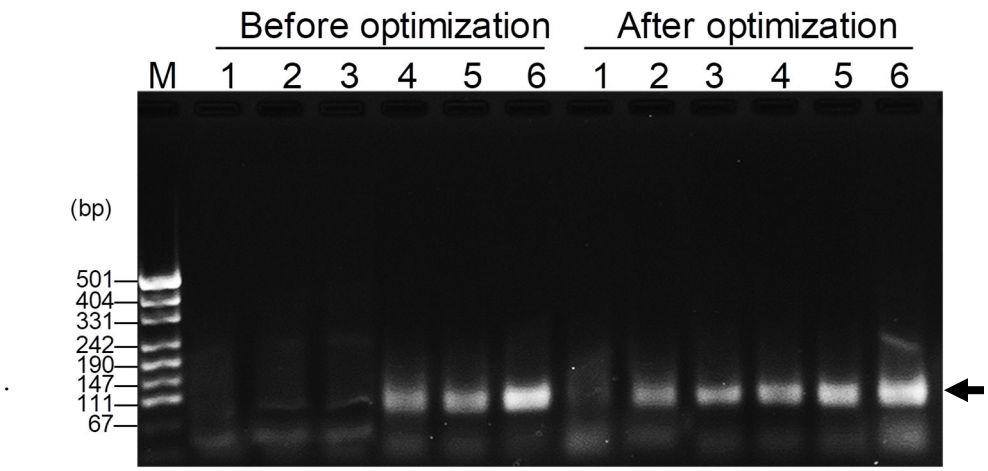

Figure 3-5. Comparison of the sensitivities of RPA before and after optimization. The reactions (30 μL) were carried out at 41ºC for 30 min. The reaction condition after optimization is 400 ng/μL uvsX, 40 ng/μL uvsY, 400 ng/μL gp32, 0.4 units/μL *Bst* DNA polymerase, 120 ng/μL creatine kinase, 2 mM DTT, 6% w/v PEG35,000, dNTPs (650 μM each), 3.5 mM ATP, 50 mM Tris-HCl buffer (pH 8.6), 40 mM CH_3COOK, 20 mM phosphocreatine, 8 mM $Mg(CH_3COO)_2$, 1 μM 2F-15 primer, and 1 μM 2R-11 primer. The reaction condition before optimization is 452 ng/μL uvsX, 70 ng/μL uvsY, 200 ng/μL gp32, 0.4 units/μL *Bst* DNA polymerase, 120 ng/μL creatine kinase, 2 mM DTT, 6.5% w/v PEG35,000, 2.5 mM ATP, dNTPs (450 μM each), 50 mM Tris-HCl buffer (pH 8.6), 40 mM CH_3COOK, 30 mM phosphocreatine, 14 mM $Mg(CH_3COO)_2$, 0.48 μM 2F-15 primer, and 0.48 μM 2R-11 primer. Initial copies of standard DNA: 0 (lane 1), 60 (lane 2), 600 (lane 3), 6×10^3 (lane 4), 6×10^5 (lane 5), and 6×10^7 (lane 6). The arrow indicates the amplified target band.

Insights into the effect of the balance between the binding and dissociation of uvsX and DNA primer on the RPA reaction efficiency

As described above, Round 2 revealed that the reaction efficiency of RPA depends on the balance of the binding and dissociation between uvsX and DNA primer. To understand this issue further, we examined the effects of the concentrations of uvsX, uvsY, gp32, and ATP on RPA efficiency. The optimized conditions obtained by Round 4 were used as standard conditions. Figure 3-6 shows the analysis of the RPA products at 30 min using agarose gel electrophoresis. An amplified DNA band was observed at 400–4,000 ng/μL uvsX, 40–400 ng/μL uvsY, 400 ng/μL gp32, and 0.35–3.5 mM ATP, while it was not observed at 40 and 120 ng/μL uvsX, 4 and 12 ng/μL uvsY, 40, 120, 1,200, and 4,000 ng/μL gp32, or 10 and 35 mM ATP. These results indicated that the optimal concentration of gp32 is narrower than that of uvsX, uvsY, and ATP, suggesting that the gp32 concentration is critical for the reaction efficiency of RPA.

It is known that uvsX, uvsY, and gp32 form a ternary complex with a ssDNA [91]. The crystal structure analysis of the uvsY-ssDNA complex reported that uvsY exists as a heptamer. The provided model showed that uvsY promotes a helical ssDNA conformation that disfavors the binding of gp32 and initiates the assembly of the ssDNA-uvsX filament [92]. We presumed that this model might be applicable to the mechanism of RPA reaction.

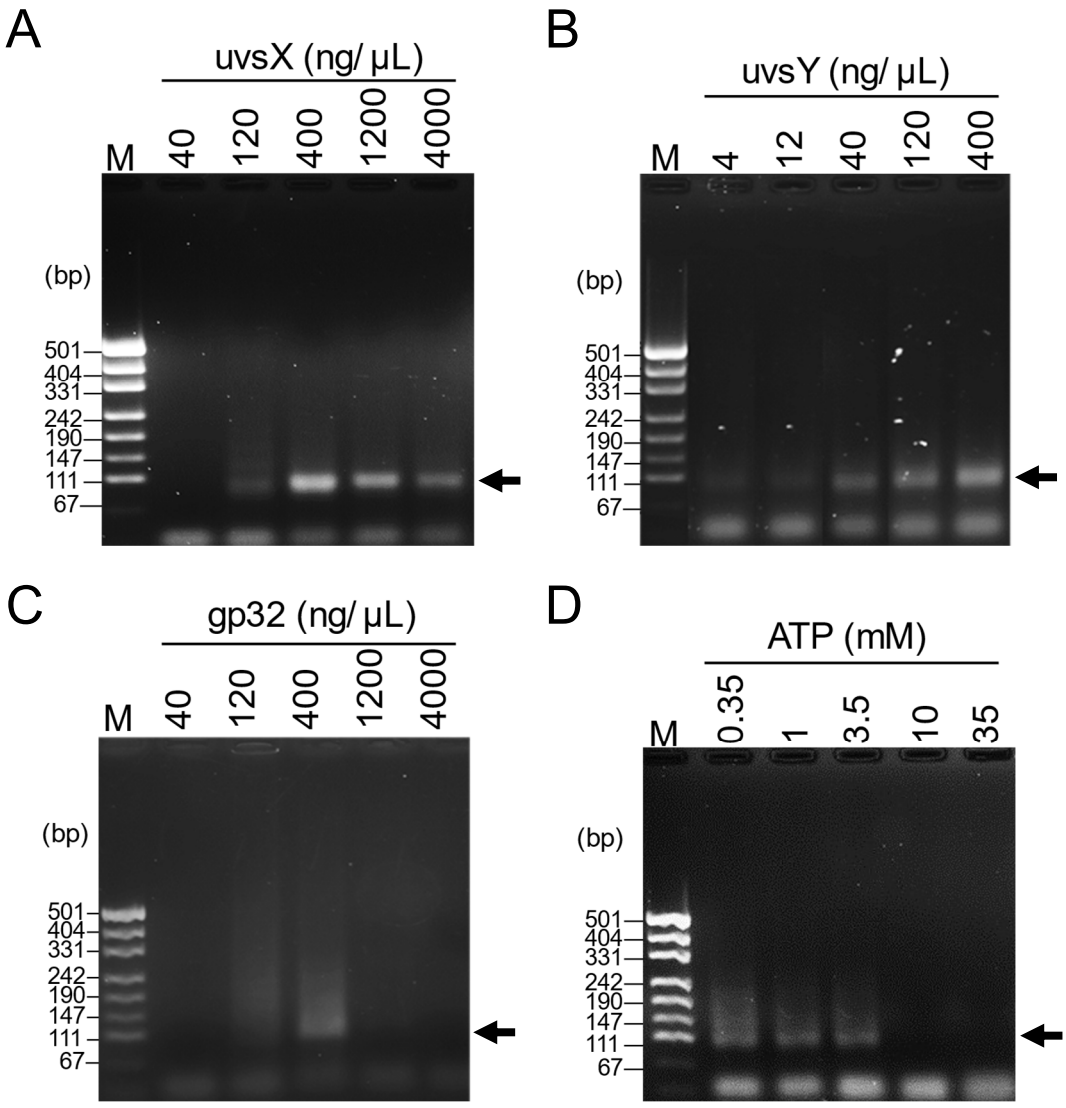

Figure 3-6. Effects of uvsX, uvsY, gp32, and ATP concentrations on RPA reaction efficiency. (A–D) The reactions (30 µL) were carried out with 40–4,000 (A) or 400 (B–D) ng/µL uvsX, 4–400 (B) or 40 (A, C, D) ng/µL uvsY, 40–4,000 (C) or 400 (A, B, D) ng/µL gp32, 0.4 units/µL *Bst* DNA polymerase, 120 ng/µL creatine kinase, 2 mM DTT, 6% w/v PEG35,000, 0.35–35 (D) or 3.5 (A–C) mM ATP, dNTPs (650 µM each), 50 mM Tris-HCl buffer (pH 8.6), 40 mM CH_3COOK, 20 mM phosphocreatine, 8 mM $Mg(CH_3COO)_2$, 1 µM 2F-15 primer, and 1 µM 2R-11 primer at 41ºC for 30 min. Initial copies of standard DNA were 6,000. The arrow indicates the amplified target band.

Conclusion

We used the Taguchi statistical method to optimize the RPA reaction conditions for the detection of SARS-CoV-2 DNA and RNA. Based on percentage contribution from Taguchi statistical analysis, uvsY, gp32, and ATP concentrations were identified as critical factors influencing the reaction rate. By applying the optimized conditions, we successfully detected as low as 60 copies of DNA and RNA, demonstrating a remarkable 1,000-fold increase in sensitivity. We hope that the Taguchi method will be employed to save valuable resources.

Chapter 4

Modified uvsY by N-terminal hexahistidine tag addition enhances efficiency of recombinase polymerase amplification*

Introduction

As described in the general introduction, RPA amplifies a specific DNA sequence at a constant temperature (37–42ºC) using Rec, SSB, and Pol [14–17]. In RPA, Rec binds to the primers to form a recombinase-primer complex. The complex scans and binds to the homologous target DNA sequence. Pol extends the primers while SSB binds to the unwound strand. By incorporating forward and reverse primers, the target sequence is amplified exponentially. Unlike PCR, RPA does not require specialized equipment such as a thermal cycler. This characteristic has made RPA particularly valuable for point-of-care applications as reported in many published papers. RPA is particularly useful for detecting pathogenic organisms and can be adapted to detect RNA, including the RNA of viruses like SARS-CoV-2, by incorporating a reverse transcriptase enzyme into the reaction [93–95]. In Chapter 2, we prepared recombinant uvsX, uvsY, and gp32 through an *E. coli* expression system and used them to examine the effects of reaction components and additives on RPA reaction efficiency [76]. In Chapter 3, we employed Taguchi

---

*The content described in this Chapter was originally published in *Molecular Biology Reports.* Kevin Maafu Juma, Teisuke Takita, Masaya Yamagata, Mika Ishitani, Kaichi Hayashi, Kenji Kojima, Koichiro Suzuki, Yuri Ando, Wakao Fukuda, Shinsuke Fujiwara, Yukiko Nakura, Itaru Yanagihara, and Kiyoshi Yasukawa (2022). Modified uvsY by N-terminal hexahistidine tag addition enhances efficiency of recombinase polymerase amplification to detect SARS-CoV-2 DNA. *Mol. Biol. Rep*., **49**, 2847–2856.

statistical method to optimize the reaction conditions for the detection of SARS-CoV-2 DNA and RNA [94]. In the two studies, uvsX, uvsY, and gp32 were expressed as N- and C-terminal $(His)_6$-tagged proteins with a thrombin recognition site. Purification was accomplished by ammonium sulfate fractionation and Ni^{2+} affinity column chromatography.

As reported in Chapter 2, upon treatment with thrombin to cleave the $(His)_6$ tag, uvsY exhibited insolubility, while uvsX and gp32 remained soluble. Therefore, we used untagged uvsX and gp32 and N- and C-terminal $(His)_6$-tagged uvsY to optimize reaction conditions using Taguchi statistical method in Chapter 3. However, the uncleaved $(His)_6$ tag may have a negative effect on RPA reaction efficiency. The $(His)_6$ tag inclusion has been reported to reduce protein solubility [96].

In this Chapter, we examined the effects of N- and C-terminal $(His)_6$ tags on uvsY's functionality in RPA, using SARS-CoV-2 DNA as a model target.

Materials and methods

Materials

UvsX and gp32 were expressed and purified as described in Chapter 2.

Construction of plasmids

Construction of pET-uvsY-NChis, previously termed pET-uvsY-2, was as described in Chapter 2. For the construction of pET-uvsY-NChis-2 (Fig. 4-1), the DNA fragment was amplified from pET-uvsY-NChis using primers UvsY-N-thrombin-del-F and UvsY-N-thrombin-del-R (Table 4-1) using 0.5 U of KOD-Plus-Neo (Toyobo) with 35 cycles at 98ºC for 10 s and 68ºC for 5 min. The amplified fragment was phosphorylated at its 5’

terminus with T7 polynucleotide kinase and self-ligated. For the construction of pET-uvsY-Nhis, the DNA fragment was amplified from pET-uvsY-NChis-2 using primers UvsY-N-His-only-F and UvsY-N-His-only-R (Table 4-1) using 0.5 U of KOD-Plus-Neo with 35 cycles at 98ºC for 10 s and 68ºC for 5 min. The amplified fragments were purified using MagExtractor PCR & Gel Clean up (Toyobo) and phosphorylated at its 5' terminus using T7 polynucleotide kinase (Toyobo) and self-ligated using a DNA ligation kit (Takara Bio).

For the construction of pET-uvsY-Chis, the 168-bp DNA fragment corresponding to 161–328 of pET-22b(+) (Merck Millipore) was inserted into the *Xba*I and *Xho*I sites of pET-28a(+) (Merck Millipore). To the *Nde*I and *Xho*I sites of the resulting plasmid, the *Nde*I- and *Xho*I-digested 411-bp uvsY DNA fragment of pET-uvsY-1 (Fig. 4-1), corresponding to DNA sequence 114,929–115,339 deposited in GenBank (KJ477686.1), was inserted. For the construction of pET-uvsY-Δhis, the DNA fragment was amplified from pET-uvsY-Chis using primers UvsY-N-His-only-F and UvsY-N-His-only-R with 35 cycles at 98ºC for 10 s and 68ºC for 5 min. The amplified fragment was phosphorylated and self-ligated.

Table 4-1. Primers used in PCR.

Primers	Sequences (5′→3′)
UvsY-N-thrombin-del-F	GGCAGCCATATGATGAGATTAGAAGATC
UvsY-N-thrombin-del-R	GTGATGATGATGATGATGGCTGCTG
UvsY-N-His-only-F	TGAGATCCGGCTGCTAACAAAGC
UvsY-N-His-only-R	TTTTCCAGCCTCAAATGCTCG

Expression of uvsY

Each of the four plasmids was transfected into *E. coli* BL21(DE3). The overnight culture of the transformants (30 mL) was added to 300 mL of L broth containing 50 μg/mL kanamycin and incubated with shaking at 37ºC. When OD_{660} reached 0.6–0.8, the culture (300 mL) was added to 2,000 mL of L broth containing 50 μg/mL kanamycin, and 2.0 mL of 0.5 M IPTG was added. Growth was continued at 30ºC for 4 h. The cells were harvested by the centrifugation of the culture at 3,000 × *g* for 10 min and suspended with 50 mL of 50 mM phosphate buffer (pH 7.2), 1 M NaCl, 2 mM PMSF, and disrupted by sonication. After centrifugation at 20,000 × *g* for 20 min, the supernatant was collected as the soluble fraction of the cells.

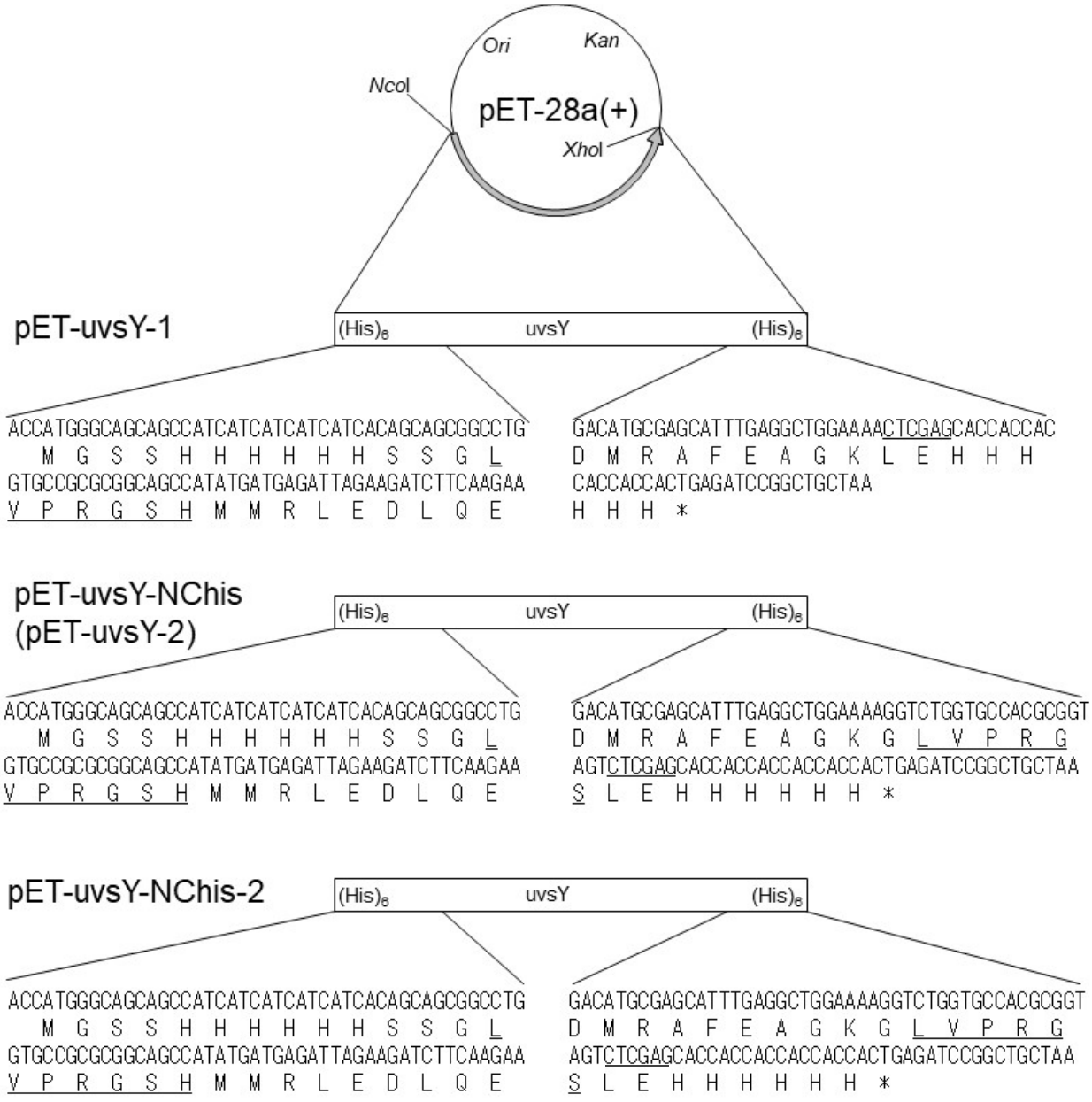

Figure 4-1. Expression plasmids. The structures of pET-uvsY-1, pET-uvsY-NChis (pET-uvsY-2), and pET-uvsY-NChis-2 are shown. The asterisk indicates the termination codon. *Xho*I site and thrombin recognition sequence are underlined.

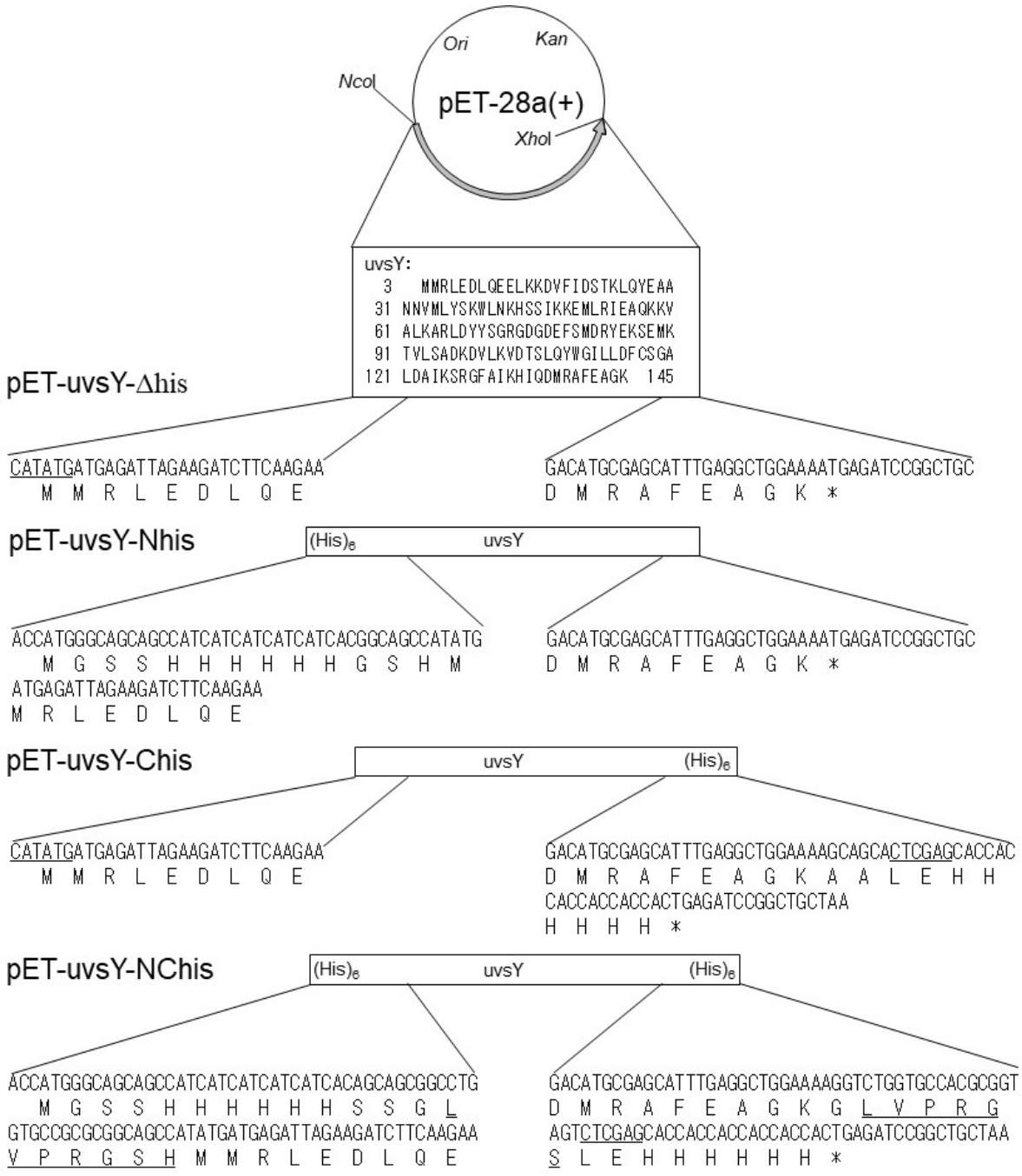

Figure 4-2. Expression plasmids. The asterisk indicates the termination codon. The thrombin recognition sequence and *Nde*I and *Xho*I sites are underlined.

Purification of uvsY-Δhis

Solid $(NH_4)_2SO_4$ was added to the soluble fraction of the cells to a final concentration of 30% saturation. Following the centrifugation at 20,000 × *g* for 20 min, the supernatant was collected and adjusted to a final concentration of 80% saturation. Following the centrifugation, the pellet was collected and dissolved in 100 mL of buffer A (50 mM Tris-HCl buffer (pH 8.0), 1 mM DTT) and applied to the column packed with Toyopearl DEAE-650M (Tosoh) equilibrated with buffer A. After washing with buffer A, the bound uvsY-Δhis was eluted with each 20 mL of buffer A containing 100, 200, and 300 mM NaCl. Each fraction (5 mL) was assessed for the presence of uvsY-Δhis by SDS-PAGE. The active fractions were collected, concentrated to 1 mL in 10 mM Tris-HCl buffer (pH 8.0) by Amicon Ultra-15 MWCO 10 k (Merck Millipore), and stored in 10 mM Tris-HCl buffer (pH 8.0), 20% v/v glycerol at –30ºC. The uvsY-Δhis concentration was determined as described in Chapter 2.

Purification of uvsY-Nhis, uvsY-Chis, and uvsY-NChis

Solid $(NH_4)_2SO_4$ was added to the soluble fraction of the cells to a final concentration of 40% saturation. In uvsY-NChis, following the centrifugation, the pellet was dissolved in 50 mL of buffer B (50 mM phosphate buffer (pH 7.2), 500 mM NaCl). In uvsY-Nhis and uvsY-Chis, following the centrifugation, the supernatant was collected and adjusted to a final concentration of 60% and 80% saturation, respectively. Following the centrifugation, the pellet was dissolved in 50 mL of buffer B. The solution was applied to a Profinity IMAC Ni-charged resin column (5 mL, Bio-Rad, Hercules, CA) equilibrated with buffer B. After washing with 100 mL of buffer B containing 100 mM imidazole, the bound enzyme was eluted with 300 mL of buffer B containing 600 mM

imidazole. The active fractions were collected and concentrated as described above. The uvsY concentration was determined by the method of Bradford as described above.

***Solubility tes*t**

UvsY (0.2 μg/mL in 50 mM Tris-HCl buffer (pH 8.6)) was incubated at 42ºC for a specified time (10–60 min) followed by the centrifugation at 15,000 × *g* for 10 min. The absorbance at 280 nm of the supernatant was measured with a Jasco spectrophotometer model V-550 (Japan Spectroscopic Company, Tokyo, Japan).

RPA reaction

The RPA detection system for SARS-CoV-2 DNA as described in Chapter 3 was used [94]. Unless otherwise indicated, the reaction condition was 400 ng/μL uvsX, 40 ng/μL uvsY, 400 ng/μL gp32, 0.4 units/μL *Bst* DNA polymerase, 120 ng/μL creatine kinase, 2 mM DTT, 6% w/v PEG35,000, 3.5 mM ATP, dNTPs (650 μM each), 50 mM Tris-HCl buffer (pH 8.6), 40 mM CH_3COOK, 20 mM phosphocreatine, 8 mM $Mg(CH_3COO)_2$, 1 μM 2F-15 primer, 1 μM 2R-11 primer at 41ºC for 30 min. The reaction was performed in a 0.2 mL PCR tube in PCR Thermal Cycler Dice (Takara Bio). The amplified products were separated on 2.0% agarose gels and stained with ethidium bromide (1 μg/mL).

Results

Design and preparation of recombinant uvsY with or without $(His)_6$ tag

The $(His)_6$ tag is known to facilitate the purification of recombinant proteins. However, it sometimes decreases the solubility and activity of proteins [96]. In Chapters 2 and 3, we expressed recombinant uvsX, uvsY, and gp32 as N- and C-terminal $(His)_6$-tagged proteins with a thrombin recognition site. In uvsX and gp32, the tags were removed by thrombin-treatment. Meanwhile, thrombin-treatment of the N- and C-terminal $(His)_6$-tagged uvsY (uvsY-NChis) resulted in precipitation. Fortunately, untreated uvsY-NChis was functional in the RPA reaction [81], indicating that the $(His)_6$ tag of uvsY does not abolish its function in RPA. However, the uncleaved $(His)_6$ tag may decrease the function of uvsY. To address this issue, we designed three new forms of uvsY, i.e., untagged uvsY (uvsY-Δhis), N-terminal $(His)_6$-tagged uvsY (uvsY-Nhis), and C-terminal $(His)_6$-tagged uvsY (uvsY-Chis). Figure 4-2 shows the *E. coli* expression plasmids for these three uvsYs and uvsY-NChis. These four genes were expressed in *E. coli* BL21(DE3) cells.

Purification was as described in Chapter 2 but with several modifications. First, polyethyleneimine treatment of the soluble fraction of the cells, which was originally included to remove NAs, was excluded. This prevented the viscosity of the solution from becoming so high that the flow rate of the successive Ni^{2+} affinity column chromatography was reduced. Second, ammonium sulfate fractionation was used instead. The ammonium sulfate concentrations at which uvsY-Δhis, uvsY-Nhis, uvsY-Chis, and uvsY-NChis precipitated were 80%, 60%, 80%, and 40% saturation, respectively, indicating that the uvsY-NChis was the least soluble. To obtain highly purified uvsY that could be used in RPA reaction, Ni^{2+} affinity chromatography was used for uvsY with

$(His)_6$ tag (uvsY-Nhis, uvsY-Chis, and uvsY-NChis), while anion exchange column chromatography was used for uvsY without $(His)_6$ tag (uvsY-Δhis). From a 2 L culture, 25, 11, 11, and 9 mg of uvsY-Δhis, uvsY-Nhis, uvsY-Chis, and uvsY-NChis, respectively, were obtained.

Figure 4-3 and 4-4 shows the results of the SDS-PAGE analysis of the active fractions of the purified enzyme preparations. The purified uvsY-Δhis, uvsY-Nhis, uvsY-Chis, and uvsY-NChis preparations yielded single bands with molecular masses of 16, 17, 17, and 22 kDa, respectively. The molecular masses of these uvsYs calculated from the amino acid sequences were 15,952, 17,419, 17,159, and 19,847 Da, respectively (Fig. 4-3), indicating that the two molecular masses were considerably different for uvsY-NChis, but were almost similar for uvsY-Δhis, uvsY-Nhis, and uvsY-Chis. These results suggested that when both the N- and C-terminal $(His)_6$ tags were present, the structure of uvsY was considerably altered.

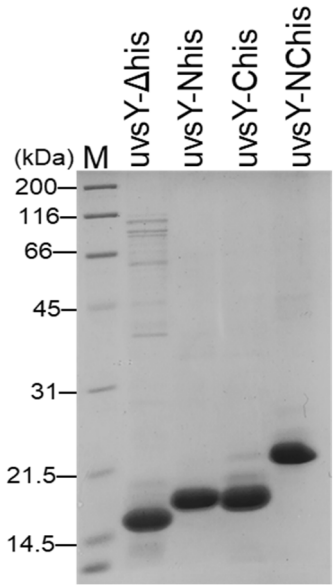

Figure 4-3. Purified uvsY preparations. SDS-PAGE was conducted under reducing conditions. Coomassie Brilliant Blue-stained 12.5% SDS-polyacrylamide gel is shown. Marker proteins (M).

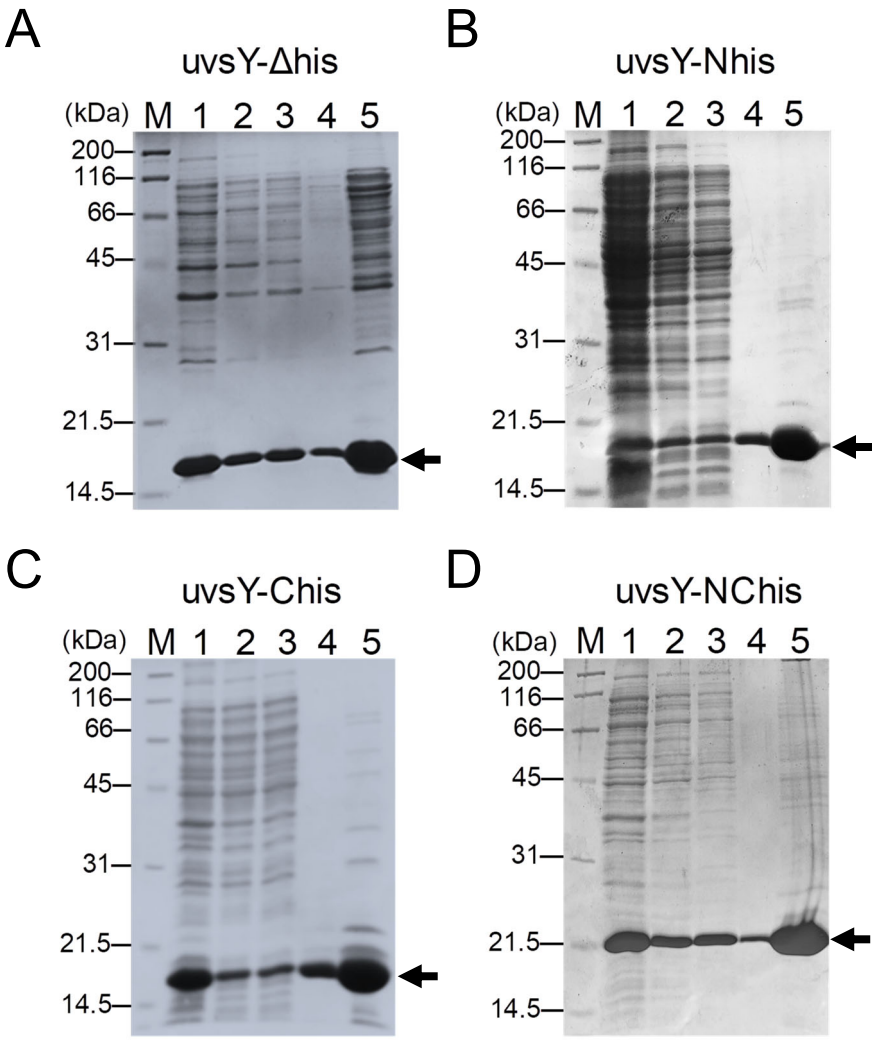

Figure 4-4. Purification of uvsY. SDS-PAGE was conducted under reducing conditions. Coomassie Brilliant Blue-stained 12.5% SDS-polyacrylamide gels are shown. Marker proteins (M), total cell extracts (lane 1), soluble fractions of the total cell extracts (lane 2), the centrifuged pellets after fractionation by ammonium sulfate (lane 3), active fractions of anion-exchange chromatography for uvsY-Δhis (A) and Ni^{2+} affinity chromatography for uvsY-Nhis (B), uvsY-Chis (C), and uvsY-NChis (D) (lane 4), and purified preparations after membrane concentration (lane 5). The arrow indicates the band corresponding to uvsY-Δhis, uvsY-Nhis, uvsY-Chis, and uvsY-NChis.

Comparison of the solubility of uvsY with or without $(His)_6$ tag

The remaining soluble protein concentration was determined after thermal treatment at 42ºC. The natural logarithm of the soluble fraction was plotted against the incubation time (Fig. 4-5). The soluble fraction of uvsY-Δhis was stable. The soluble fraction of uvsY-Nhis decreased to 15% at 60 min. The soluble fractions of uvsY-Chis and uvsY-NChis decreased more rapidly than did uvsY-Nhis, and decreased to less than 5% at 60 min. These results indicated that the solubility was in the order of uvsY-Δhis > uvsY-Nhis > uvsY-Chis ≈ uvsY-NChis, suggesting that the presence of $(His)_6$ tag, especially the C-terminal $(His)_6$ tag, reduced the solubility of uvsY.

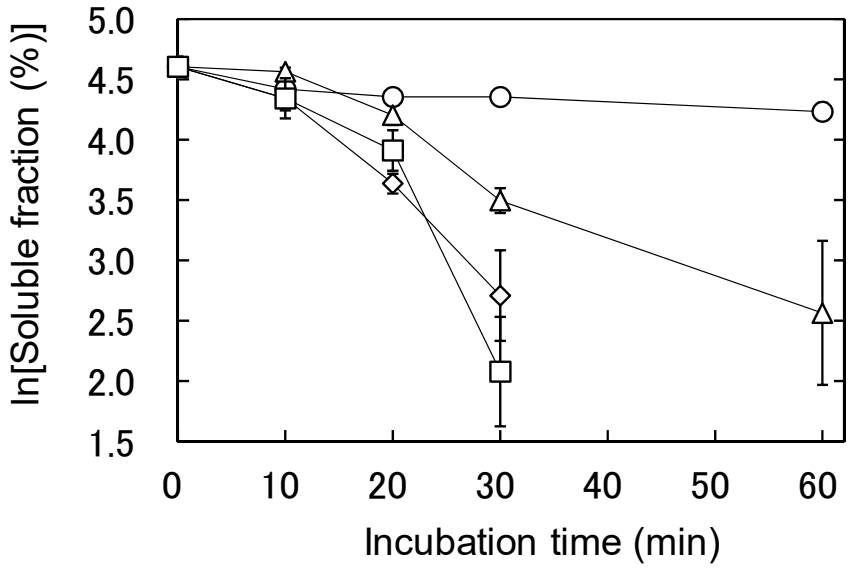

Figure 4-5. Effects of thermal incubation on the solubility of uvsY. UvsY-Δhis (open circle), uvsY-Nhis (open triangle), uvsY-Chis (open square), or uvsY-NChis (open diamond) each at 0.2 μg/mL was incubated at 42ºC for the indicated durations. Then, the soluble uvsY concentration was determined. The soluble fraction was defined as the ratio of the concentration of soluble uvsY with incubation for the indicated durations to that without incubation. Error bars indicate SD values. The average of triplicate determination is shown.

Comparison of the optimal concentration of uvsY with or without $(His)_6$ tag in RPA

The effect of each uvsY concentration on the RPA reaction efficiency was examined using the detection system of SARS-CoV-2 DNA established in Chapter 3. Figure 4-6 shows the analysis of the products in the RPA reaction with each uvsY using agarose gel electrophoresis. The uvsY concentrations at which amplified DNA band was observed were 10–20 ng/μL for uvsY-Δhis, 10–40 ng/μL for uvsY-Nhis, 10–100 ng/μL for uvsY-Chis, and 40–100 ng/μL for uvsY-NChis. Non-specific bands were observed at 10–100 ng/μL uvsY-Δhis.

In Chapter 3, we reported that uvsY concentrations that are too low or excessive are detrimental to the reaction [94]. These findings were also evident for uvsX, gp32, and ATP [94]. Thus, our results suggested that the specific activity of uvsY-Nhis was higher than those of the other three uvsYs. We set 20, 20, 80, and 60 ng/μL as the optimal concentrations of uvsY-Δhis, uvsY-Nhis, uvsY-Chis, and uvsY-NChis, respectively, and conducted the subsequent experiments.

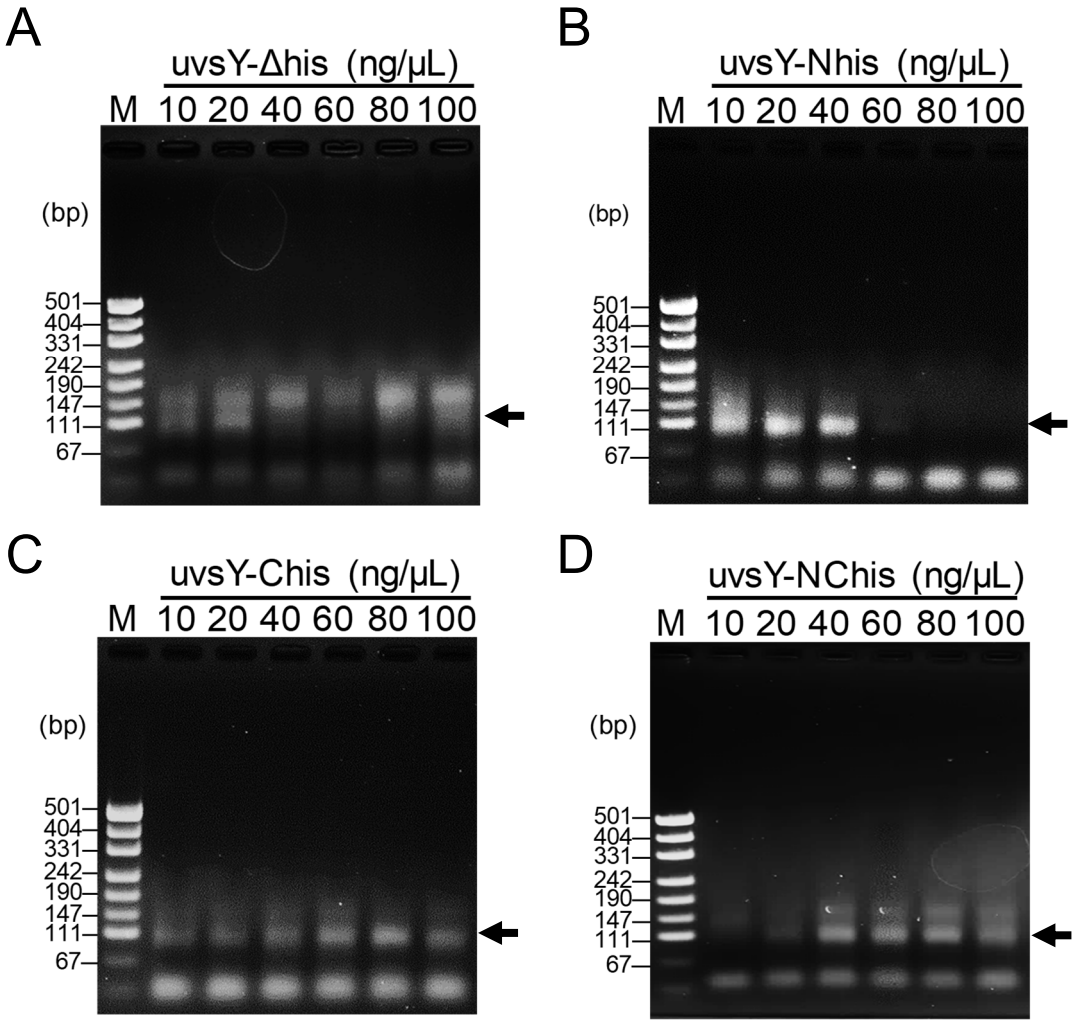

Figure 4-6. Effects of the concentrations of uvsY on RPA reaction efficiency. The reactions were carried out with 10, 20, 40, 60, 80, and 100 ng/μL uvsY-Δhis (A), uvsY-Nhis (B), uvsY-Chis (C), or uvsY-NChis (D) at 41ºC for 30 min. Initial copies of standard DNA were 6,000. The arrow indicates the amplified target band.

Comparison of sensitivity and speed of RPA reaction using uvsY with or without $(His)_6$ tag

For comparison of sensitivity, RPA reaction was carried out using each uvsY with 60−6×10^7 copies of standard DNA at 41ºC for 30 min. In the analysis of the products in the subsequent electrophoresis, the minimal initial copy numbers of standard DNA from which the amplified products were observed were 6×10^5, 60, 600, and 600 copies for the RPA with uvsY-Δhis, uvsY-Nhis, uvsY-Chis, and uvsY-NChis, respectively (Fig. 4-7). Several non-specific bands were observed at 0−6×10^3 copies for the RPA with uvsY-Δhis (lanes 1−4 in Fig. 4-7 A). This might be due to the fact that uvsY-Δhis was less functional as the loading factor because Ni^{2+} affinity chromatography cannot be used for its purification, and the uvsY-Δhis preparation contained more impurities, than other three uvsY preparations.

For comparison of speed, the RPA reaction was carried out using each uvsY with 6,000 copies of standard DNA at 41ºC for 10−60 min. The minimal reaction time at which the amplified products were observed were 20, 20, 30, and 20 min for the RPA with uvsY-Δhis, uvsY-Nhis, uvsY-Chis, and uvsY-NChis, respectively (Fig. 4-8). More importantly, the RPA with uvsY-Nhis exhibited clearer bands than that with either of other three uvsYs. The results have revealed that the reaction efficiency of RPA with N-terminal tagged uvsY (uvsY-Nhis), was highest while that with untagged uvsY (uvsY-Δhis) was the lowest.

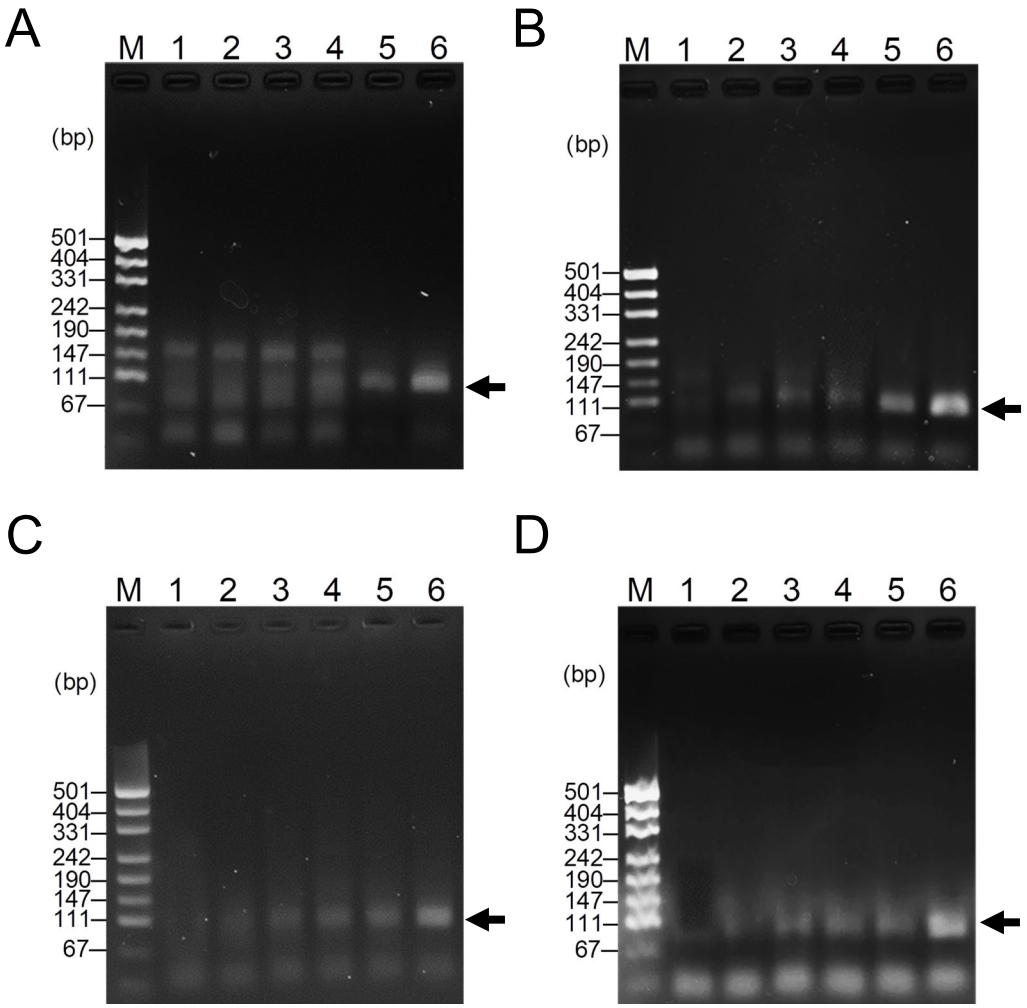

Figure 4-7. Effects of initial copies on the RPA reaction. The reactions were carried out with 20 ng/μL uvsY-Δhis (A), 20 ng/μL uvsY-Nhis (B), 80 ng/μL uvsY-Chis (C), or 60 ng/μL uvsY-NChis (D) at 41ºC for 30 min. Initial copies of standard DNA: 0 (lane 1), 60 (lane 2), 600 (lane 3), 6×10^3 (lane 4), 6×10^5 (lane 5), and 6×10^7 (lane 6). The arrow indicates the amplified target band.

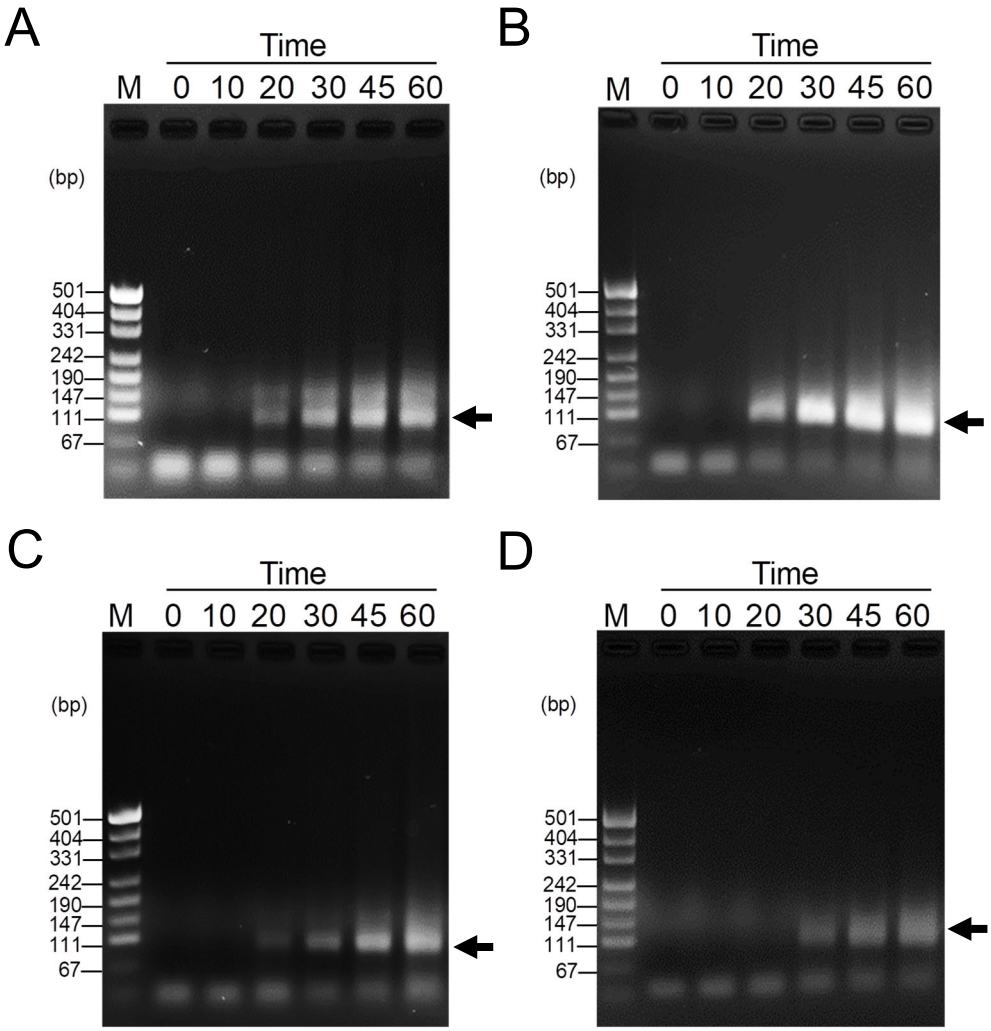

Figure 4-8. Effects of reaction time on RPA reaction efficiency. The reactions were carried out with 20 ng/μL uvsY-Δhis (A), 20 ng/μL uvsY-Nhis (B), 80 ng/μL uvsY-Chis (C), or 60 ng/μL uvsY-NChis (D) at 41ºC for 0–60 min. Initial copies of standard DNA was 6,000. The arrow indicates the amplified target band.

Discussion

It was first reported by gel-shift assay that uvsX, uvsY, and gp32 form a ternary complex with ssDNA [91]. The presence of the ternary complex was also observed using surface plasmon resonance and isothermal titration calorimetry [92]. However, the binding of uvsY to ssDNA lessens the subsequent binding of the ssDNA to gp32 [92]. Thus, uvsY and gp32 bind to ssDNA competitively. In the RPA process, this competition should be adjusted to achieve a high reaction efficiency by optimizing the concentrations of uvsX, uvsY, gp32, and ATP. If the binding of uvsY to DNA primer is not strong enough, the binding of uvsX to DNA primer will also not be strong enough. Thus, the DNA primer cannot invade dsDNA, preventing it from binding to the target sequence. In contrast, if the binding of uvsY to DNA primer is too strong, the binding of uvsX to the DNA primer will also be too strong, and uvsX will remain occupied even after the elongation starts. This will prevent another nucleoprotein from binding to the target sequence and initiating elongation.

The first crystallographic analysis of uvsY reported that uvsY exists as a hexamer [97]. A more recent crystallographic analysis revealed that it exists as a heptamer and that one uvsY molecule consists of four α-helices (H1–H4: H1, E5–Y14; H2, L21–S65; H3, K80–S88; and H4, K91–E134) [92]. When viewed from the top of the heptamer, H4 is located inside, whereas H1, H2, and H3 are located outside. In one heptamer, seven N-terminal residues are located apart from each other and seven C-terminal residues are located close together. In this study, the presence of a C-terminal $(His)_6$ tag of uvsY reduced its function in RPA (Figs. 4-6, 4-7, and 4-8). In Chapter 2, we reported that cleavage of the $(His)_6$ tag by thrombin rendered uvsY-NChis insoluble [81]. These results might be explained as follows. In the heptameric assembly, C-terminal peptides

containing $(His)_6$ tag and thrombin recognition sequence in close proximity to each other alter the uvsY structure unfavorably, leading to decreased activity and precipitation by thrombin-treatment. The results of solubility test that uvsY-Δhis exhibited higher solubility than the other three uvsYs (Fig. 4-5) supports this hypothesis. As for its low activity (Figs. 4-6, 4-7, and 4-8), we presumed that the preparation contained some impurities, such as NA, that inhibited the RPA reaction. Such impurities can be removed using Ni^{2+} affinity chromatography.

Conclusion

We prepared four forms of uvsY: untagged uvsY (uvsY-Δhis), N-terminal tagged uvsY (uvsY-Nhis), C-terminal tagged uvsY (uvsY-Chis), and N- and C-terminal tagged uvsY (uvsY-NChis) and assessed their performance in the RPA reaction. RPA with uvsY-Nhis demonstrated superior reaction efficiency compared to uvsY-Δhis, uvsY-Chis, and uvsY-NChis. These findings demonstrated that the inclusion of $(His)_6$ tag might enhance the performance of proteins. However, it is essential to assess each protein individually to determine the specific impact of the $(His)_6$ tag on its performance.

Chapter 5

Recombinase polymerase amplification using novel thermostable strand-displacing DNA polymerases from *Aeribacillus pallidus* and *Geobacillus zalihae*

Introduction

Instead of using high temperature to achieve the denaturation of the dsDNA target for amplification, RPA technique is performed at a constant temperature of around 41ºC, using Rec enzyme to form a complex with ssDNA primer. The complex then searches for homologous sequence on the dsDNA target and binds to the target sequence. The unwound strand is stabilized by SSB. The primers are extended by Pol activity resulting in accumulation of amplicons consisting of the sequence between forward and reverse primers [14–17]. Unlike PCR, RPA does not require a thermal cycler, making it potentially suitable for on-site detection. By integrating the amplification reaction with DNA extraction and amplified product detection techniques, RPA holds promise for the rapid and convenient identification of various pathogens. Since the first report in 2006 [14], the T4 phage Rec, uvsX and uvsY, T4 phage SSB, gp32, and *Bst* strand-displacing DNA polymerase (*Bst*-Pol) have been consistently used in studies.

---

*The content described in this Chapter was originally published in *Journal of Bioscience and Bioengineering.* Kevin Maafu Juma, Eisuke Inoue, Kengo Asada, Wakao Fukuda, Kenta Morimoto, Masaya Yamagata, Teisuke Takita, Kenji Kojima, Koichiro Suzuki, Yukiko Nakura, Itaru Yanagihara, Shinsuke Fujiwara, and Kiyoshi Yasukawa (2023). Recombinase polymerase amplification using novel thermostable strand-displacing DNA polymerases from *Aeribacillus pallidus* and *Geobacillus zalihae*. *J. Biosci. Bioeng.*, **135**, 282–290.

In Chapter 2, we prepared Rec and SSB and used them to examine the effects of pH, temperature, and various additives on the efficiency of RPA. We established RPA and RT-RPA systems to detect the SARS-CoV-2 DNA and RNA, respectively and optimized the reaction conditions using a statistical method in Chapter 3. Strand-displacing DNA polymerase facilitated continuous replication of DNA without the need for thermal cycling, making it a critical component of isothermal DNA amplification processes. The commonly utilized Pol is a large fragment of *Bst*-Pol, which lacks 5′→3′ and 3′→5′ exonuclease activities. For effective strand-displacement, characteristics such as strand-displacement activity, processivity, and thermostability are desired.

In this Chapter, we isolated thermophilic bacteria strains: *Aeribacillus pallidus* (H1) and *Geobacillus zalihae* (C1). From this, we identified novel thermostable Pols. Additionally, we prepared recombinant forms of these polymerases, known as H1-Pol and C1-Pol, and compared their performance in RPA with a commercially available large fragment of *Bst*-Pol.

Materials and methods

Materials

UvsX and gp32 were expressed in *E. coli* and purified as described in Chapter 2. N-terminal $(His)_6$-tagged uvsY protein was purified as described in Chapter 4.

Isolation of thermophilic bacteria

Tap water (5 mL) containing 1% w/v soluble starch and 0.1 g of compost fermented at 70ºC (Hyuga Farm, Sanda, Japan) were cultured. Grown cells were transferred to CS1 medium (1% w/v soluble starch, 0.5% w/v polypeptone, 0.5% w/v yeast extract, 0.05%

w/v K_2HPO_4, and 0.01% w/v $MgSO_4$. $7H_2O$) and incubated for two days at 70ºC. Grown cells were re-inoculated to fresh CS1 medium and enriched by further cultivating at 70ºC. Cells were spread onto CS1 azure agar plates containing 2.0% w/v agar and 0.25% w/v starch azure (Sigma Chemical, St. Louis, Mo) instead of soluble starch. Halo-forming colony which shows an efficient amylase secretion was then selected for microscopic observation to confirm rod-cell shape with endospore formation. Cells were pure-cultivated in a CS1 liquid medium, and chromosomal DNAs were extracted from the obtained cells. The 16S rRNA genes were amplified by PCR using 27f-16S rRNA-Fw and 1492r-16S rRNA-Rv (Table 5-1) as described previously [98].

Cloning, expression, and purification of H1-Pol and C1-Pol

DNA polymerase genes were amplified by PCR from H1-Pol using primers Aeripol-Fw and Aeripol-Rv and from C1 using Geobacillus-Fw and Geobacillus-Rv. Amplified DNAs were sequenced. H1-Pol and C1-Pol DNAs were amplified by PCR with primers pET28a-Aeripol-Fw and pET28a-Aeripol-Rv for H1-Pol and pET28a-Geobacillus-Fw and pET28a-Geobacillus-Rv for C1-Pol, digested with *Eco*RI and *Xba*I, and inserted into the corresponding sites of plasmid pET28a. The constructs were designated pET28-H1pol and pET28a-C1pol, respectively. *E. coli* BL21(DE3) cells were transformed with each of these two plasmids.

H1-Pol and C1-Pol were expressed and purified as follows. The overnight culture of the transformants (2 mL) was added to 200 mL of L broth containing 20 μg/mL kanamycin and 30 μg/mL chloramphenicol and incubated with shaking at 37ºC. When OD_{660} reached 0.4, 200 μL of 1 M IPTG was added. Growth was continued at 37ºC overnight. The cells were harvested, suspended with buffer A (50 mM Tris-HCl buffer

(pH 8.0), 400 mM NaCl), and disrupted by sonication. After centrifugation at 14,000 × *g* for 10 min at 4ºC, the supernatant was collected and incubated at 60ºC for 10 min. After centrifugation at 14,000 × *g* for 10 min at 4ºC, the supernatant was collected and applied to the column packed with a Ni^{2+}-sepharose (His60 Ni Superflow Resin (2 mL), Takara Bio) equilibrated with buffer A. After washing with buffer A containing 25 mM imidazole, the bound enzyme was eluted with each of buffer A containing 100, 200, or 500 mM imidazole. Each fraction was assessed for the presence of enzyme by 10% SDS-PAGE. Active fractions with imidazole concentrations of 100 mM were collected and dialyzed overnight against buffer B (10 mM Tris-HCl buffer (pH 7.1), 50 mM KCl, 1 mM DTT, 0.1 mM ethylenediaminetetraacetic acid (EDTA), 0.1% v/v Triton X-100) containing 50% v/v glycerol. The solution was recovered and stored at –30ºC until use.

Strand-displacing DNA polymerase assay

Strand-displacing DNA polymerase assay was carried out according to the manufacturer's instructions (New England BioLabs). Briefly, a hybrid (Fx-M13) was prepared by mixing primer Fx and M13mp18 ssDNA (Takara Bio) (Table 5-1). The reaction (10 μL) was carried out in an Isothermal Amplification Buffer (New England BioLabs) containing 1.5 mM $MgSO_4$, dNTPs (0.2 mM each), 1 M betaine, 200 ng M13 mp18 ssDNA, 200 nM Fx-M13 and 150 ng H1-Pol or C1-Pol at 50–60ºC for 30 min. The amplified products were separated on 1.0% agarose gels and stained with ethidium bromide (1 μg/mL).

ssDNA-dependent DNA polymerase assay

The rolling circle DNA synthesis reaction (10 μL) was carried out in 1× ThermoPol Reaction Buffer (New England BioLabs) containing 1.5 mM $MgSO_4$, dNTPs (0.2 mM each), 1 M betaine, 200 ng M13 mp18 ssDNA, 200 nM M13mp18Rv primer, and 100 ng H1-Pol, 100 ng C1-Pol, or 10 units *Bst*-Pol at 60ºC for 10 min. After the reaction, the 5 reaction solutions were gathered and boiled at 100ºC for 10 min followed by phenol chloroform extraction. The synthesized DNA was obtained by ethanol precipitation.

For the quantification of the synthesized DNA, the real-time PCR was carried out as described previously [98] using primers M13mp18Fw and M13mp18Rv (Table 5-1) and PowerUP SYBR Green Master Mix (Thermo Fisher Scientific, Waltham, MA) for 2 min at 50ºC, 2 min at 95ºC, 25 cycles of 15 s at 95ºC, 15 s at 58ºC, and 1 min at 72ºC followed by 15 s at 95ºC, 20 s at 60ºC, and 15 s at 95ºC. The cycle threshold required in PCR to reach a constant fluorescent intensity (Ct value) was obtained using the supplied software.

Preparation of standard DNA

The 233-bp DNA fragment of the urease subunit β (UreB) gene from *Ureaplasma parvum* serovar 3, corresponding to DNA sequence 519–751 deposited in GenBank (AF085732.1), was previously cloned by PCR. From this DNA fragment, the same DNA fragment was amplified by PCR using primers UreB28F3 and UreB260R3 (Table 5-1) and *Taq* polymerase (Toyobo) under 35 cycles of 30 s at 95ºC, 30 s at 55ºC, and 30 s at 72ºC, and purified using MagExtractor (Toyobo). The concentration of purified DNA was determined spectrophotometrically at 260 nm and stored at –20ºC for subsequent use.

RPA reaction

Figure 5-7 shows the target UreB DNA and the primers. The reaction condition was 400 ng/μL uvsX, 40 ng/μL uvsY, 600 ng/μL gp32, indicated concentrations of H1-Pol, C1-Pol, or *Bst*-Pol, 120 ng/μL creatine kinase, 2 mM DTT, 6% w/v PEG35,000, 3.5 mM ATP, dNTPs (650 μM each), 50 mM Tris-HCl buffer (pH 8.6), 40 mM CH_3COOK, 20 mM phosphocreatine, 14 mM $Mg(CH_3COO)_2$, 1 μM UreB28F3 primer, 1 μM UreB260R3 primer at 41ºC. The reaction was performed in a 0.2 mL PCR tube in PCR Thermal Cycler Dice (Takara Bio). The amplified products were separated on 2.0% agarose gels and stained with ethidium bromide (1 μg/mL). The intensities of the DNA bands were quantified using the ImageJ software (http://imagej.nih.gov/ij/).

Table 5-1. Oligonucleotides used in PCR and RPA.

Primers	Sequences (5′→3′)
27f-16S rRNA-Fw	AGAGTTTGATCCTGGCTCAG
1492r-16S rRNA-Rv	GGCTACCTTGTTACGACTT
Aeripol-Fw	CGACGGTGAAACAGTCATCAT
Aeripol-Rv	GGCCATGATACGATAACTTCAT
Geobacillus-Fw	GCRTGGTACAATAGRACAAGGA
Geobacillus-Rv	CGRCGRATCGTTTCCACYTC
pET28a-Aeripol-Fw	CGCGGATCCGAATTCGTGACAAAGAAGCTAGTTTTAATTGATG
pET28a-Aeripol-Rv	GTGGTGGTGCTCGAGTTATTTCGCTTCATACCACGTA
pET28a-Geobacillus-Fw	AGCCATATGGCTAGCATGAGATTGAAAAAAAAGCTTGTTT
pET28a-Geobacillus-Rv	CTCGAGTGCGGCCGCTTATTTCGCGTCATACCACGT
Fx	GTTTTCCCAGTCACGACGTTGTA
M13mp18Rv	GTTTTCCCAGTCACGACGTTGTA
M13mp18Fw	CTCTCCCCGCGCGTTGGCCGATTC
UreB28F	CCAGGTAAATTAGTACCAGG
UreB28F1	CCAGGTAAATTAGTACCAGGGGCAA
UreB28F2	CCAGGTAAATTAGTACCAGGGGCAATTAAT
UreB28F3	CCAGGTAAATTAGTACCAGGGGCAATTAATTTCGC
UreB260R	CCTGATGGAATATCGAAACG
UreB260R1	CCTGATGGAATATCGAAACGTCGTC
UreB260R2	CCTGATGGAATATCGAAACGTCGTCCATAA
UreB260R3	CCTGATGGAATATCGAAACGTCGTCCATAAGCAAC

Lyophilization of RPA reagents

The following solutions were mixed: 292 µL of 4.11 mg/mL uvsX in 20% v/v glycerol, 10 mM Tris-HCl buffer (pH 8.0); 197 µL of 9.14 mg/mL gp32 in 20% v/v glycerol, 10 mM Tris-HCl buffer (pH 8.0); and 75 µL of 0.32 mg/mL H1-Pol or 150 µL of 0.80 mg/mL C1-Pol in 50% v/v glycerol, 50 mM KCl, 1 mM DTT, 0.1 mM EDTA, 0.1% v/v Triton X-100, 10 mM Tris-HCl buffer (pH 7.1). The mixed solution was applied to PD-10 gel filtration column (GE Healthcare) equilibrated with 25 mL of 10 mM $(CH_3COO)NH_4$ buffer (pH 6.0). After sample application, the column was washed with 1.84 mL (H1-Pol) or 1.76 mL (C1-Pol) of 10 mM $(CH_3COO)NH_4$ buffer (pH 6.0). The enzymes were eluted with 1.5 mL with the same buffer as above. To the fraction, the following solutions were added: 75 µL of 2 M Tris-HCl buffer (pH 8.6), 40 µL of 3 M CH_3COOK, 900 µL of 20% w/v PEG35,000, 50 µL of 120 mM DTT, 78 µL of dNTPs (25 mM each) in water, 100 µL of 30 µM DNA primer UreB28F3, 100 µL of 30 µM DNA primer UreB260R3, 50 µL of 1.2 M phosphocreatine, 70 µL of 150 mM ATP, 467 µL of 30% w/v trehalose, 50 µL of 7.2 mg/mL creatine kinase in water, and 28 µL of 4.3 mg/mL uvsY in 20% v/v glycerol, 10 mM Tris-HCl buffer (pH 8.0). The mixed solution was frozen at –80ºC for 1 h followed by drying using EYELA-FD1000 (Tokyo Rikakikai, Tokyo, Japan) freeze dryer at 50 Pa, –50ºC, for 16 h.

Nucleotide sequence accession number

The nucleotide sequences of DNA polymerase and 16S rDNA from *A. pallidus* strain H1 reported in this study have been submitted to the DDBJ nucleotide sequence database under the accession numbers LC720966 and LC720964, respectively. Those of *G. zalihae* strain C1 were LC720965 and LC720963, respectively.

Results and discussion

Screening of novel thermophiles which produce DNA polymerase with strand-displacement activity

DNA polymerases with strand-displacement activity are mainly derived from *G. stearothermophilus* and utilized in various isothermal DNA amplifications such as LAMP and RPA *etc*. *Geobacillus* sp. microbes are hence considered as a potential producer of DNA polymerase with strand-displacement activity. To obtain a novel DNA polymerase with efficient strand-displacement activity, thermophilic *Bacillus* cells were focused and screened from a natural thermal environment. Thermophilic *Bacillus*-related strains show rod shape with endospore, secrete amylase, and utilize starch as a carbon source.

Two strains, which we termed H1 and C1, were isolated from the compost fermented at 70ºC (Hyuga Farm). Both strains H1 and C1 grew optimally at 60ºC (Fig. 5-1 A), and both showed typical rod-cell shapes with endospore (data not shown). Based on the sequence analysis of 16S rDNA, strains H1 and C1 were classified as *A. pallidus* and *G. zalihae* (Fig. 5-1 B).

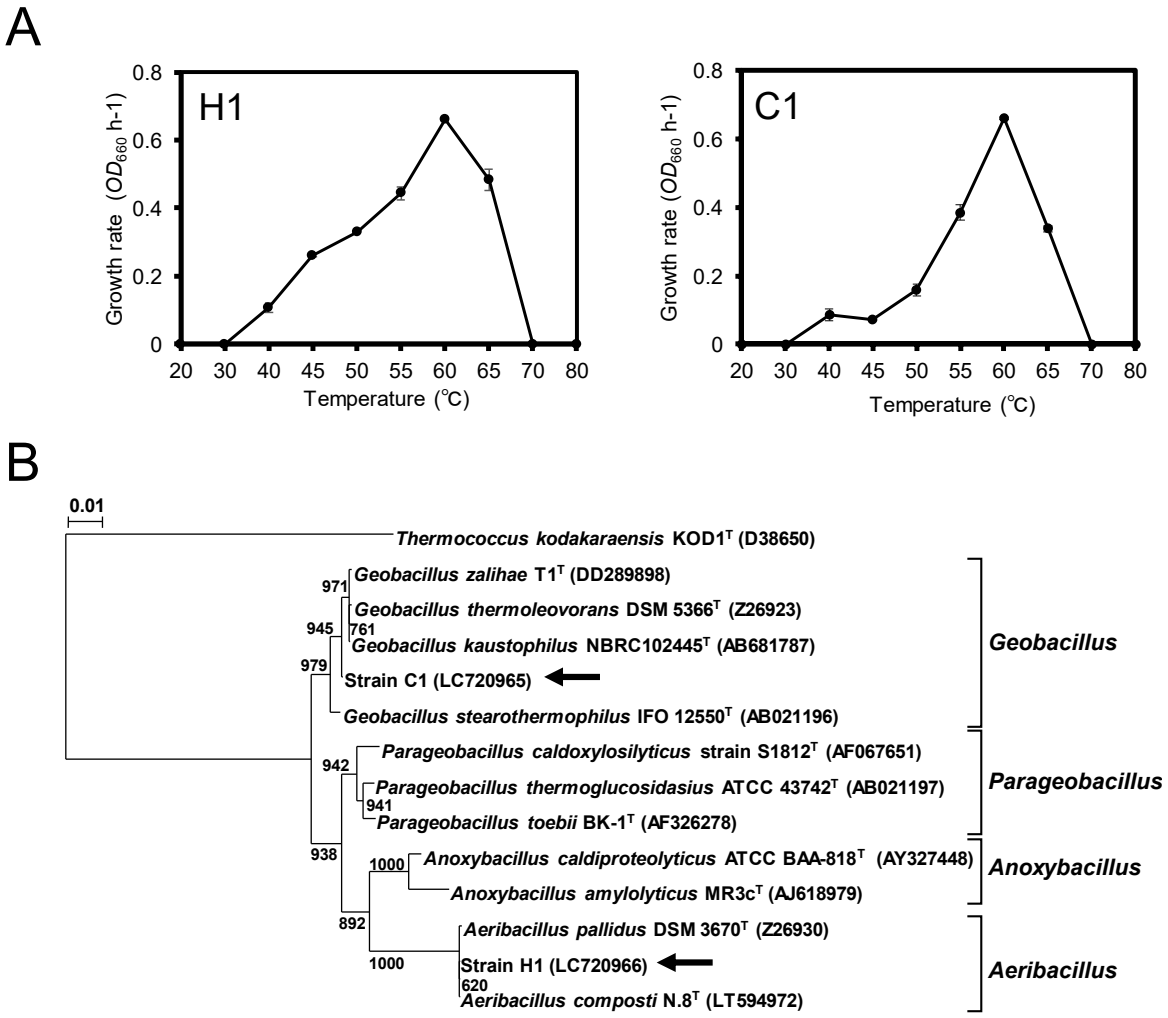

Figure 5-1. Phylogenetic neighbor-joining tree of the members of thermophilic bacteria including the strains H1 and C1 based on the 16S rDNA sequences. (A) Effects of the temperature on the specific growth rates of strains H1 and C1. The growth rates were calculated from a linear regression analysis along the logarithmic phase of the growth curves. (B) The 16S rDNA sequences were obtained from the GenBank/EMBL/DDBJ database. The sequence of *T. kodakaraensis* KOD1 was included as an outgroup. 0.01 means 1 base substitution per 100 nucleotide positions. The arrows indicate the positions of H1 and C1. Accession numbers are shown in parentheses.

Sequence analysis of DNA polymerases of strains H1 and C1

DNA polymerase genes were amplified from strains H1 and C1, respectively. Amplified DNAs were sequenced, and deduced amino acid sequences Gly581–Ile612 were compared with those of other known DNA polymerases derived from thermophilic *Bacillus* strains (Fig. 5-2 and 5-3). The C1 DNA polymerase (C1-Pol) was closely located to the *Bst*-Pol which is derived from *G. stearothermophilus*, formally named *B. stearothermophilus*, in the phylogenetic tree. By contrast, H1 DNA polymerase (H1-Pol) was found in another branch as shown in the tree. As both H1-Pol and C1-Pol showed slight amino acid sequence differences in the conserved region of DNA polymerase, we expected different properties in strand-displacement activity.

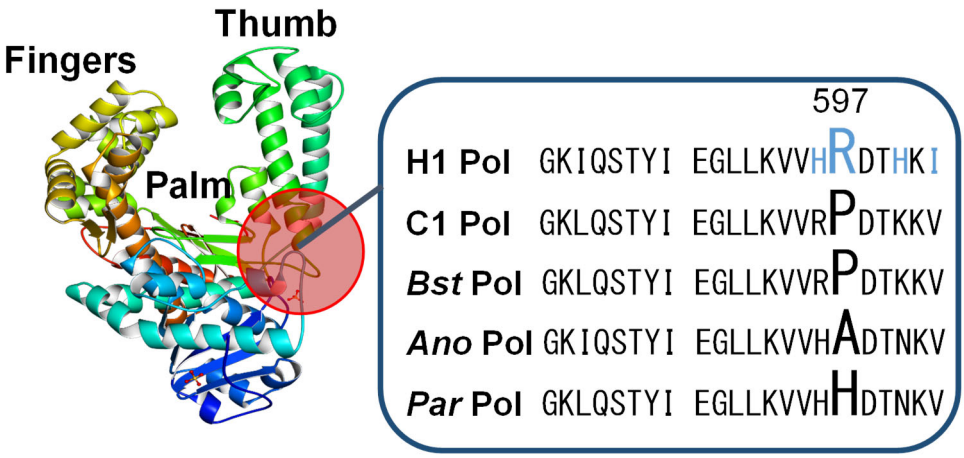

Figure 5-2. Multiple sequence alignment of DNA polymerases. *Ano*-Pol and *Par*-Pol indicate DNA polymerases from *Anoxybacillus caldiproteolyticus* U458 (QPA30338) and *Parageobacillus toebii* NBRC107807T (QIQ31661), respectively.

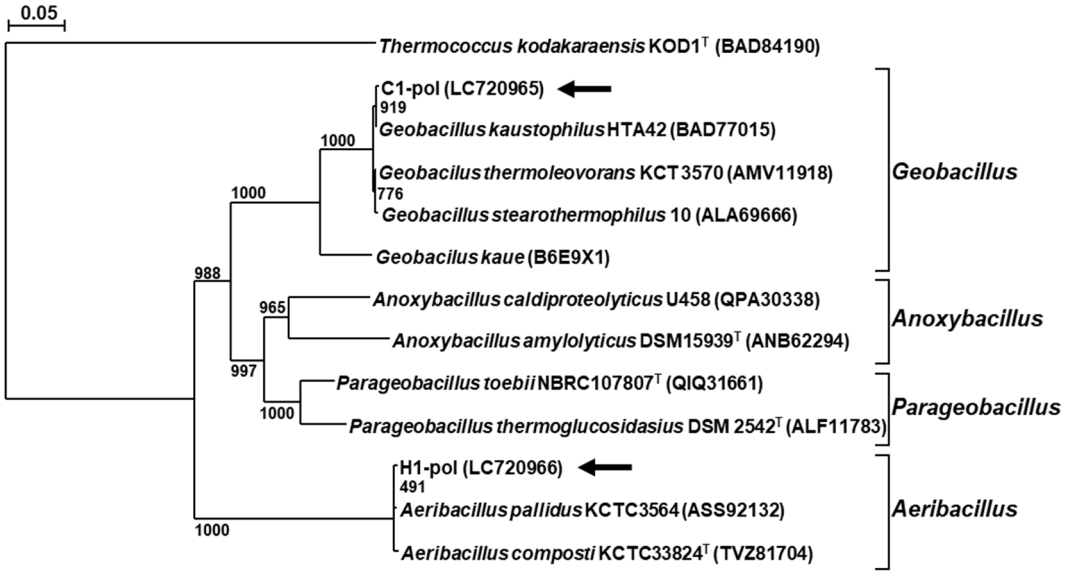

Figure 5-3. Phylogenetic tree based on the amino acid sequence of DNA polymerase. The sequences were obtained from the GenBank/EMBL/DDBJ database. The sequence of *T. kodakaraensis* KOD1 was included as an outgroup. 0.05 means 1 base substitution per 20 amino acid positions. The arrows indicate the positions of H1 and C1. Accession numbers are shown in parentheses.

Characterization of H1-Pol and C1-Pol

E. coli expression plasmids for H1-Pol and C1-Pol were constructed with pET28a. These two genes were expressed in *E. coli* BL21(DE3) cells. The transformants were cultured, and H1-Pol and C1-Pol were purified from the cells. Fig. 5-4 shows the results of the SDS-PAGE analysis of the purified H1-Pol and C1-Pol. They yielded uniform bands with molecular masses of 100 and 99 kDa, respectively. The concentration of the in-house H1-Pol and C1-Pol enzymes was determined by measuring their mass (mg/mL) with spectrophotometry, using an absorbance of 280 nm. On the other hand, the quantification of the commercially available *Bst*-Pol enzyme was based on its enzymatic activity (units/mL).

To evaluate DNA synthesis and strand-displacement activity, we first performed strand-displacing DNA polymerase assay. The rolling circle DNA synthesis reaction was carried out with H1-Pol, C1-Pol, or *Bst*-Pol using M13 circular ssDNA, M13mp18, as a template and Fx (Table 5-1) as a primer. *Taq* DNA polymerase was also used as a thermostable DNA polymerase without strand-displacement activity. *Taq* DNA polymerase produced the dsDNA corresponding to the replication form of M13 DNA in agarose gel (Fig. 5-5). In contrast, in H1-Pol, C1-Pol, and *Bst*-Pol, larger-sized smear patterns were observed, showing that rolling circle DNA synthesis arose beyond the primer-annealed region. The smear band increased in H1-Pol, C1-Pol, and *Bst*-Pol when the reaction temperature increased. This might be due to the fact that the chain dissociation activity increased as the reaction temperature increased.

We next performed ssDNA-dependent DNA polymerase assay. The rolling circle DNA synthesis reaction was carried out with H1-Pol, C1-Pol, or *Bst*-Pol, using M13mp18 as a template and M13mp18Rv (Table 5-1) as a primer. The synthesized DNA was

quantified by real-time PCR. As shown in Fig. 5-6, the Ct value of H1-Pol was significantly lower than that of C1-Pol, indicating that the rolling circle DNA synthesis activity of H1-Pol was significantly higher than that of C1-Pol. As both H1-Pol and C1-Pol possessed typical strand-displacement activity, these enzymes were applied for the RPA reaction.

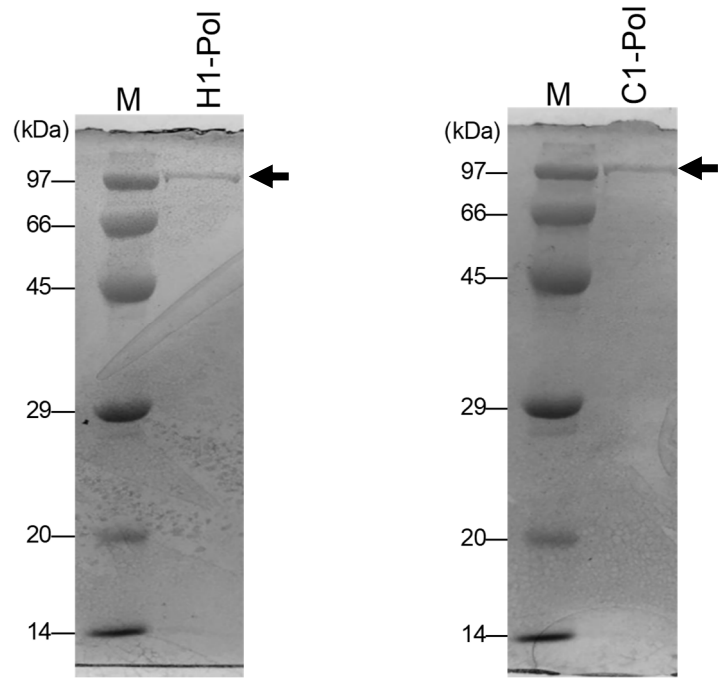

Figure 5-4. SDS-PAGE under reducing conditions. Coomassie Brilliant Blue-stained 10% SDS polyacrylamide gels of purified H1-Pol or C1-Pol are shown. Marker proteins (M).

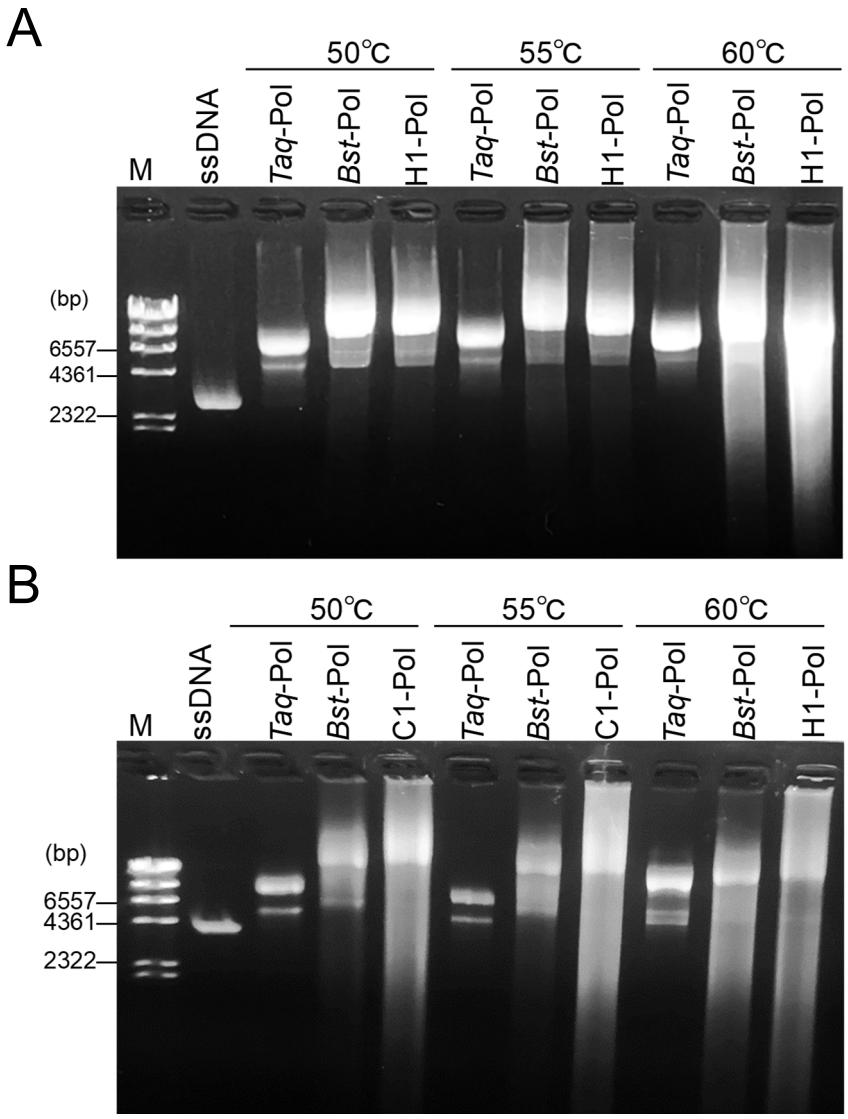

Figure 5-5. DNA synthesis pattern at various temperatures. M13mp18 was used as a template. *Taq*-Pol (DNA polymerase without strand-displacing activity); *Bst*-Pol (DNA polymerase with strand-displacement activity); H1-Pol (A); C1-Pol (B). M, λ phage DNA digested with *Hind*III (23,130-, 9,416-, 6,557-, 4,361-, 2,322-, 2,027-, and 564-bp).

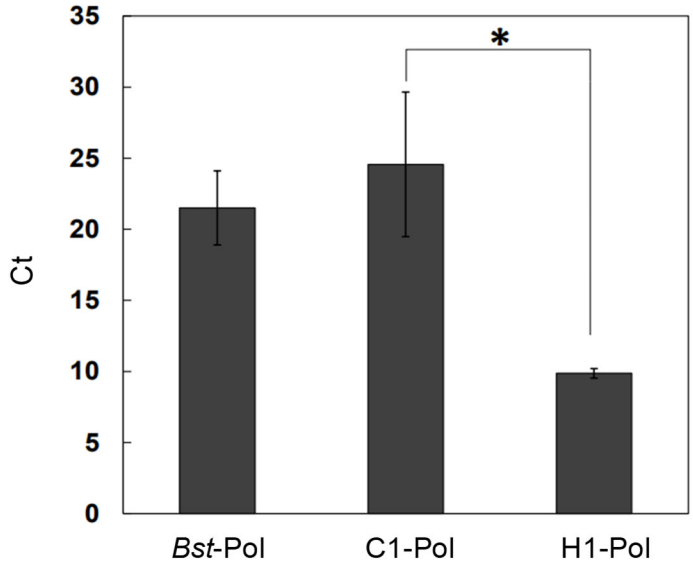

Figure 5-6. ssDNA-dependent DNA polymerase activity. Ct is the cycle threshold required in PCR to reach a constant fluorescent intensity. *, significantly different ($p < 0.05$) by Student's *t*-test.

Establishment of the RPA detection system of UreB

For the comparison of H1-Pol, C1-Pol, and *Bst*-Pol for their performances in RPA reaction, we established a detection system of UreB. *Ureaplasma* is a bacterium that is commonly found in people's urinary or genital tract. UreB gene has been used as a target to detect *Ureaplasma* DNA [99–103]. We designed four forward and three reverse primers (Table 5-1) and selected one combination (UreB28F3 and UreB260R3) that exhibited the best performance in sensitivity. The size of the amplified product by the primer combination was 233-bp (Fig. 5-7).

Figure 5-7. Nucleotide and amino acid sequence of the target UreB DNA and the primers. The arrows indicate the regions to which primers bind.

Effects of Pol concentration on the RPA reaction efficiency

We evaluated the effects of concentrations of H1-Pol, C1-Pol, or *Bst*-Pol on the RPA reaction efficiency. RPA was carried out with the initial copy number of 6×10^6 copies of standard DNA at 41ºC for 30 min. Figure 5-8 shows the agarose gel analysis of the amplified RPA products. The concentrations at which the 233-bp target DNA band was observed were 0.6–60 ng/μL for H1-Pol, 0.8–160 ng/μL for C1-Pol, and 0.05–2.0 units/μL for *Bst*-Pol, and those at which the target band was observed clearly were 2.0–20 ng/μL for H1-Pol, 2.0–80 ng/μL for C1-Pol, and 0.1–0.5 units/μL for *Bst*-Pol. When the result obtained with H1-Pol and that obtained with C1-Pol were compared, the lowest concentration at which the reaction proceeded was almost the same (0.6–0.8 ng/μL), while the highest concentration at which the reaction proceeded was considerably different (20 ng/μL for H1-Pol and 80 ng/μL for C1-Pol). The former might be attributed to the fact that H1-Pol and C1-Pol have similar processivity, and the latter might be due to the fact that the non-specific binding to the template primer of H1-Pol more easily occurs than that of C1-Pol. We reported such non-specific binding to template-primer in HIV-1 reverse transcriptase [104] and MMLV reverse transcriptase [74]. We set 8 ng/μL for H1-Pol, 40 ng/μL for C1-Pol, and 0.2 units/μL for *Bst*-Pol as the optimal concentrations and conducted the subsequent experiments.

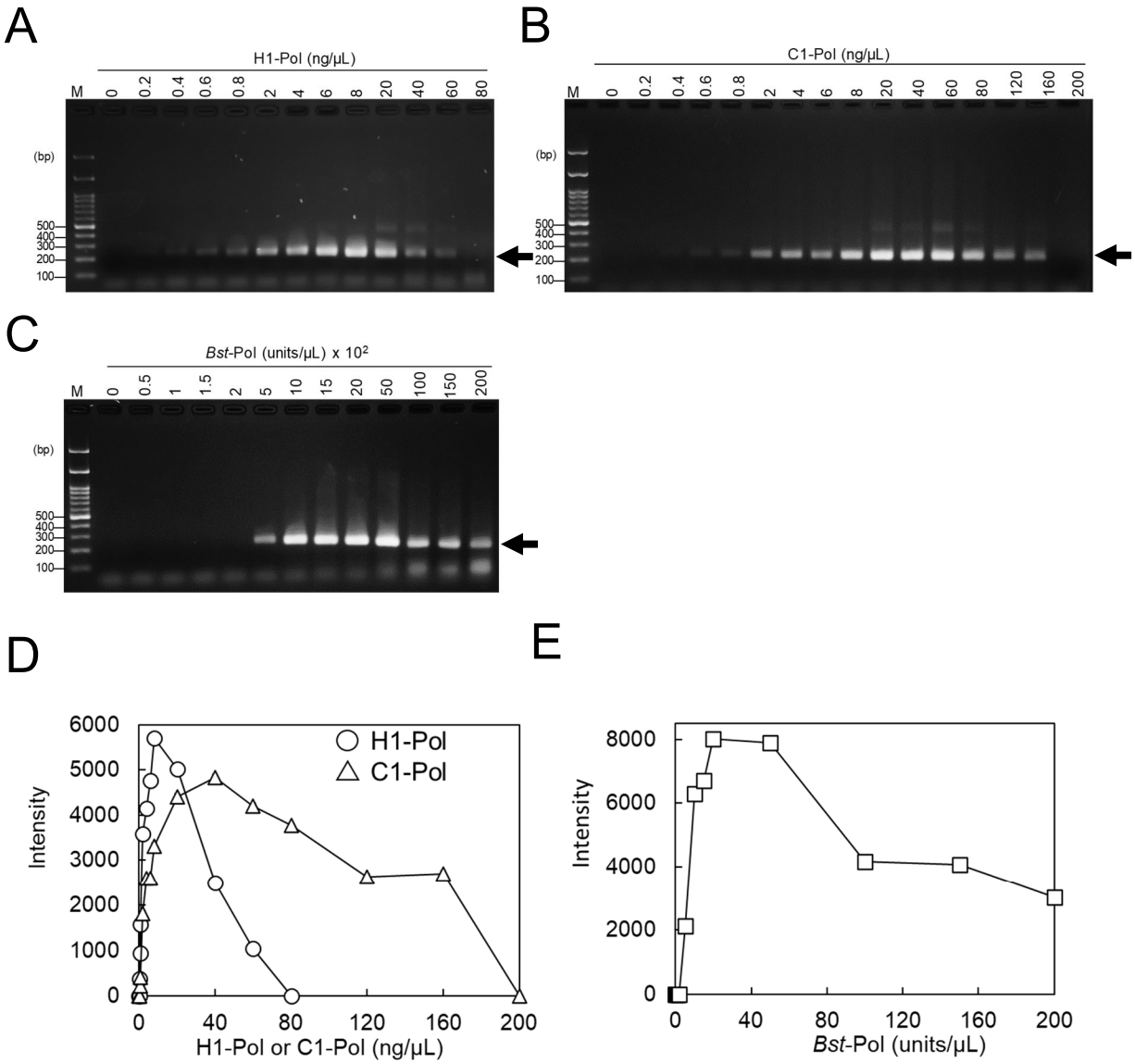

Figure 5-8. Effects of the Pol concentrations on RPA reaction efficiency. The reactions were carried out with 0–80 ng/μL H1-Pol (A), 0–200 ng/μL C1-Pol (B), or 0–2 units/μL *Bst*-Pol (C) at 41ºC for 30 min. Initial copies of standard DNA were 6×10^6. The amplified products were separated on 2.0% agarose gels and stained with ethidium bromide (1 μg/mL). The arrow indicates the target band (A–C). ImageJ analysis (D, E). H1-Pol (circle), C1-Pol (triangle), and *Bst*-Pol (square).

Sensitivities of the RPA reaction with H1-Pol, C1-Pol, or Bst-Pol

We next compared the sensitivities of RPA reaction with H1-Pol, C1-Pol, or *Bst*-Pol. RPA was performed with initial copy number of 0–6 × 10^6 copies of standard DNA at 41ºC for 30 min. Amplified RPA products were analyzed by agarose gel electrophoresis (Fig. 5-9). In the RPA with H1-Pol or C1-Pol, the 233-bp target DNA bands were weakly observed for 600 copies and clearly observed for 6,000 or more copies. In the RPA with *Bst*-Pol, the target band was not observed for 600 copies but was observed for 6,000 or more copies. These results indicated that the sensitivities of RPA reaction with H1-Pol or C1-Pol were higher than that with *Bst*-Pol, suggesting that the binding ability to template-primer of H1-Pol and C1-Pol is slightly higher than that of *Bst*-Pol.

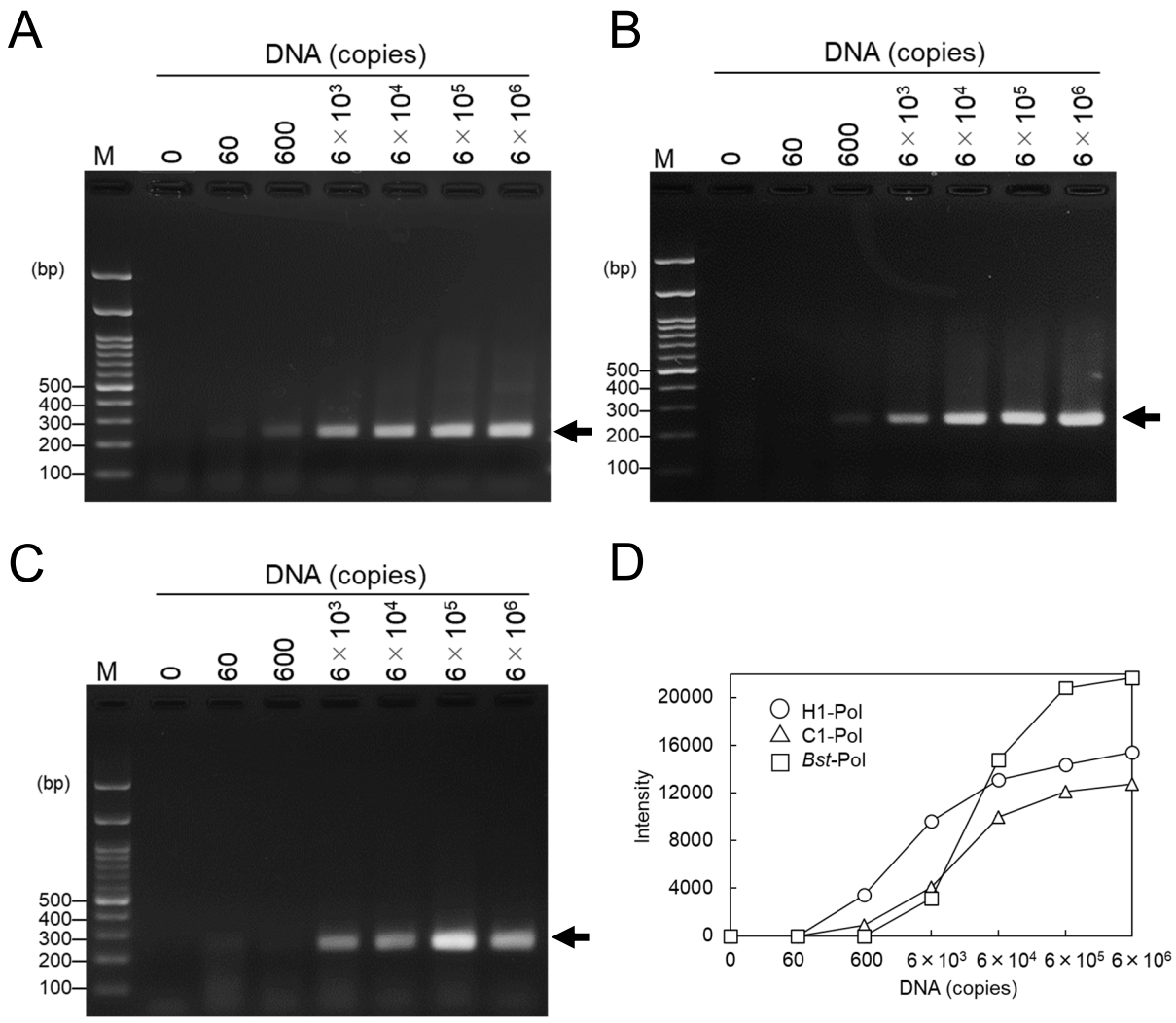

Figure 5-9. Effects of initial copies on RPA reaction. The reactions were carried out with 8 ng/μL H1-Pol (A), 40 ng/μL C1-Pol (B), or 0.2 units/μL *Bst*-Pol (C) at 41ºC for 30 min. Initial copies of standard DNA were 0–6 × 10^6. The amplified products were separated on 2.0% agarose gels and stained with ethidium bromide (1 μg/mL). The arrow indicates the target band (A–C). ImageJ analysis (D). H1-Pol (circle), C1-Pol (triangle), and *Bst*-Pol (square).

Rapidness of the RPA reaction with H1-Pol, C1-Pol, or Bst-Pol

RPA was performed with initial copy number of 6×10^6 copies of standard DNA at 41ºC for 0–60 min. Amplified RPA products were analyzed by agarose gel electrophoresis (Fig. 5-10). In the RPA with H1-Pol, the 233-bp target DNA band was weakly observed for 10 min and clearly observed for 20–60 min. In the RPA with C1-Pol or *Bst*-Pol, the target band was not observed for 10 min but was observed for 20–60 min. These results indicated that the rapidness of RPA reactions with H1-Pol, C1-Pol, and *Bst*-Pol are similar, suggesting that the processivity of these three enzymes is almost the same.

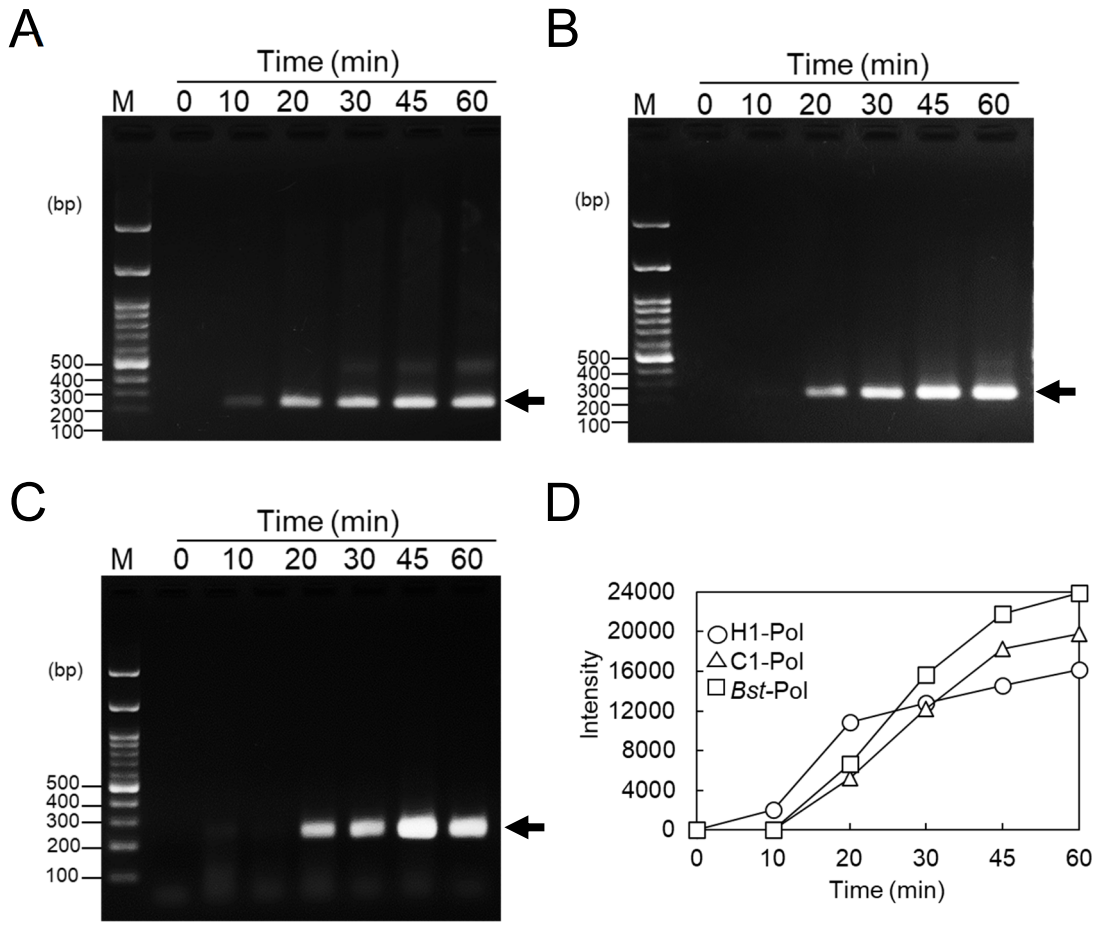

Figure 5-10. Effects of reaction time on RPA reaction. The reactions were carried out with 8 ng/μL H1-Pol (A), 40 ng/μL C1-Pol (B), or 0.2 units/μL *Bst*-Pol (C) at 41ºC for 0–60 min. Initial copies of standard DNA were 6×10^6. The amplified products were separated on 2.0% agarose gels and stained with ethidium bromide (1 μg/mL). The arrow indicates the target band (A–C). ImageJ analysis (D). H1-Pol (circle), C1-Pol (triangle), and *Bst*-Pol (square).

Thermostabilities of H1-Pol, C1-Pol, and Bst-Pol

We compared the thermostabilities of three DNA polymerases. H1-Pol, C1-Pol, and *Bst*-Pol were incubated at 56–84ºC for 10 min. Amplified RPA products were analyzed by agarose gel electrophoresis (Fig. 5-11). The highest temperatures at which the target 233-bp band was amplified were 62ºC for H1-Pol, 70ºC for C1-Pol, and 66ºC for *Bst*-Pol. These results suggested that thermostability of Pol was in the order of C1-Pol > *Bst*-Pol > H1-Pol.

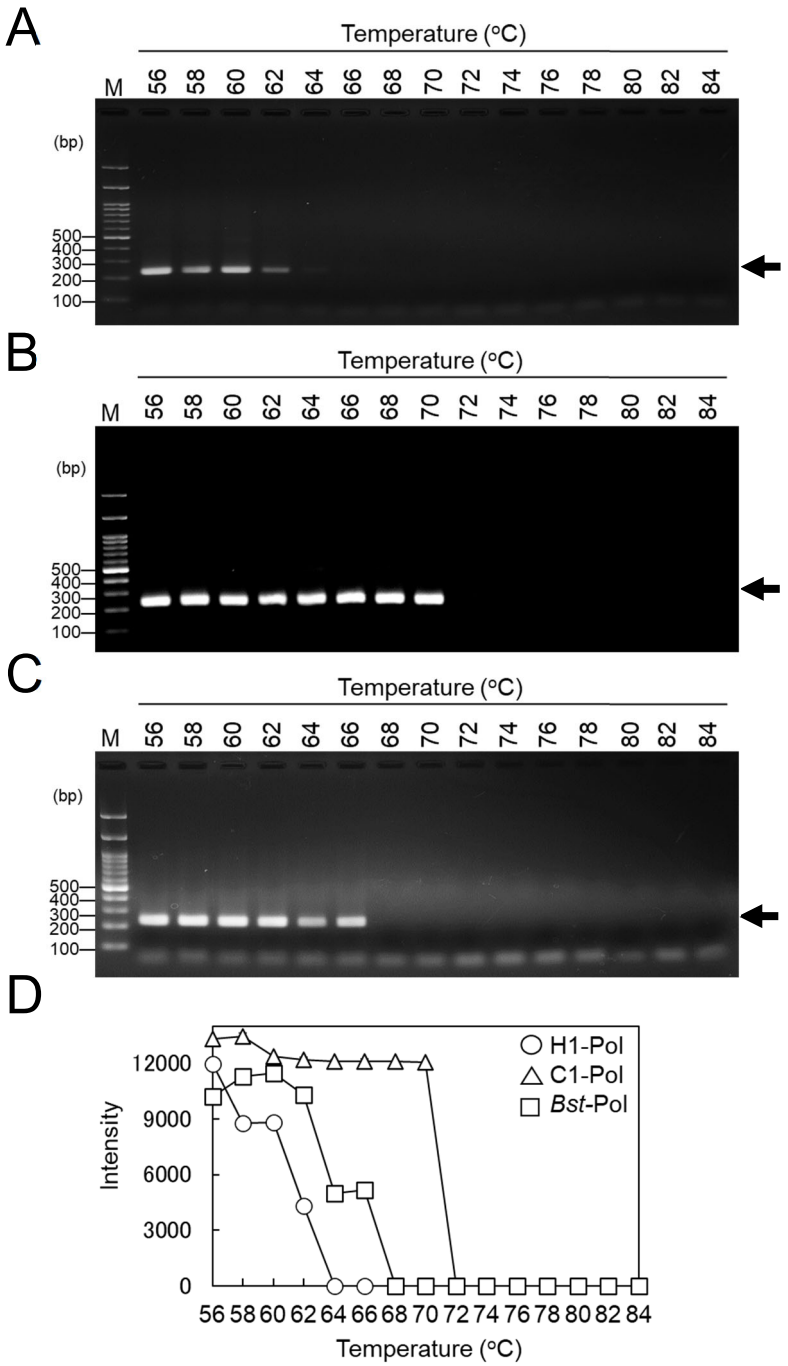

Figure 5-11. Thermostabilities of Pol. The enzymes (10 µL of 320 ng/µL H1-Pol, 800 ng/µL C1-Pol, or 8 units/µL *Bst*-Pol in a PCR tube) were incubated for 10 min between 56–84ºC. The RPA reactions were carried out with 8 ng/µL H1-Pol (A), 40 ng/µL C1-Pol (B), or 0.2 units/µL *Bst*-Pol (C) at 41ºC for 30 min. Initial copies of standard DNA were 6×10^6. The amplified products were separated on 2.0% agarose gels and stained with ethidium bromide (1 µg/mL). The arrow indicates the target band (A–C). ImageJ analysis (D). H1-Pol (circle), C1-Pol (triangle), and *Bst*-Pol (square).

Performance of lyophilized RPA reagents

As we mentioned, the disadvantage of RPA is instability for storage. To solve this problem, we applied lyophilization of RPA solutions and optimized the condition. Experimental details are described in Materials and Methods. Preparation of lyophilized reagents used for RPA reagents consists of three steps: 1) Removal of glycerol present in enzyme preparation, except uvsY, by gel filtration chromatography; 2) preparation of a mixture of all the reagents, except for $Mg(CH_3COO)_2$ solution; and 3) lyophilization of the mixture using 4% w/v trehalose. UvsY was not applied to PD-10 because it precipitated as soon as glycerol was removed (data not shown).

We prepared lyophilized RPA reagents containing H1-Pol or C1-Pol, each equivalent to 100 tests. In each reagent, the concentrations of uvsX, uvsY, gp32, and either H1-Pol or C-Pol at the time of reaction were set as 400, 40, 600, and 8 or 40 ng/μL, respectively, which were the same as those used for liquid reagents. After lyophilization, we dissolved the reagents in water and evaluated their performance. RPA was performed with an initial copy number of 0–6×10^6 copies of standard DNA at 41ºC for 30 min (Fig. 5-12). The lowest initial copy number at which the amplified band was observed was 600 copies for the RPA reagents containing H1-Pol, whereas that for C1-Pol was 6×10^4 copies, thus indicating that the sensitivity of the lyophilized RPA reagents was indistinguishable from that for the liquid ones in the case of H1-Pol, while the former reagents were less sensitive than the latter ones for C1-Pol.

Next, we evaluated the storage stability of the lyophilized RPA reagents containing H1-Pol. It is anticipated that enzymes denature during storage; therefore, two types of reagents (Reagents A and B) were prepared and stored at 20ºC. In Reagent A, the concentrations of uvsX, uvsY, gp32, and H1-Pol used at the time of reaction were the

same as the ones described above, whereas they were twice as much in Reagent B. RPA was performed with initial copy number of 0–6×10^6 copies of standard DNA at 41ºC for 30 min (Fig. 5-13). The lowest initial copy number (600 copies) at which the amplified band was observed was stable at days 0–14 in both Reagents. These results indicated that the lyophilized RPA reagents containing H1-Pol had good storage stability.

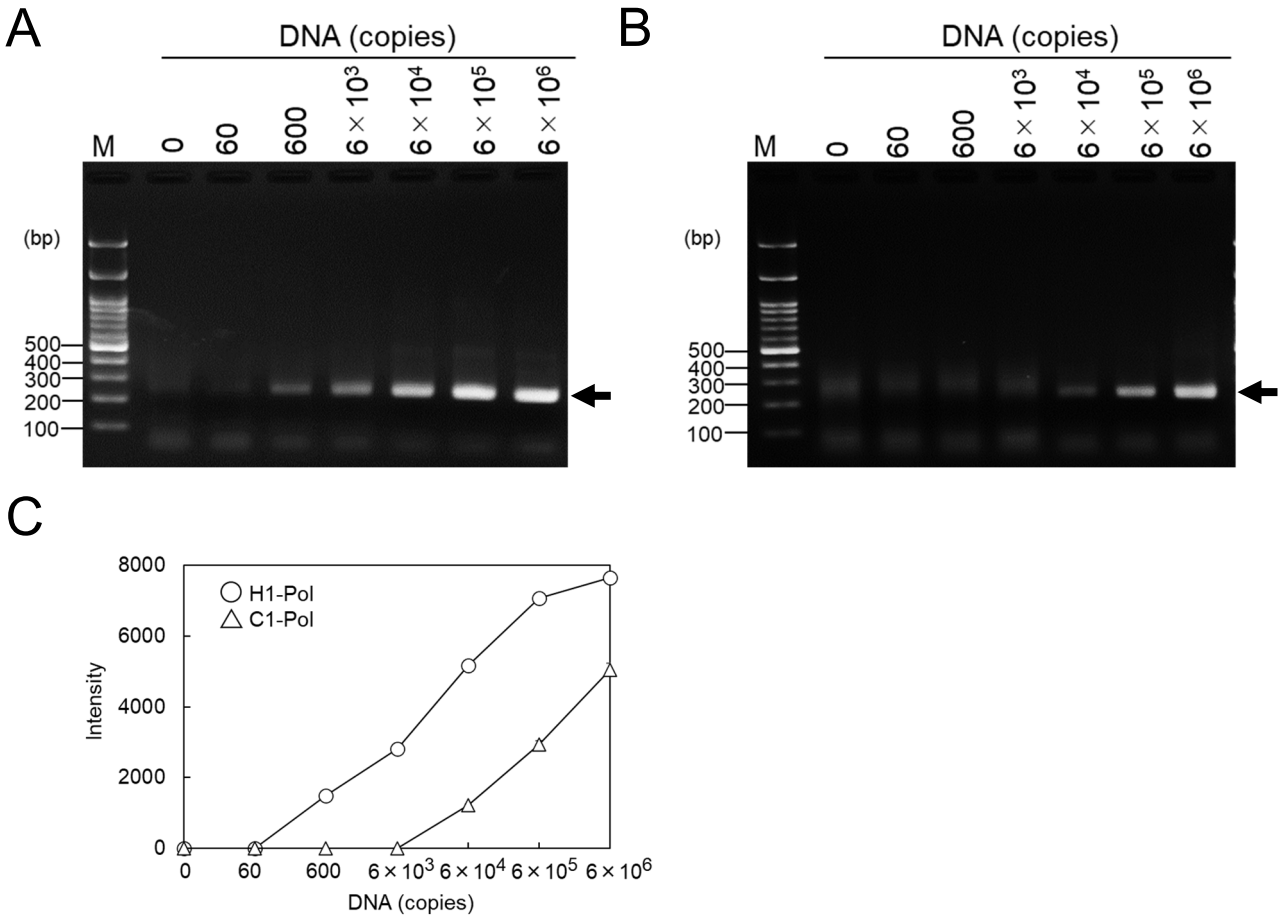

Figure 5-12. Effects of initial copies on the RPA reaction using lyophilized reagents containing H1-Pol or C1-Pol. The reactions were carried out with 400 ng/μL uvsX, 40 ng/μL uvsY, 600 ng/μL gp32, and 8 ng/μL H1-Pol (A) or 40 ng/μL C1-Pol (B) at 41ºC for 30 min. Initial copies of standard DNA were 0–6×10^6. The amplified products were separated on 2.0% agarose gels and stained with ethidium bromide (1 μg/mL). The arrow indicates the target band (A, B). ImageJ analysis (C). H1-Pol (circle) and C1-Pol (triangle).

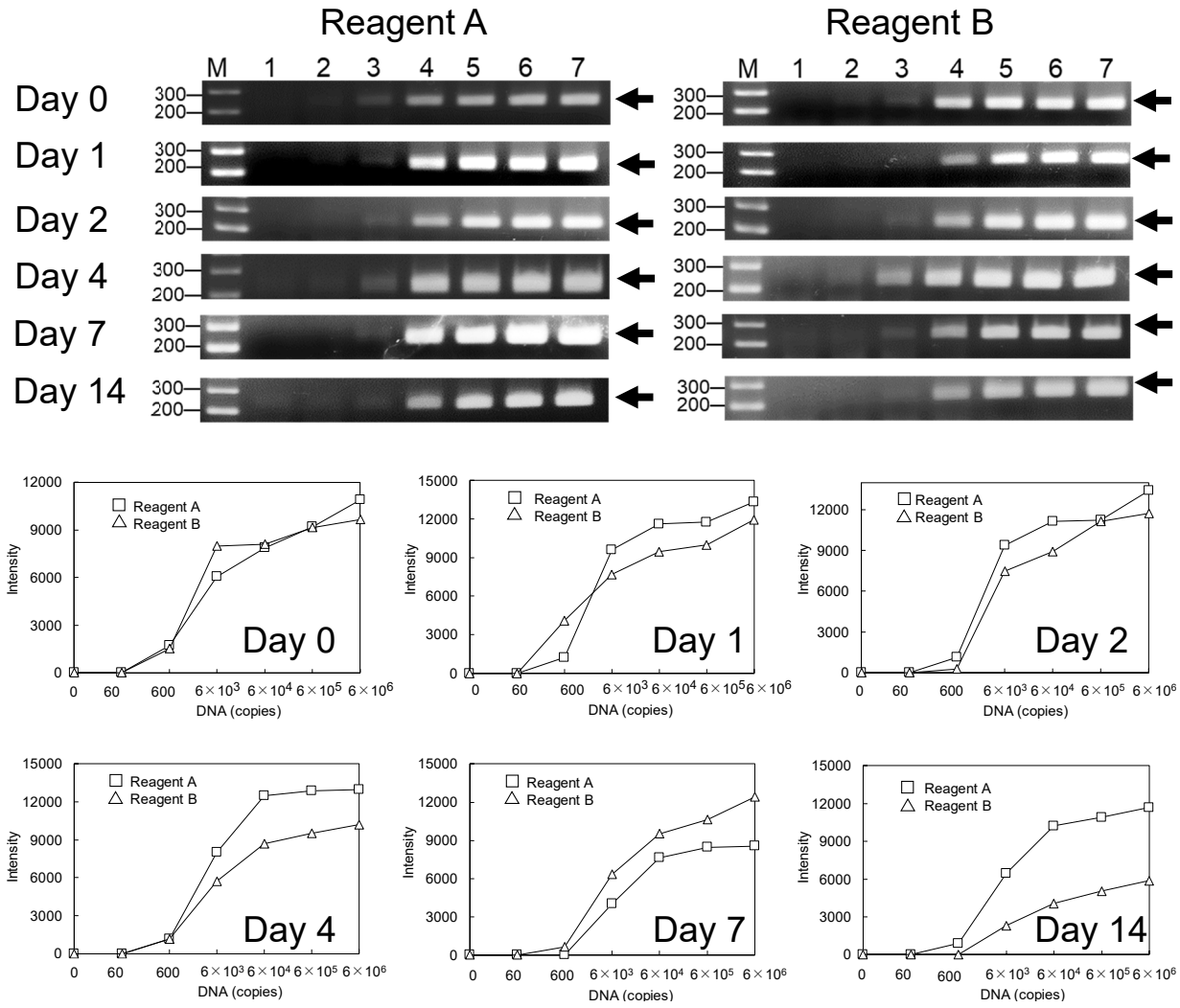

Figure 5-13. Effects of initial copies on the RPA reaction using lyophilized reagents containing H1-Pol. The lyophilized reagents were stored at 20ºC for 0–14 days. The reaction was carried out with 400 ng/µL uvsX, 40 ng/µL uvsY, 600 ng/µL gp32, and 8 ng/µL H1-Pol for Reagent A and 800 ng/µL uvsX, 80 ng/µl uvsY, 1,200 ng/µL gp32, and 16 ng/µL H1-Pol for Reagent B, each at 41ºC for 30 min. Marker (M), initial standard DNA copies were: 0 (lane 1), 60 (lane 2), 600 (lane 3) 6×10^3 (lane 4), 6×10^4 (lane 5), 6×10^5 (lane 6) and 6×10^6 (lane 7). The arrow indicates the target band (upper panel). ImageJ analysis (lower panel). Reagent A (square) and Reagent B (triangle).

Insights into the performance of H1-Pol and C1-Pol in RPA

The efficiency of isothermal amplification depends on the performance of DNA polymerase. Especially, the strand-displacement activity, protein stability, and DNA synthesis activity all play important roles in achieving successful DNA amplification. In the present study, our newly isolated DNA polymerase (H1-Pol) from *A. pallidus* strain H1 showed superior performance in RPA to detect UreB DNA. When we compare the protein stability of H1-Pol with those of *Bst*-Pol and C1-Pol, H1-Pol did not show higher stability than the other two (Fig. 5-11). Hence, the reason for the improvement by H1-Pol in RPA might be H1-Pol's enzymatic property, probably its higher processivity and strand-displacement activity.

Comparison of the amino acid sequence of these three enzymes reveals that four amino acid residues were different in the conserved region which is involved in strand-displacement activity (Figs. 5-2, 5-3). One of the unique points is the 597th position of H1-Pol where Arg is occupied while Pro is occupied in C1-Pol and *Bst*-Pol, Ala is occupied in *Anoxybacillus caldiproteolyticus*, and His is occupied in *Parageobacillus toebii*. This position is located at the end of the α-helix structure and is essential to form a thumb shape in the DNA polymerase molecule. In H1-Pol, Arg597 seems to be involved in helix stabilization, and its basic property would play some role in enhancing strand-displacement by incorporating substrate dNTP more efficiently while maintaining template DNA at the thumb domain. However, clear molecular mechanisms are unknown. A further precise study using mutant enzymes is in progress.

C1-Pol and H1-Pol contain exonuclease domains in the amino-terminal region. *Bst*-Pol which has been used in RPA in previous studies, is a Klenow-like fragment lacking a 3'→5' exonuclease domain although the original *Bst* DNA polymerase contains an

exonuclease domain. Our successful RPA with C1-Pol and H1-Pol indicates that the exonuclease activity of DNA polymerase does not affect amplification. Having 3'→5' exonuclease activity is rather desirable to avoid the misincorporation of unstable nucleotides during RPA.

The disadvantage of RPA is the instability of the mixed protein components in the solution. To solve this problem, we tried lyophilization of RPA components. Lyophilization is a low-temperature dehydration process that involves freezing the product, lowering pressure, then removing the ice by sublimation. Some biopharmaceutical products such as monoclonal antibodies require lyophilization for stability. Generally, NA-relating enzymes are stored at around −30ºC in the presence of 30–50% v/v glycerol because they are easily denatured. Trehalose, a natural non-reducing disaccharide in which two glucose units are linked in α1→1 linkage is thought to be the most effective stabilizer of enzymes during lyophilization [105]. According to the glass theory, trehalose stabilizes freeze-dried enzymes by forming glasses and increasing the glass transition temperature, the temperature above which a transition from viscous to fluid state occurs [106]. It is also known that glycerol in enzyme preparation should be removed before lyophilization. As for the mechanism, it was reported that glycerol has a plasticizing effect on the glasses trehalose formed during the primary drying stage, reducing the bioprotective effect of trehalose [107]. Here, we applied lyophilization for RPA components. After several condition trials, we found that PD-10 gel filtration column treatment using a volatile $(CH_3COO)NH_4$ solution as an equivalent buffer before freezing process is an important step to achieve lyophilization while maintaining RPA activity. The lyophilized RPA reagents containing H1-Pol, but not C1-Pol, exhibited the same performance as the corresponding liquid one (Fig. 5-12) and were stable at 20ºC (Fig. 5-

13). It is unknown why C1-Pol was more affected by lyophilization than H1-Pol. The success in lyophilization provides flexibility in the fabrication of RPA reagents, leading to the expansion of the use of RPA in various fields.

The major advantages of RPA over other NA amplification methods are that the reaction is isothermal and the reaction temperature is closer to the normal human body temperature, thereby eliminating the need for any specialized equipment to obtain the required temperature. Thus, RPA is the ideal NA amplification method for point-of-care diagnosis targeting pathogenic organisms. However, the major limitation of RPA is that RPA kits are sold only by two companies: TwistDx and Jiangsu Qitian Gene Biotechnology (Ningbo, China). In addition, these kits are liquid kits that must be stored in a frozen state, but not lyophilized kits that can be stored at room temperature. Thus, researchers face difficulties in developing effective RPA reagents. To address this issue, we developed two novel thermostable DNA polymerases that can be used for both liquid and lyophilized RPA reagents. Our results pave the way for use of RPA in various fabrications.

Conclusion

Two novel thermostable strand-displacing DNA polymerases were isolated, one from a thermophilic bacterium *A. pallidus* (H1) and the other from *G. zalihae* (C1). The RPA with H1-Pol or C1-Pol was more sensitive than that with *Bst*-Pol. The sensitivity of lyophilized RPA reagents with H1-Pol was indistinguishable from that of the corresponding liquid one. These results suggested that H1-Pol is attractive as a strand-displacing DNA polymerase in RPA.

Chapter 6

Detection of SARS-CoV-2 spike protein D614G mutation using µTGGE *

Introduction

Understanding the infection mechanism, disease transmission and severity, and guiding public interventions, it is essential to study mutations that occur within key viral genes. One of the important mutations in the SARS-CoV-2 genome is the missense located in the spike (S) protein, which led to the substitution of amino acid from aspartic acid (D) with glycine (G) at residue 614. This mutation is known as the D614G and has been shown to affect the infectivity of SARS-CoV-2 *in vitro* and *in vivo* [108, 109].

To prevent, control, and manage human diseases caused by mutations including SARS-CoV-2, an accurate, quick, and simple detection method that can be used at point-of-care is highly desired. DNA sequencing assay is the industry 'gold standard' for mutation analysis [110–113]. However, this assay is time-consuming, costly, and requires a specialized laboratory. Micro temperature gradient gel electrophoresis (µTGGE) is a mutation analysis assay of DNA fragments based on their specific T_m, (temperature at which half of the dsDNA separates into ssDNA). It is a miniaturized version

---

*The content described in this Chapter has been accepted for publication in *Molecular Biology Reports.* Kevin Maafu Juma, Kenta Morimoto, Vishnu Sharma, Kirti Sharma, Radhika Biyani, Manish Biyani, Teisuke Takita, and Kiyoshi Yasukawa. Detection of SARS-CoV-2 spike protein D614G mutation using µTGGE. *Mol. Biol. Rep.*, in press.

of temperature gradient gel electrophoresis (TGGE) that allows for higher resolution and improved detection of small differences in the T_m.

The μTGGE analysis involves running the PCR products on a polyacrylamide gel with a temperature gradient. As the temperature increases, the DNA fragments denature and migrate through the gel based on their unique T_m. Any sequence variations or mutations can be identified by comparing the μTGGE patterns of the PCR products from different samples on the gel [61]. This assay has been used in genome profiling for fungal discrimination [114] and for detecting mammalian cell mutagens [115]. Recently, the application of μTGGE for rapid RNA testing of SARS-CoV-2 variants Alpha Wuhan-Hu-1 and Delta B.1.617.2 types using RICCA and portable PalmPAGE system was reported [116].

In Chapter 3, we successfully established an RPA system for detecting SARS-CoV-2 DNA and RNA. However, due to the ongoing mutations in the virus since its initial identification in late 2019 [108, 109], there is a growing need for additional techniques to study these mutations. To address this, this Chapter focuses on the development of a detection system using μTGGE to precisely identify the D614 and G614 mutations in the spike proteins of SARS-CoV-2.

Materials and methods

Materials

The 220-nt ssDNA corresponding to DNA sequence 23,301–23,520 of SARS-CoV-2 gene S deposited in GenBank (MN908947.3) and target primers, were purchased from Eurofins Genomics (Tokyo, Japan).

Synthesis of the 220-bp DNA fragment containing D614 or G614 used for PCR as a template

The 220-bp target sequences of D614 and G614 variants were amplified by PCR from 220nt-1 and 220nt-2, respectively, using F1 and R6 primers (Table 6-1). The PCR reaction was carried out using Premix Ex *Taq* Hot Start (Takara Bio) under 25 cycles of 5 s at 98ºC, 5 s at 58ºC, and 30 s at 72ºC. The PCR products of D614 and G614 were stored at –30ºC until use.

Synthesis of the 80–120-bp DNA fragments containing D614 or G614 used for μTGGE analysis

The reaction mixture (25 μL) for PCR was prepared by mixing 11 μL of water, 12.5 μL of Premix Ex *Taq* Hot Start, 0.5 μL of 10 μM forward primer, 0.5 μL of 10 μM reverse primer and 0.5 μL of D614 or G614 DNA. The cycling parameters were 94ºC for 2 min, followed by 25 cycles at 98ºC for 5 s, 58ºC for 5 s, and 72ºC for 30 s with a final extension at 72ºC, for 2 min. The amplified products were separated on 2.0% agarose gels and stained with ethidium bromide (1 μg/mL). The melting curves of target gene fragments for μTGGE analysis were predicted using uMelt software, a web-based tool [117].

Table 6-1. Oligonucleotides used in PCR.

Primers	Sequences (5′→3′)
220nt-1	AGACACTTGAGATTCTTGACATTACACCATGTTCT
	TTTGGTGGTGTCAGTGTTATAACACCAGGAACAAA
	TACTTCTAACCAGGTTGCTGTTCTTTATCAGGATGT
	TAACTGCACAGAAGTCCCTGTTGCTATTCATGCAG
	ATCAACTTACTCCTACTTGGCGTGTTTATTCTACAG
	GTTCTAATGTTTTTCAAACACGTGCAGGCTGTTTAA
	TAGGGGC
220nt-2	AGACACTTGAGATTCTTGACATTACACCATGTTCT
	TTTGGTGGTGTCAGTGTTATAACACCAGGAACAAA
	TACTTCTAACCAGGTTGCTGTTCTTTATCAGGGTGT
	TAACTGCACAGAAGTCCCTGTTGCTATTCATGCAGA
	TCAACTTACTCCTACTTGGCGTGTTTATTCTACAGGT
	TCTAATGTTTTTCAAACACGTGCAGGCTGTTTAATAG
	GGGC
F1	AGACACTTGAGATTCTTGAC
F2	ATTACACCATGTTCTTTTGG
F3	TGGTGTCAGTGTTATAACAC
F4	CAGGAACAAATACTTCTAAC
F5	CAGGTTGCTGTTCTTTATCAGG
R1	CTTCTGTGCAGTTAACA
R2	TGCATGAATAGCAACAGGGA
R3	CAAGTAGGAGTAAGTTGATC
R4	AACCTGTAGAATAAACACGC
R5	ACGTGTTTGAAAAACATTAG
R6	GCCCCTATTAAACAGCCTG

Table 6-2. PCR primer combinations and expected amplicon size.

	Primer combination		Amplicon size (bp)
No.	Forward	Reverse	
1	F1	R1	120
2	F1	R2	140
3	F1	R3	160
4	F1	R4	180
5	F1	R5	200
6	F1	R6	220
7	F2	R1	100
8	F2	R2	120
9	F2	R3	140
10	F2	R4	160
11	F2	R5	180
12	F2	R6	200
13	F3	R1	80
14	F3	R2	100
15	F3	R3	120
16	F3	R4	140
17	F3	R5	160
18	F3	R6	180
19	F4	R1	60
20	F4	R2	80
21	F4	R3	100
22	F4	R4	120
23	F4	R5	160
24	F4	R6	180
25	F5	R1	40
26	F5	R2	60
27	F5	R3	80
28	F5	R4	100
29	F5	R5	120
30	F5	R6	140

µTGGE analysis

This procedure is important for the extraction of DNA sequence information without the need for sequencing [118]. The PCR products were run on 6% w/v polyacrylamide gel, acrylamide and bis-acrylamide (19:1) containing 90 mM TBE buffer (0.1 M Tris, 0.09 M boric acid, 0.001 M EDTA) (pH 8.4) and 6.5 M urea using a temperature gradient generator (Lifetech Co. Ltd, Japan). A 9 µL of the PCR product was electrophoresed at 100 V for 10 min at a linear temperature gradient of 15–55ºC in 1 × TBE running buffer. After electrophoresis, the gel was stained with 300 µL of 10 × SYBR gold (Thermo Fischer Scientific, Waltham, MA, USA) and visualized using the fluorescence imager, SAYAKA-IMAGER (DRC, Tokyo, Japan). Each analysis was performed in triplicate.

Results and discussion

µTGGE principle for D614 and G614 mutation detection

To develop a simple, highly sensitive, and point-of-care mutation analysis system, µTGGE has been introduced and demonstrated to highly discriminate point mutations [62]. Fragment design and optimization before µTGGE analysis is an important step for a successful µTGGE method. In particular, it is important to consider: (1) NA fragment length and (2) the position of mutation at the 3′-terminal end, center, or 5′-terminal end of the fragment. By employing the dry lab approach, a computer program (uMelt) is used to predict regions that show variations that are suitable for µTGGE analysis. The positions at the 3′-terminal end, center, and 5′-terminal end are optimized followed by fragment length (Fig. 6-1 A). The uMelt software interactively calculates and visualizes the mean helicity and the dissociation probability at each sequence position at temperatures within the temperature range. Predicted curves display the mean helicity as a function of temperature or as derivative plots [117]. After optimization, the best candidates are subjected to µTGGE analysis.

When the PCR product is applied on polyacrylamide gel with a temperature gradient, DNA undergoes three melting patterns as follows: (1) initial melting, where the dissociation of hydrogen bonds holding the DNA bases begins; (2) mid melting, where the hydrogen bond dissociation continues; and (3) end melting, where the hydrogen bonds dissociate entirely from each other resulting in ssDNA [61]. In the illustration, the mid melting pattern of D614 is shorter than that of G614 (Fig. 6-1 B). By comparing the µTGGE migration pattern between the D614 and G614, the differences can easily be discriminated.

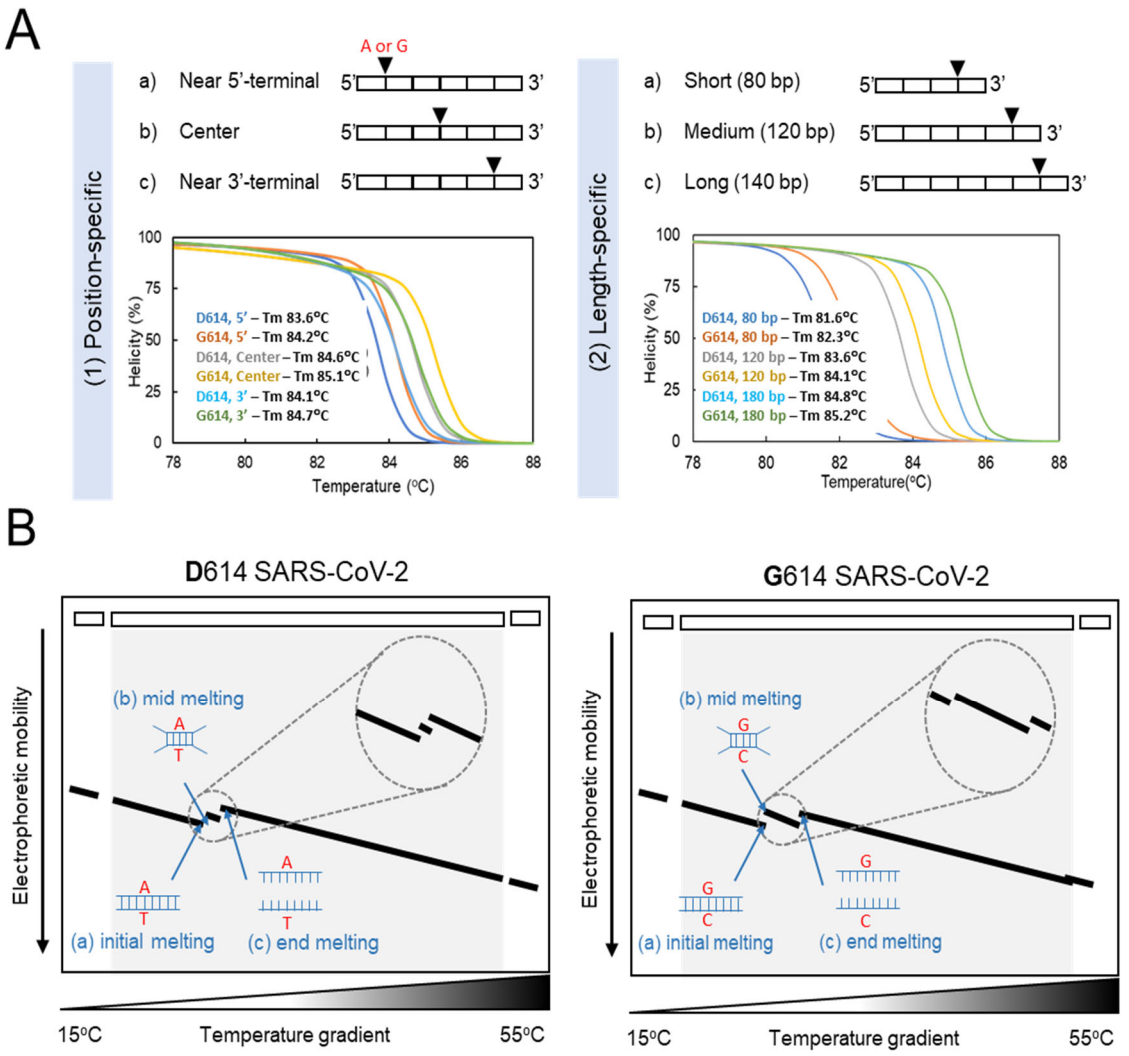

Figure 6-1. µTGGE principle for D614 and G614 mutation detection. (A) NA design and optimization and NA melting curve prediction. (B) Schematic illustration of migration patterns of D614 and G614. In µTGGE, a sample migrates through a temperature gradient gel, producing a unique pattern based on T_m.

D614 and G614 design for μTGGE analysis

The nucleotide sequence of the standard DNA is shown in Fig. 6-2. First, the 220-bp fragment of D614 was amplified by PCR using F1 and R6 primers with 220nt-1 as a template (Table 6-1). G614 was prepared in the same way with 220nt-2 as a template. To synthesize templates for μTGGE analysis, we designed five forward primers (F1–F5) and six reverse primers (R1–R6) (Table 6-1). PCR was carried out with previously prepared D614 and G614 as templates using primers listed in Table 6-1. Figure 6-3 shows the agarose gel results of the amplified PCR products. The expected amplicon size is shown in Table 6-2. Target bands were observed with all the primer combinations.

The ability to predict the shape and position of melting curves is essential for assay design and optimization. We predicted the DNA melting curves of D614 and G614 using uMelt web-based software. The D614 and G614 variants contain adenine (A) and guanine (G), respectively, at position 23,343 of the SARS-CoV-2 sequence (GenBank NC_045512.2.). Figure 6-4 shows the predicted DNA melting curves. The 80-, 120-, and 140-bp size fragments amplified with primer combinations No. 13, 1, and 16, respectively, were examined (Table 6-2). When the 80-bp fragments of D614 and G614 were compared, the G614 curve shifted to the right, similar observations were made with the 120- and 140-bp fragments. We attribute the shift to the presence of G in G614 which binds with C through three hydrogen bonds as compared to A in D614 which binds with T through two hydrogen bonds. These results indicated that the predicted T_m was in the order of 140-bp > 120-bp > 80-bp while the variation was 80-bp > 120-bp > 140-bp. Based on the melting curves predicted by uMelt, amplified fragments with primer combinations No. 13, 1, and 16 yielding 80-, 120-, and 140-bp, respectively (Table 6-2), were chosen as candidates for μTGGE analyses. These results also suggest that uMelt is a convenient tool

for designing and optimizing high-resolution melting experiments by predicting PCR product melting curves.

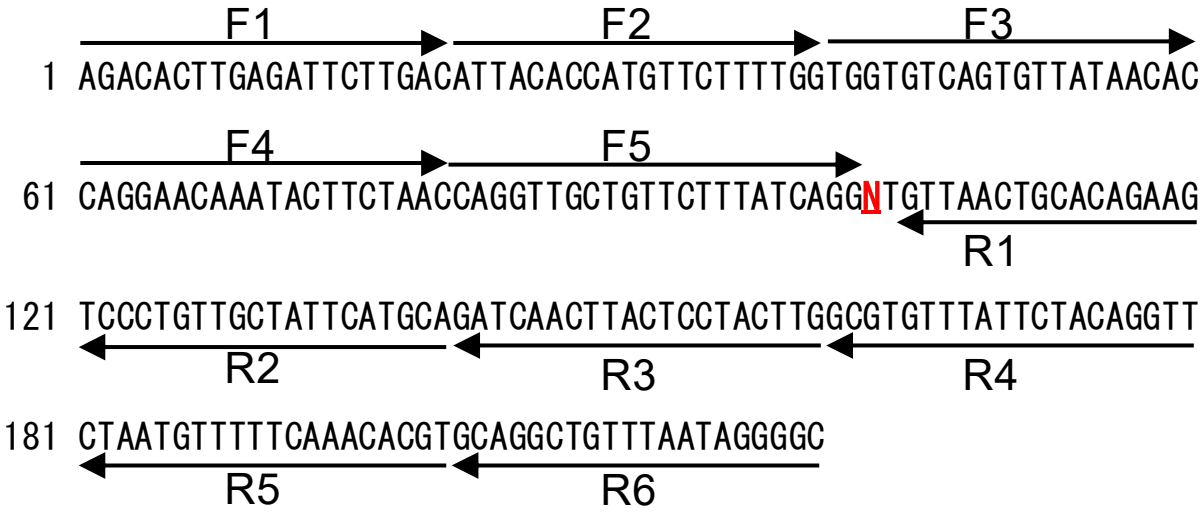

Figure 6-2. Nucleotide sequence of the regions targeted by the primers in PCR. The underlined N (in red) denotes the mutation position, adenine (A) in D614 and guanine (G) in G614. The base position corresponds to that described in the sequences deposited in GenBank (MN908947.3).

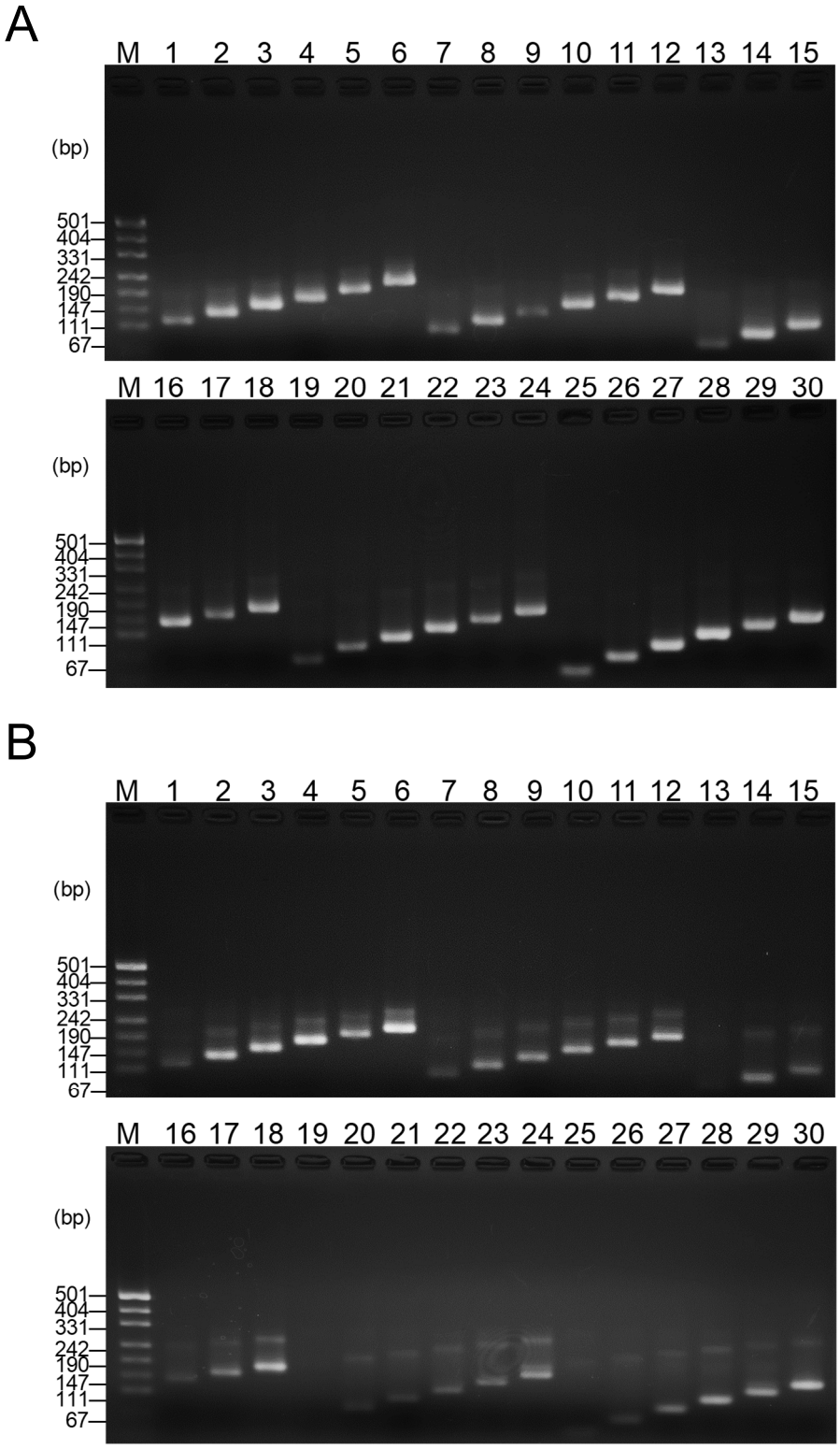

Figure 6-3. Agarose gel electrophoresis of the amplified PCR products. PCR was carried out with D614 (A) or G614 (B) as a template with primer combinations listed in Table 6-2. Amplified products were applied on 2.0% agarose gel followed by staining with ethidium bromide (1 μg/mL).

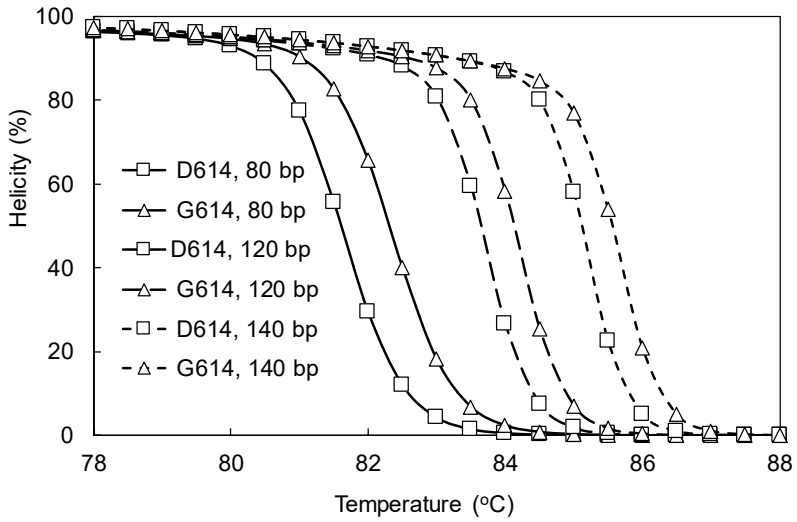

Figure 6-4. Theoretical prediction of melting curves of PCR products. The uMelt web software was used to optimize fragments for μTGGE analysis. D614 (square), G614 (triangle), 80-bp (solid line), 120-bp (long dashed line), and 140-bp (dashed line).

Effects of position of D614 and G614 mutation on μTGGE pattern

The position of mutation at the terminal positions of the DNA fragment has been reported to affect μTGGE analysis [61]. We evaluated the effects of specific-positioning of D614 and G614 variants on the μTGGE migration pattern. The 120-bp DNA fragments of D614 and G614 were designed with mutations near the 3′-terminal end, center, and the 5′-terminal end. The PCR products were applied on 6% polyacrylamide gel at a linear temperature gradient of 15–55ºC. Figure 6-5 shows μTGGE pattern. The initial, mid, and end melting patterns near the 3′-terminal and 5′-terminal ends were clearly distinguished on the gel. In particular, the mid melting pattern of D614 was shorter than that of G614. However, the mid melting at the center of the fragment was connected with end melting. These results suggest that mutation near the 5′-terminal or 3′-terminal end is superior to one at the center of the fragment for μTGGE analysis.

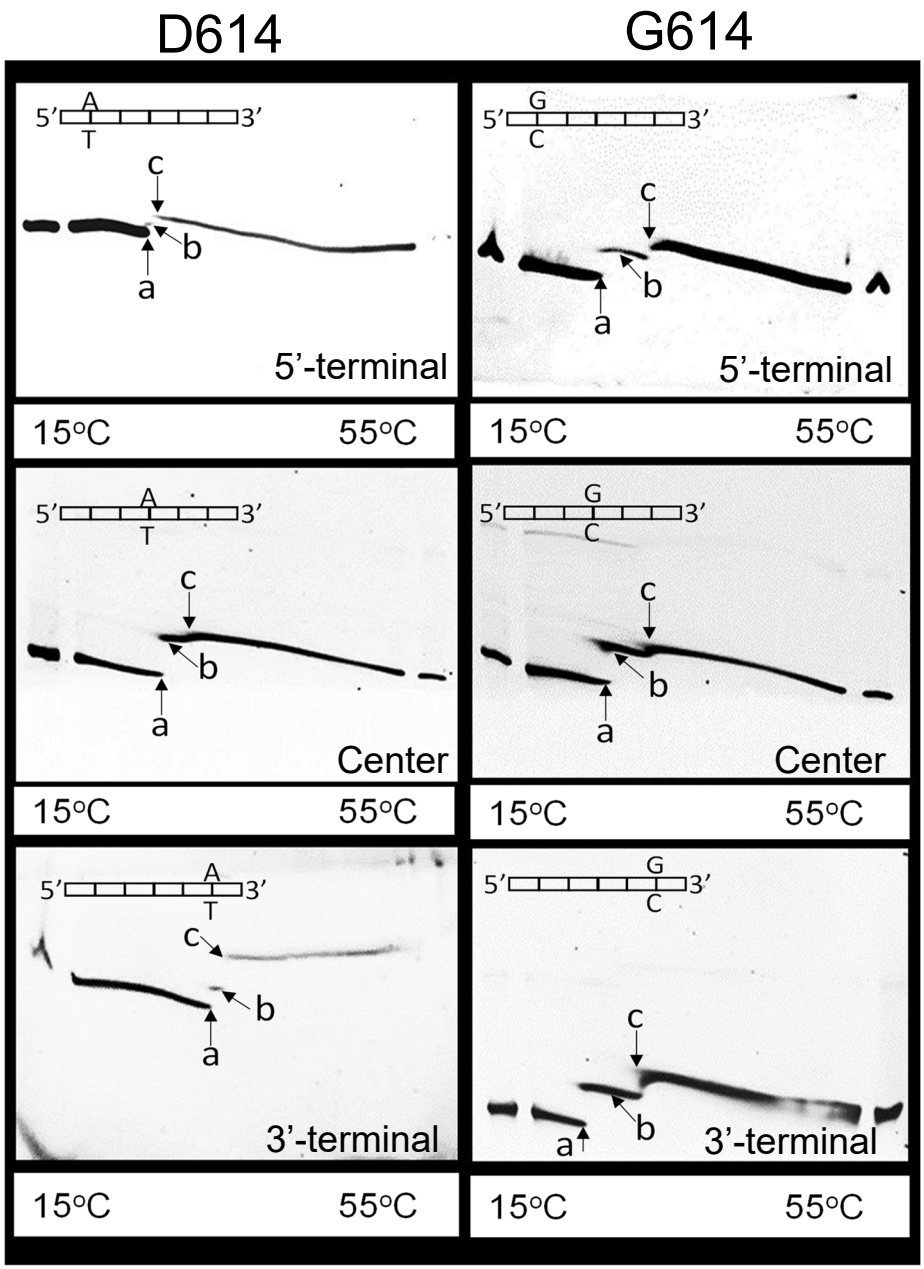

Figure 6-5. Effects of position of mutation on the μTGGE migration pattern. The standard DNA fragments of 120-bp with D614 and G614 mutation near the 5′-terminal end (upper panel), center (middle panel), or 3′-terminal end (lower panel) were prepared. Initial melting (a), mid melting (b), and end melting (c). The PCR product was applied on 6% polyacrylamide gel at a linear temperature gradient of 15–55ºC followed by staining using 10 × SYBR gold.

Effects of fragment length of D614 and G614 on µTGGE pattern

We examined the effects of DNA fragment length on the µTGGE migration pattern. The 80-, 120-, and 140-bp PCR products each of D614 and G614 were applied on 6% polyacrylamide gel at a linear temperature gradient of 15–55ºC. Figure 6-6 shows the µTGGE migration pattern. In the 80-bp, the initial, mid, and end melting patterns were clustered making it difficult to discriminate between D614 and G614 variants. In the 120-bp, the initial, mid, and end melting patterns were clearly different. Especially the mid melting pattern (the position between initial melting and end melting) was shorter in D614 than in G614. Similarly, in 140-bp, the initial, mid, and end melting patterns were clearly different in D614 and G614 variants. The mid melting pattern was shorter in D614 than in G614. A similar observation in the melting pattern was reported when RNA editing detection using µTGGE analysis was performed [61]. Based on these findings, the 120-bp fragment size was chosen for subsequent analyses.

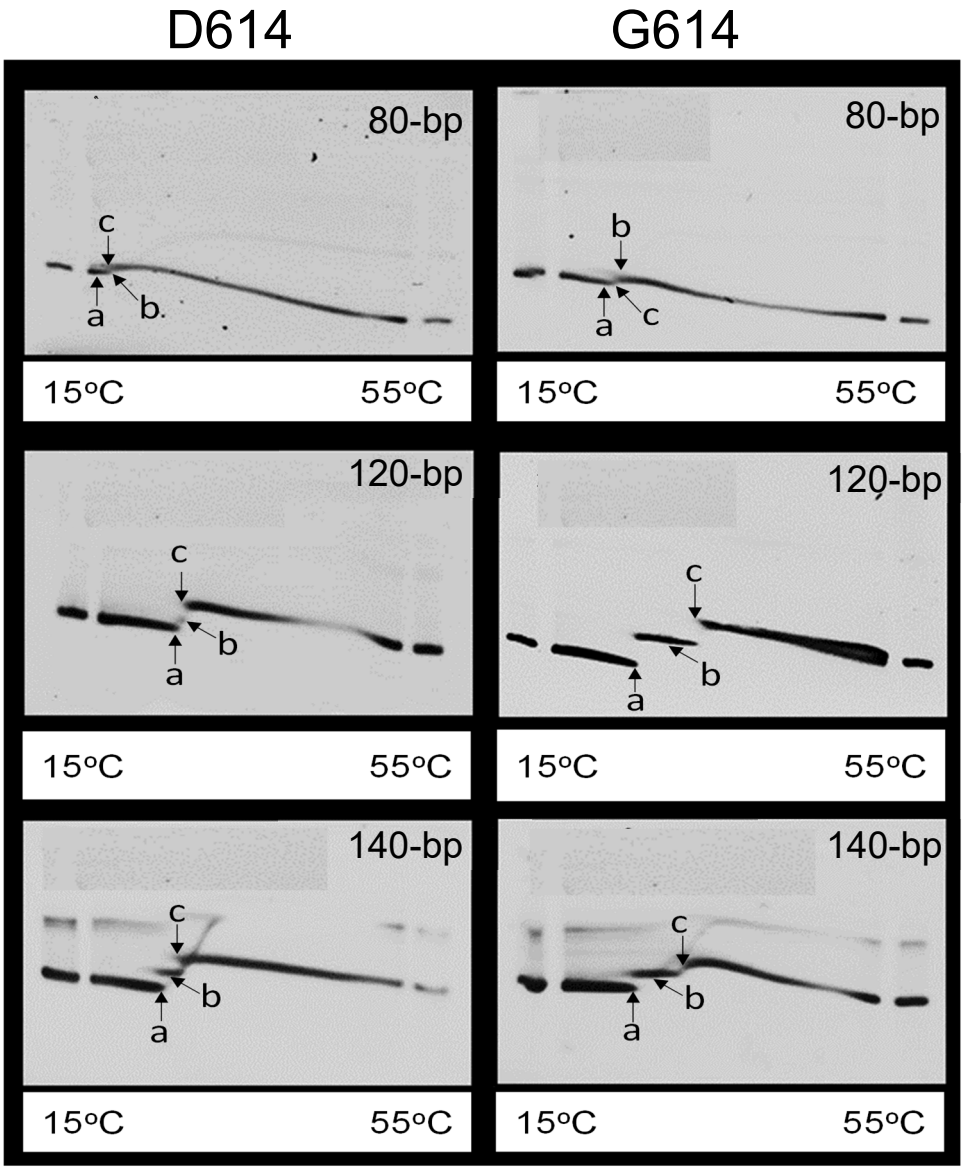

Figure 6-6. Effects of DNA fragment length on μTGGE migration pattern. The standard DNA fragments of 80-bp (upper panel), 120-bp (middle panel), or 140-bp (lower panel) were prepared with D614 and G614. Initial melting (a), mid melting (b), and end melting (c). The PCR product was applied on 6% polyacrylamide gel at a linear temperature gradient of 15–55ºC followed by staining using 10 × SYBR gold.

Conclusion

We developed a detection technique using μTGGE to distinguish between the D614 and G614 variants of the SARS-CoV-2 spike protein. The mid melting pattern of the D614 variant was shorter than that of the G614 variant. These findings demonstrated the capability of μTGGE to rapidly, accurately, and cost-effectively identify the SARS-CoV-2 spike protein D614 and G614 variants without the need for sequencing. This assay holds great potential for practical application at the point-of-care, enabling efficient mutation analysis in SARS-CoV-2 and other pathogens.

Summary

Chapter 1

We developed assays for the detection of RYMV DNA or RNA using three different techniques: PCR, RPA, and RNA-specific amplification. The sensitivities were in the range of several copies of the target DNA for PCR and RPA and dozens of copies of the target RNA for RNA-specific amplification. The cycle numbers or reaction times required for amplification from 10^9 copies of the target DNA or RNA were 15 cycles (27 min) for the PCR-based system and 5 min for RPA, and 10 min for RNA-specific amplification-based systems. These results suggested that isothermal RPA and RNA-specific amplification-based detection systems are more suitable for the rapid identification of RYMV-infected rice plants compared to the PCR-based system. Implementing these advanced detection systems will enable rapid and accurate diagnosis of RYMV, aiding in the timely implementation of measures to mitigate its impact on rice production.

Chapter 2

We prepared recombinant recombinases and a single-stranded DNA-binding protein from T4 phage and used them to examine the effects of reaction conditions and additives on the efficiency of RPA. The optimal pH was 7.5–8.0, the optimal potassium acetate concentration was 40–80 mM, and the optimal reaction temperature was 37–45ºC. DMSO at 5% v/v and formamide at 5% v/v inhibited the reaction. These results indicated that RPA exhibits a broader range of optimal reaction conditions. This flexibility opens up new possibilities for conducting RPA under various conditions. Furthermore, the study highlights the suitability of RPA for point-of-care applications, emphasizing its potential

for on-site and rapid diagnostic testing.

Chapter 3

We optimized the reaction conditions of RPA using Taguchi statistical method to enhance the sensitivity and rapidness using *in vitro* synthesized SARS-CoV-2 DNA and RNA targets. After evaluating the concentration of each component, uvsY, gp32, and ATP concentrations were rate-determining factors. In particular, the balance between the binding and dissociation of uvsX and DNA primer was precisely adjusted. Under the optimized conditions, 60 copies of the target DNA and RNA were detected, which was a 1,000-fold increase in sensitivity. These results underscore the flexibility in fabricating RPA reagents, leading to expanded applications of RPA in diverse fields.

Chapter 4

We examined the effects of the N- and C-terminal $(His)_6$ tags of uvsY on its function in RPA to detect SARS-CoV-2 DNA. The minimal initial copy numbers of standard DNA from which the amplified products were observed were 6×10^5, 60, 600, and 600 copies for the RPA with uvsY-Δhis, uvsY-Nhis, uvsY-Chis, and uvsY-NChis, respectively. The minimal reaction time at which the amplified products were observed were 20, 20, 30, and 20 min for the RPA with uvsY-Δhis, uvsY-Nhis, uvsY-Chis, and uvsY-NChis, respectively. The RPA with uvsY-Nhis exhibited clearer bands than that with either of the other three uvsYs. The reaction efficiency of RPA with uvsY-Nhis was the highest, suggesting that uvsY-Nhis is suitable for use in RPA.

Chapter 5

We optimized the lyophilization conditions for RPA with newly isolated thermostable DNA polymerases for storage at room temperature. We isolated two novel thermostable strand-displacing DNA polymerases from *A. pallidus* (H1) and *G. zalihae* (C1) and evaluated their performances in RPA reaction. The minimal initial copy numbers of standard DNA from which the amplified products were observed were 600, 600, and 6,000 copies for RPA with H1-Pol, C1-Pol, and *Bst*-Pol, respectively. Lyophilized RPA reagents containing H1-Pol exhibited the same performance as the corresponding liquid RPA reagents. In addition, lyophilized RPA reagents with H1-Pol showed almost the same activity after two weeks of storage at room temperature as the freshly prepared liquid RPA reagents. These results suggested that lyophilized RPA reagents with H1-Pol are preferable to liquid RPA reagents for on-site use.

Chapter 6

We developed a detection system of SARS-CoV-2 spike protein D614 and G614 variants using μTGGE. The *in vitro* synthesized SARS-CoV-2 spike protein D614 and G614 gene fragments were amplified using PCR and subjected to μTGGE analysis. The migration patterns of D614 and G614 on the polyacrylamide gel were clearly different and easily distinguished by μTGGE. In particular, the mid melting pattern of D614 was shorter than that of G614. These results demonstrated the ability of μTGGE to detect SARS-CoV-2 spike protein D614 and G614 variants, quickly, accurately, and cost-effectively without the need for sequencing. Therefore, the assay has a great potential for application at point-of-care for mutation assay in SARS-CoV-2 and other pathogens.

References

1. Saiki, R.K., Scharf, S., Faloona, F., Mullis, K.B., Horn, G.T., Erlich, H.A., and Arnheim, N. (1985) Enzymatic amplification of beta-globin genomic sequences and restriction site analysis for diagnosis of sickle cell anemia. *Science*, **230**, 1350–1354
2. Seki, M., Kim, C.K., Hayakawa, S., and Mitarai, S. (2018) Recent advances in tuberculosis diagnostics in resource-limited settings. *Eur. J. Clin. Microbiol. Infect. Dis*., **37**, 1405–1410
3. Zimmerman, P.A., King, C.L., Ghannoum, M., Bonomo, R.A., and Procop, G.W. (2021) Molecular diagnosis of SARS-COV-2: assessing and interpreting nucleic acid and antigen tests. *Pathog. Immun*., **6**, 135–156
4. Kievits, T., van Gemen, B., van Strijp, D., Schkkink, P., Dircks, M., Adriaanse, H., Malek, L., Sooknanan, R., and Lens, P. (1991) NASBA isothermal enzymatic *in vitro* nucleic acid amplification optimized for the diagnosis of HIV-1 infection. *J. Virol. Methods*, **35**, 273–286
5. Walker, G.T., Fraiser, M.S., Schram, J.L., Little, M.C., Nadeau, J.G., and Malinowski, D.P. (1992) Strand displacement amplification-an isothermal, *in vitro* DNA amplification technique. *Nucleic Acids Res*., **20**, 1691–1696
6. Lizardi, P.M., Huang, X., Zhu, Z., Bray-Ward, P., Thomas, D.C., and Ward, D.C. (1998) Mutation detection and single-molecule counting using isothermal rolling-circle amplification. *Nat. Genet.*, **19**, 225–232
7. Vincent, M., Xu, Y., and Kong, H. (2004) Helicase-dependent isothermal DNA amplification. *EMBO Rep.*, **5**, 795–800
8. Notomi, T., Okayama, H., Masubuchi, H., Yonekawa, T., Watanabe, K., Amino, N.,

and Hase, T. (2000) Loop-mediated isothermal amplification of DNA. *Nucleic Acids Res*., **28**, e63

9. Yan, L., Zhou, J., Zheng, Y., Gamson, A.S., Roembke, B.T., Nakayama, S., and Sintim, H.O. (2014) Isothermal amplified detection of DNA and RNA. *Mol. Biosyst*., **10**, 970–1003
10. Chien, A., Edgar, D.B., and Trela, J.M. (1976) Deoxyribonucleic acid polymerase from the extreme thermophile *Thermus aquaticus*. *J. Bacteriol*., **127**, 1550–1557
11. Pavlov, A.R., Pavlova, N.V., Kozyavkin., S.A., and Slesarev, A.I. (2004) Recent developments in the optimization of thermostable DNA polymerases for efficient applications. *Trends Biotechnol*., **22**, 253–260
12. Tabor, S., and Richardson, C.C. (1995) A single residue in DNA polymerases of the *Escherichia coli* DNA polymerase I family is critical for distinguishing between deoxy- and dideoxyribonucleotides. *Proc. Natl. Acad. Sci. USA*, **92**, 6339–6343
13. Pavlov, A.R., Belova, G.I., Kozyavkin, S.A., and Slesarev, A.I. (2002) Helix-hairpin-helix motifs confer salt resistance and processivity on chimeric DNA polymerases. *Proc. Natl. Acad. Sci. USA*, **99**, 13510–13515
14. Piepenburg, O., Williams, C.H., Stemple, D.L., and Armes, N.A. (2006) DNA detection using recombination proteins. *PLoS Biol*., **4**, e204
15. Lobato, I.M. and O'Sullivan, C.K. (2018) Recombinase polymerase amplification: Basics, applications and recent advances. *Trends Analyt. Chem*., **98**, 19–35
16. Li, J., Macdonald, J., and von Stetten, F. (2019) Review: a comprehensive summary of a decade development of the recombinase polymerase amplification. *Analyst*, **144**, 31–67
17. Mustafa, A.M. (2022) Critical insight into recombinase polymerase amplification

technology. *Expert Rev. Mol. Diagn*., **22**, 725–737

18. Deng, W., Wang, S., Wang, L., Lv, C., Li, Y., Feng, T., Qin, Z., and Xu, J. (2022) Laboratory evaluation of a basic recombinase polymerase amplification (RPA) assay for early detection of *Schistosoma japonicum*. *Pathogens*, **11**, 319
19. Tan, M., Liao, C., Liang, L., Yi, X., Zhou, Z., and Wei, G. (2022). Recent advances in recombinase polymerase amplification: principle, advantages, disadvantages and applications. *Front. Cell. Infect. Microbiol.*, **12**, 1019071
20. Qian, J., Boswell, S.A., Chidley, C., Lu, Z.X., Pettit, M.E., Gaudio, B.L., Fajnzylber, J.M., Ingram, R.T., Ward, R.H., Li, J.Z., and Springer, M. (2020) An enhanced isothermal amplification assay for viral detection. *Nat. Commun*., **11**, 5920
21. Behrmann, O., Bachmann, I., Spiegel, M., Schramm, M., Abd El Wahed, A., Dobler, G., Dame, G., and Hufert, F.T. (2020) Rapid detection of SARS-CoV-2 by low volume real-time single tube reverse transcription recombinase polymerase amplification using an exo probe with an internally linked quencher (Exo-IQ). *Clin. Chem*., **66**, 1047–1054
22. Wang, P., Ma, C., Zhang, X., Chen, L., Yi, L., Liu, X., Lu, Q., Cao, Y., and Gao, S. (2021) A ligation/recombinase polymerase amplification assay for rapid detection of SARS-CoV-2. *Front. Cell. Infect. Microbiol*., **11**, 680728
23. Shelite, T.R., Uscanga-Palomeque, A.C., Castellanos-Gonzalez, A., Melby, P.C., and Travi, B.L. (2021) Isothermal recombinase polymerase amplification-lateral flow detection of SARS-CoV-2, the etiological agent of COVID-19. *J. Virol. Methods*, **296**, 114227
24. Singpanomchai, N., Akeda, Y., Tomono, K., Tamaru, A., Santanirand, P., and Ratthawongjirakul, P. (2021) Rapid detection of multidrug-resistant tuberculosis

based on allele-specific recombinase polymerase amplification and colorimetric detection. *PLoS One*, **16**, e0253235

25. Liu, P., Wang, X., Liang, J., Dong, Q., Zhang, J., Liu, D., Wang, S., Bi, J., Liu, W., Wang, Z., Chen, L., Liu, L., Huang, X., and Zhang, G. (2022) A recombinase polymerase amplification-coupled Cas12a mutant-based module for efficient detection of streptomycin-resistant mutations in *Mycobacterium tuberculosis*. *Front. Microbiol*., **12**, 796916
26. Ma, Q., Liu, H., Ye, F., Xiang, G., Shan, W., and Xing, W. (2017) Rapid and visual detection of *Mycobacterium tuberculosis* complex using recombinase polymerase amplification combined with lateral flow strips. *Mol. Cell. Probes*, **36**, 43–49
27. Davi, S.D., Kissenkötter, J., Faye, M., Böhlken-Fascher, S., Stahl-Hennig, C., Faye, O., Faye, O., Sall, A.A., Weidmann, M., Ademowo, O.G., Hufert, F.T., Czerny, C.P., and Abd El Wahed, A. (2019) Recombinase polymerase amplification assay for rapid detection of Monkeypox virus. *Diagn. Microbiol. Infect. Dis.*, **95**, 41–45
28. Mao, L., Ying, J., Selekon, B., Gonofio, E., Wang, X., Nakoune, E., Wong, G., and Berthet, N. (2022) Development and characterization of recombinase-based isothermal amplification assays (RPA/RAA) for the rapid detection of monkeypox virus. *Viruses*, **14**, 2112
29. Wei, J., Wang, W., Yu, Q., Zhang, M., Xue, F., Fan, B., Zhang, T., Gao, Y., Li, J., Meng, X., and Pang, B. (2023) MASTR Pouch: Palm-size lab for point-of-care detection of Mpox using recombinase polymerase amplification and CRISPR technology. *Sens. Actuators B Chem*., **390**, 133950
30. Lalremruata, A., Nguyen, T.T., McCall, M.B.B., Mombo-Ngoma, G., Agnandji, S.T., Adegnika, A.A., Lell, B., Ramharter, M., Hoffman, S.L., Kremsner, P.G., and

Mordmüller, B. (2020) Recombinase polymerase amplification and lateral flow assay for ultrasensitive detection of low-density *Plasmodium falciparum* infection from controlled human malaria infection studies and naturally acquired infections. *J. Clin. Microbiol.*, **58**, e01879-19

31. Lai, M.Y., Abdul Hamid, M., Jelip, J., Mudin, R.N., and Lau, Y.L. (2023) Lateral Flow Recombinase polymerase amplification assays for the detection of human *Plasmodium* species. *Am. J. Trop. Med. Hyg.*, **108**, 882–886
32. Louizi, C., Khan, M.A.A., Faisal, K., Chowdhury, R., Ghosh, P., Hossain, F., Nisansala, T., Ranasinghe, S., Moreno, J., Alvar, J., Mondal, D., Buhl, T., Lüder, C.G.K., and Abd El Wahed, A. (2023) Assessment of pan-*Leishmania* detection by recombinase polymerase amplification assay. *Diagn. Microbiol. Infect. Dis.*, **105**, 115862
33. Mondal, D., Ghosh, P., Khan, M.A., Hossain, F., Böhlken-Fascher, S., Matlashewski, G., Kroeger, A., Olliaro, P., and Abd El Wahed, A. (2016) Mobile suitcase laboratory for rapid detection of *Leishmania donovani* using recombinase polymerase amplification assay. *Parasit. Vectors*, **9**, 281
34. Khan, M.A.A., Faisal, K., Chowdhury, R., Ghosh, P., Hossain, F., Weidmann, M., Mondal, D., and Abd El Wahed, A. (2021) Development of quantitative rapid isothermal amplification assay for *Leishmania donovani*. *Diagnostics*, **11**, 1963
35. Wang, F., Wang, Y., Liu, X., Wang, L., Wang, K., Xu, C., Huang, G., and Gao, X. (2022) Rapid, simple, and highly specific detection of *Streptococcus pneumoniae* with visualized recombinase polymerase amplification. *Front. Cell. Infect. Microbiol.*, **12**, 878881
36. Kersting, S., Rausch, V., Bier, F.F., and von Nickisch-Rosenegk, M. (2018) A

recombinase polymerase amplification assay for the diagnosis of a typical pneumonia. *Anal. Biochem.*, **550**, 54–60

37. Jauset-Rubio, M., Tomaso, H., El-Shahawi, M.S., Bashammakh, A.S., Al-Youbi, A. O., and O'Sullivan, C.K. (2018) Duplex lateral flow assay for the simultaneous detection of *Yersinia pestis* and *Francisella tularensis*. *Anal. Chem.*, **90**, 12745–12751
38. Fang, W., Cai, Y., Zhu, L., Wang, H., and Lu, Y. (2020) Rapid and highly sensitive detection of toxigenic *Vibrio cholerae* based on recombinase-aided amplification combining with lateral flow assay. *Food Anal. Methods*, **14**, 687–696
39. Wang, P., Liao, L., Ma, C., Zhang, X., Yu, J., Yi, L., Liu, X., Shen, H., Gao, S., and Lu, Q. (2021) Duplex On-site detection of *Vibrio cholerae* and *Vibrio vulnificus* by recombinase polymerase amplification and three-segment lateral flow strips. *Biosensors*, **11**, 151
40. Green, H., Tillmar, A., Pettersson, G., and Montelius, K. (2019) The use of FTA cards to acquire DNA profiles from postmortem cases. *Int. J. Leg. Med.*, **133**, 1651–1657
41. Siegel, C.S., Stevenson, F.O., and Zimmer, E.A. (2017) Evaluation and comparison of FTA card and CTAB DNA extraction methods for non-agricultural taxa. *Appl. Plant Sci*., **5**, 1600109
42. Rathore, H., Biyani, R., Kato, H., Takamura, Y., and Biyani, M. (2019) Palm-size and one-inch gel electrophoretic device for reliable and field-applicable analysis of recombinase polymerase amplification. *Anal. Methods*, **11**, 4969–4976
43. Hu, J., Wang, Y., Ding, H., Jiang, C., Geng, Y., Sun, X., Jing, J., Gao, H., Wang, Z., and Dong, C. (2020) Recombinase polymerase amplification with polymer flocculation sedimentation for rapid detection of *Staphylococcus aureus* in food

samples. *Int. J. Food Microbiol.*, **331**, 108691

44. Koo, K.M., Wee, E.J., Mainwaring, P.N., and Trau, M. (2016) A simple, rapid, low-cost technique for naked-eye detection of urine-isolated TMPRSS2:ERG gene fusion RNA. *Sci. Rep*., **6**, 30722
45. Wee, E.J., Ha Ngo, T., and Trau, M. (2015) A simple bridging flocculation assay for rapid, sensitive and stringent detection of gene specific DNA methylation. *Sci. Rep.*, **5**, 15028
46. Khaliliazar, S., Ouyang, L., Piper, A., Chondrogiannis, G., Hanze, M., Herland, A., and Hamedi, M.M. (2020) Electrochemical detection of genomic DNA utilizing recombinase polymerase amplification and stem-loop probe. *ACS Omega*, **5**, 12103–12109
47. Tsaloglou, M.N., Nemiroski, A., Camci-Unal, G., Christodouleas, D.C., Murray, L.P., Connelly, J.T., and Whitesides, G.M. (2018) Handheld isothermal amplification and electrochemical detection of DNA in resource-limited settings. *Anal. Biochem.*, **543**, 116–121
48. del Río, J.S., Yehia Adly, N., Acero-Sánchez, J.L., Henry, O.Y., and O'Sullivan, C.K. (2014) Electrochemical detection of *Francisella tularensis* genomic DNA using solid-phase recombinase polymerase amplification. *Biosens. Bioelectron.*, **54**, 674–678
49. Kober, C., Niessner, R., and Seidel, M. (2018) Quantification of viable and non-viable *Legionella* spp. by heterogeneous asymmetric recombinase polymerase amplification (haRPA) on a flow-based chemiluminescence microarray. *Biosens. Bioelectron.*, **100**, 49–55
50. Qing, L., Boon, K.L.L., Swee, Y.L., Wen, Y.T., Zhonghua, G., Jaehoon, C., Mi, K.P.,

and Timothy, B. (2018) Label-free, real-time and multiplex detection of *Mycobacterium tuberculosis* based on silicon photonic microring sensors and asymmetric isothermal amplification technique (SPMS-AIA). *Sens. Actuators B Chem*., **255**, 1595–1603

51. Dao, T.N.T., Lee, E.Y., Koo, B., Jin, C.E., Lee, T.Y., and Shin, Y. (2018) A microfluidic enrichment platform with a recombinase polymerase amplification sensor for pathogen diagnosis. *Anal. Biochem.*, **544**, 87–92
52. Lau, H.Y., Wang, Y., Wee, E.J., Botella, J.R., and Trau, M. (2016) Field demonstration of a multiplexed point-of-care diagnostic platform for plant pathogens. *Anal. Chem.*, **88**, 8074–8081
53. Koo, K.M., Wee, E.J., Mainwaring, P.N., Wang, Y., and Trau, M. (2016) Toward precision medicine: a cancer molecular subtyping nano-strategy for RNA biomarkers in tumor and urine. *Small*, **12**, 6233–6242
54. Toldrà, A., Jauset-Rubio, M., Andree, K.B., Fernández-Tejedor, M., Diogène, J., Katakis, I., O'Sullivan, C.K., and Campàs, M. (2018) Detection and quantification of the toxic marine microalgae *Karlodinium veneficum* and *Karlodinium armiger* using recombinase polymerase amplification and enzyme-linked oligonucleotide assay. *Anal. Chim. Acta*, **1039**, 140–148
55. Obradovic, J., Jurisic, V., Tosic, N., Mrdjanovic, J., Perin, B., Pavlovic, S., and Djordjevic, N. (2013) Optimization of PCR conditions for amplification of GC-Rich EGFR promoter sequence. *J. Clin. Lab. Anal.*, **27**, 487–493
56. Dhatterwal, P., Mehrotra, S., and Mehrotra, R. (2017) Optimization of PCR conditions for amplifying an AT-rich amino acid transporter promoter sequence with high number of tandem repeats from *Arabidopsis thaliana*. *BMC Res. Notes*, **10**, 638

57. Rychlik, W., Spencer, W.J., and Rhoads, R.E. (1990) Optimization of the annealing temperature for DNA amplification *in vitro*. *Nucleic Acids Res.*, **18**, 6409–6412

58. Fargette, D., Konate, G., Fauquet, C., Muller, E., Peterschmitt, M., and Thresh, J.M. (2006) Molecular ecology and emergence of tropical plant viruses. *Annu. Rev. Phytopathol.*, **44**, 235–260

59. Pinel-Galzi, A., Traoré, O., Séré, Y., Hébrard, E., and Fargette, D. (2015) The biogeography of viral emergence: rice yellow mottle virus as a case study. *Curr. Opin. Virol.*, **10**, 7–13

60. Yassi, M.N., Ritzenthaler, C., Brugidou, C., Fauquet, C., and Beachy, R.N. (1994) Nucleotide sequence and genome characterization of rice yellow mottle virus RNA. *J. Gen. Virol.*, **75**, 249–257

61. Ruchika, Tshukahara, T., and Biyani, M. (2020) A nonsequencing approach for the rapid detection of RNA editing. *J. Vis. Exp*., **182**, e63591

62. Biyani, M. and Nishigaki, K. (2001) Hundredfold productivity of genome analysis by introduction of micro temperature-gradient gel electrophoresis. *Electrophoresis,* **22**, 23–28

63. Kouassi, N.K., N'Guessan, P.N., Albar, L., Fauquet, C.M., and Brigidou, C. (2005) Distribution and characterization of Rice yellow mottle virus: A threat to African farmers. *Plant Disease*, **89**, 124–133

64. Sekiya, N., Nakajima, T., Oizumi, N., Kurosawa, C., Tibanyendela, N., Peter, M.A., Tomitaka, M., and Natsuaki, K.T. (2022) Agronomic practices preventing local outbreaks of rice yellow mottle virus disease revealed by spatial autoregressive analysis. *Agron. Sustain. Dev*., **42**, 15

65. Longué, R.D., Zinga, I., Semballa, S., Barro, N., and Traoré, O. (2016) Detection and

serological characterization of rice yellow mottle virus in Central African Republic. *Agric. Sci*., **7**, 911–919

66. Opalka, N., Brugidou, C., Bonneau, C., Nicole, M., Beachy, R.N., Yeager, M., and Fauquet, C. (1998) Movement of rice yellow mottle virus between xylem cells through pit membranes. *Proc. Natl. Acad. Sci. USA*, **95**, 3323−3328
67. Choi, H., Cho, W.K., Yu, J., Lee, J.S., and Kim, K.H. (2013) Highly specific detection of five exotic quarantine plant viruses using RT-PCR. *Plant Pathol*., **29**, 99–104
68. Ishiguro, T., Saitoh, J., Horie, R., Hayashi, T., Ishizuka, T., Tsuchiya, S., Yasukawa, K., Kido, T., Nakaguchi, Y., Nishibuchi, M., and Ueda, K. (2003) Intercalation activating fluorescence DNA probe and its application to homogeneous quantification of a target sequence by isothermal sequence amplification in a closed vessel. *Anal. Biochem*., **314**, 77–86
69. Yasukawa, K., Agata, N., and Inouye, K. (2010) Detection of *cesA* mRNA from *Bacillus cereus* by RNA-specific amplification. *Enzyme Microb. Technol*., **46**, 391–396
70. Fargette, D., Pinel, A., Halimi, H., Brugidou, C., Fauquet, C., and Van, R.M. (2002) Comparison of molecular and immunological typing of isolates of Rice yellow mottle virus. *Arch. Virol.*, **147**, 583–596
71. Qiao, Y., Nakayama, J., Ikeuchi, T., Ito, M., Kimura, T., Kojima, K., Takita, T., and Yasukawa, K. (2020) Kinetic analysis of inhibition of α-glucosidase by leaf powder from *Morus australis* and its component iminosugars. *Biosci. Biotechnol. Biochem.*, **84**, 2149–2156
72. Nishimura, K., Higashiya, K., Ueshima, N., Abe, T., and Yasukawa, K. (2020) The roles of histidine and tyrosine residues in the active site of collagenase in *Grimontia*

hollisae. *J. Food Sci.*, **85**, 535–544

73. Okano, H., Katano, Y., Baba, M., Fujiwara, A., Hidese, R., Fujiwara, S., Yanagihara, I., Hayashi, T., Kojima, K., Takita, T., and Yasukawa, K. (2017) Enhanced detection of RNA by MMLV reverse transcriptase coupled with thermostable DNA polymerase and DNA/RNA helicase. *Enzyme Microb. Technol*., **96**, 111–120
74. Okano, H., Baba, M., Yamasaki, T., Hidese, R., Fujiwara, S., Yanagihara, I., Ujiiye, T., Hayashi, T., Kojima, K., Takita, T., and Yasukawa, K. (2017) High sensitive one-step RT-PCR using MMLV reverse transcriptase, DNA polymerase with reverse transcriptase activity, and DNA/RNA helicase. *Biochem. Biophys. Res. Commun.*, **487**, 128–133
75. Grunenwald, H. (2003) Optimization of polymerase chain reactions. *Methods Mol. Biol.*, **226**, 89–100
76. Juma, K.M., Kojima, K., Takita, T., Natsuaki, K.T., and Yasukawa, K. (2021) Comparison of sensitivity and rapidness of PCR, recombinase polymerase amplification, and RNA-specific amplification for detection of Rice yellow mottle virus. *J. Biol. Macromol*., **21**, 27–32
77. Chen, G., Dong, J., Yuan, Y., Li, N., Huang, X., Cui, X., and Tang, Z. (2016) A general solution for opening double-stranded DNA for isothermal amplification. *Sci. Rep.*, **6**, 34582
78. Spiess, A.N., Mueller, N., and Ivell, R. (2004) Trehalose is a potent PCR enhancer: lowering of DNA melting temperature and thermal stabilization of *Taq* polymerase by the disaccharide trehalose. *Clin. Chem.*, **50**, 1256–1259
79. Yasukawa, K., Konishi, A., and Inouye, K. (2010) Effects of organic solvents on the reverse transcription reaction catalyzed by reverse transcriptases from avian

myeloblastosis virus and Moloney murine leukemia virus. *Biosci. Biotechnol. Biochem*., **74**, 1925–1930

80. Hubé, F., Reverdiau, P., Iochmann, S., and Gruel, Y. (2005) Improved PCR method for amplification of GC-rich DNA sequences. *Mol. Biotechnol.*, **31**, 81–84
81. Kojima, K., Juma, K.M., Akagi, S., Hayashi, K., Takita, T., O'Sullivan, C.K., Fujiwara, S., Nakura, Y., Yanagihara, I., and Yasukawa, K. (2021) Solvent engineering studies on recombinase polymerase amplification. *J. Biosci. Bioeng*., **131**, 219–224
82. Thanakiatkrai, P. and Welch, L. (2012) Using the Taguchi method for rapid quantitative PCR optimization with SYBR Green I. *Int. J. Legal Med.*, **126**, 161–165
83. Yasukawa, K., Mizuno, M., Konishi, A., and Inouye, K. (2010) Increase in thermal stability of Moloney murine leukaemia virus reverse transcriptase by site-directed mutagenesis. *J. Biotechnol.*, **150**, 299–306
84. Corman, V.M., Landt, O., Kaiser, M., Molenkamp, R., Meijer, A., Chu, D.K.W., Bleicker, T., Brünink, S., Schneider, J., Schmidt, M.L., Mulders, D.G.J.C., Haagmans, B.L., van der Veer, B., van den Brink, S., Wijsman, L., Goderski, G., Romette, J.L., Ellis, J., Zambon, M., Peiris, M., Goossens, H., Reusken, C., Koopmans, M.P.G., and Drosten, C. (2020) Detection of 2019 novel coronavirus (2019-nCoV) by real-time RT-PCR. *Euro Surveill*., **25**, 2000045
85. Ishino, Y. (2020) Studies on DNA-related enzymes to elucidate molecular mechanisms underlying genetic information processing and their application in genetic engineering. *Biosci. Biotechnol. Biochem*., **84**, 1749–1766
86. Yasukawa, K., Yanagihara, I., and Fujiwara, S. (2020) Alteration of enzymes and their application to nucleic acid amplification (Review). *Int. J. Mol. Med*., **46**, 1633–

1643

87. Hidese, R., Kawato, K., Nakura, Y., Fujiwara, A., Yasukawa, K., Yanagihara, I., and Fujiwara, S. (2018) Thermostable DNA helicase improves the sensitivity of digital PCR. *Biochem. Biophys. Res. Commun.*, **495**, 2189–2194
88. Roperch, J.P., Benzekri, K., Mansour, H., and Incitti, R. (2015) Improved amplification efficiency on stool samples by addition of spermidine and its use for non-invasive detection of colorectal cancer. *BMC Biotechnol*., **15**, 41
89. Kikuchi, A., Sawamura, T., Kawase, N., Kitajima, Y., Yoshida, T., Daimaru, O., Nakakita, T., and Itoh, S. (2010) Utility of spermidine in PCR amplification of stool samples. *Biochem. Genet.*, **48**, 428–432
90. Luo, G.C., Yi, T.T., Jiang, B., Guo, X.L., and Zhang, G.Y. (2019) Betaine-assisted recombinase polymerase assay with enhanced specificity. *Anal. Biochem.*, **575**, 36–39
91. Hashimoto, K. and Yonesaki, T. (1991) The characterization of a complex of three bacteriophage T4 recombination proteins, uvsX protein, uvsY protein, and gene 32 protein, on single-stranded DNA. *J. Biol. Chem*., **266**, 4883–4888
92. Gajewski, S., Waddell, M.B., Vaithiyalingam, S., Nourse, A., Li, Z., Woetzel, N., Alexander, N., Meiler. J., and White, S.W. (2016) Structure and mechanism of the phage T4 recombination mediator protein UvsY. *Proc. Natl. Acad. Sci. USA*, **113**, 3275–3280
93. Wu, T., Ge, Y., Zhao, K., Zhu, X., Chen, Y., Wu, B., Zhu, F., Zhu, B., and Cui, L. (2020) A reverse-transcription recombinase-aided amplification assay for the rapid detection of N gene of severe acute respiratory syndrome coronavirus 2 (SARS-CoV-2). *Virology*, **549**, 1–4

94. Juma, K.M., Takita, T., Ito, K., Yamagata, M., Akagi, S., Arikawa, E., Kojima, K., Biyani, M., Fujiwara, S., Nakura, Y., Yanagihara, I., and Yasukawa, K. (2021) Optimization of reaction condition of recombinase polymerase amplification to detect SARS-CoV-2 DNA and RNA using a statistical method. *Biochem. Biophys. Res. Commun.*, **56**, 195–200

95. Lau, Y.L., Ismail, I.B., Mustapa, N.I.B., Lai, M.Y., Tuan Soh, T.S., Haji Hassan, A., Peariasamy, K.M., Lee, Y.L., Abdul Kahar, M.K.B., Chong, J., and Goh, P.P. (2021) Development of a reverse transcription recombinase polymerase amplification assay for rapid and direct visual detection of Severe Acute Respiratory Syndrome Coronavirus 2 (SARS-CoV-2). *PLoS One*, **16**, e0245164

96. Terpe, K. (2003) Overview of tag protein fusions: from molecular and biochemical fundamentals to commercial systems. *Appl. Microbiol. Biotechnol*., **60**, 523–533

97. Xu, H., Beernink, H.T.H., Rould, M.A., and Morrical, S.W. (2006) Crystallization and preliminary X-ray analysis of bacteriophage T4 UvsY recombination mediator protein. *Acta Crystallogr. Sect. F. Struct. Biol. Cryst. Commun*., **62**, 1013–1015

98. Sano, S., Yamada, Y., Shinkawa, T., Kato, S., Okada, T., Higashibata, H., and Fujiwara, S. (2012) Mutations to create thermostable reverse transcriptase with bacterial family A DNA polymerase from *Thermotoga petrophila* K4. *J. Biosci. Bioeng.*, **113**, 315–321

99. Namba, F., Hasegawa, T., Nakayama, M., Hamanaka, T., Yamashita, T., Nakahira, K., Kimoto, A., Nozaki, M., Nishihara, M., Mimura, K., Yamada, M., Kitajima, H., Suehara, N., and Yanagihara, I. (2010) Placental features of chorioamnionitis colonized with *Ureaplasma* species in preterm delivery. *Pediatr. Res.*, **67**, 166–172

100. Mallard, K., Schopfer, K., and Bodmer, T. (2005) Development of real-time PCR for

the differential detection and quantification of *Ureaplasma urealyticum* and *Ureaplasma parvum*. *J. Microbiol. Methods*, **60**, 13–19

101. Glass, J.I., Lefkowitz, E.J., Glass, J.S., Heiner, C.R., Chen, E.Y., and Cassell, G.H. (2000) The complete sequence of the mucosal pathogen *Ureaplasma urealyticum*. *Nature*, **12**, 757–762

102. Mikami, Y., Fuwa, K., Arima, E., Suda, Y., Yanagihara, I., and Ibara, S. (2021) Validation of the loop-mediated isothermal amplification method for rapid and sensitive detection of *Ureaplasma* species in respiratory tracts of preterm infants. *PLoS One*, **16**, e0247618

103. Pavlidis, I., Spiller, O.B., Sammut Demarco, G., MacPherson, H., Howie, S.E.M., Norman, J.E., and Stock, S.J. (2020) Cervical epithelial damage promotes *Ureaplasma parvum* ascending infection, intrauterine inflammation and preterm birth induction in mice. *Nat. Commun*., **11**, 199

104. Konishi, A., Shinomura, M., and Yasukawa, K. (2013) Enzymatic characterization of human immunodeficiency virus type 1 reverse transcriptase for use in cDNA synthesis. *Appl. Biochem. Biotechnol.*, **169**, 77e87

105. Matejtschuk, P. (2007) Lyophilization of proteins. *Methods Mol. Biol.*, **368**, 59–72

106. Crowe, L.M., Reid, D.S., and Crowe, J.H. (1996) Is trehalose special for preserving dry biomaterials? *Biophys. J.*, **71**, 2087–2093

107. Starciuc, T., Guinet, Y., Paccou, L., and Hedoux, A. (2017) Influence of a small amount of glycerol on the trehalose bioprotective action analyzed in situ during freeze-drying of lyzozyme formulations by micro-raman spectroscopy. *J. Pharm. Sci*., **106**, 2988–2997

108. Gazali, F.M., Nuhamunada, M., Nabilla, M.R., Supriyati, E., Hakim, M.S., Arguni,

E., Daniwijaya, E.W., Nuryastuti, T., Haryana, S.M., Wibawa, T., and Wijayanti, N. (2021) Detection of SARS-CoV-2 spike protein D614G mutation by qPCR-HRM analysis. *Heliyon*, **7**, e07936

109. Meng, Q., Wang, X., Wang, Y., Dang, L., Liu, X., Ma, X., Chi, T., Wang, X., Zhao, Q., Yang, G., Liu, M., Huang, X., and Ma, P. (2021) Detection of the SARS-CoV-2 D614G mutation using engineered Cas12a guide RNA. *Biotechnol. J.*, **16**, e2100040
110. Crossley, B.M., Bai, J., Glaser, A.L., Maes, R.K., Porter, E., Killian, M.L., Clement T., and Toohey-Kurth, K.L. (2020) Guidelines for Sanger sequencing and molecular assay monitoring. *J. Vet. Diagn. Invest*., **32**, 767–775
111. Mardis, E. (2017) DNA sequencing technologies: 2006–2016. *Nat. Protoc*., **12**, 213–218
112. Eren, K., Taktakoğlu, N., and Pirim, I. (2022) DNA sequencing methods: From past to present. *Eurasian J. Med*., **54**, 47–56
113. Sloan, D.B., Broz, A.K., Sharbrough, J., and Wu, Z. (2018) Detecting rare mutations and DNA damage with sequencing-based methods. *Trends Biotechnol*., **36**, 729–740
114. Agarwal, T., Komazaki, S., Sharma, H., and Biyani, M. (2014) Rapid and molecular discrimination of host-specific fungal plant pathogens in pulse crops using genome profiling. *Curr. Sci*., **107**, 1704–1710
115. Kumari. P., Gautam, S.G., Baba, M., Tsukiashi, M., Matsuoka, K., Yasukawa, K., and Nishigaki, K. (2017) DNA-based mutation assay GPMA (genome profiling-based mutation assay): reproducibility, parts-per-billion scale sensitivity, and introduction of a mammalian-cell-based approach. *J. Biochem*., **162**, 395–401
116. Biyani, M. and Yasukawa, K. (2022) A non-sequencing approach for rapid RNA testing of SARS-CoV-2 variants using RICCA and PalmPAGE system. *J. IEIE Jpn.*,

42, 109–112

117. Dwight, D., Palais, R., and Wittwer, C.T. (2011) uMELT: prediction of high-resolution melting curves and dynamic melting profiles of PCR products in a rich web application. *Bioinformatics*, **27**, 1019–1020

118. Nishigaki, K., Saito, A., Takashi, H., and Naimuddin, M. (2000) Whole genome sequence-enabled prediction of sequences performed for random PCR products of *Escherichia coli*. *Nucleic Acids Res*., **28**, 1879–1884

Acknowledgments

This research was carried out at the Laboratory of Enzyme Chemistry, Division of Food Science and Biotechnology, Graduate School of Agriculture, Kyoto University, Japan, from April 2019 to March 2024.

I would like to express my deepest gratitude to Professor Kiyoshi Yasukawa of Kyoto University for his unwavering guidance, kind support, and constant encouragement throughout my academic journey. His mentorship has been instrumental in shaping the course of this research.

I am also indebted to Assistant Professor Teisuke Takita of Kyoto University for his insightful comments and guidance, which significantly enriched the quality of this study.

A special note of appreciation goes to Professor Manish Biyani of Japan Advanced Institute of Science and Technology (JAIST) for his exceptional guidance, which has been indispensable to the success of this study.

Furthermore, I wish to acknowledge the valuable advice provided by Dr. Kenji Kojima, former Assistant Professor at Kyoto University and current Associate Professor at Himeji Dokkyo University. I am also grateful to Dr. Misato Baba and Dr. Qiao Ying for their technical advice and fruitful discussions.

I want to express my heartfelt gratitude to Professor Shinsuke Fujiwara from the Department of Biosciences at the School of Biological and Environmental Sciences at Kwansei-Gakuin University. His unwavering support and invaluable guidance have been instrumental.

I sincerely thank Director Itaru Yanagihara from the Department of Developmental Medicine at the Research Institute of Osaka Women's and Children's Hospital for his valuable support and guidance throughout this journey.

I thank Dr. Keiko T. Natsuaki, a former Tokyo University of Agriculture professor, for her valuable guidance and support.

I am also profoundly grateful to Masaya Yamagata, Mika Ishitani, and Kenji Ito, former technical assistants at Kyoto University, for their invaluable assistance during the experimental phase.

I thank all members of the Laboratory of Enzyme Chemistry for their unwavering support throughout this research. Special thanks goes to AMGEN scholars Leila Jamal and Kavyashree Tewari for their technical assistance.

I am sincerely thankful for the financial support provided by the ABE-Initiative from JICA, Toyota-Tsusho, Support for Pioneering Graduate Students presented by the Kyoto University Graduate Division, and the Japan Society for the Promotion of Science (JSPS). Additionally, I extend my gratitude to Japanese taxpayers.

Finally, I extend my deepest gratitude to my family members: my late father Cyburn Juma, my late mother Alice Juma, and my late brother Michael Juma. I also want to acknowledge the unwavering support and encouragement from my wife, Irene Kerubo Moturi, and my son, Ryan Maafu Juma. Additionally, I am immensely grateful to my circle of friends whose consistent moral support has served as an indispensable driving force throughout my academic journey. Their unwavering belief in me has been truly invaluable.

KEVIN MAAFU JUMA

List of publications

Original papers

1. **Juma, K.M.**, Kojima, K., Takita, T., Natsuaki, K.T., and Yasukawa, K. (2021) Comparison of sensitivity and rapidness of PCR, recombinase polymerase amplification, and RNA-specific amplification for detection of Rice yellow mottle virus. *J. Biol. Macromol.*, **21**, 27–32
2. Kojima, K., **Juma K.M.**, Akagi, S., Hayashi, K., Takita, T., O'Sullivan, C.K., Fujiwara, S., Nakura, Y., Yanagihara, I., and Yasukawa, K. (2021) Solvent engineering studies on recombinase polymerase amplification. *J. Biosci. Bioeng.*, **131**, 219–224
3. **Juma, K.M.**, Takita, T., Ito, K., Yamagata, M., Akagi, S., Arikawa, E., Kojima, K., Biyani, M., Fujiwara, S., Nakura, Y., Yanagihara, I., and Yasukawa, K. (2021) Optimization of reaction condition of recombinase polymerase amplification to detect SARS-CoV-2 DNA and RNA using a statistical method. *Biochem. Biophys. Res. Commun*., **567**, 195–200
4. **Juma, K.M.**, Takita, T., Yamagata, M., Ishitani, M., Hayashi, K., Kojima, K., Suzuki, K., Ando, Y., Fukuda, W., Fujiwara, S., Nakura, Y., Yanagihara, I., and Yasukawa, K. (2022) Modified uvsY by N-terminal hexahistidine tag addition enhances efficiency of recombinase polymerase amplification to detect SARS-CoV-2 DNA. *Mol. Biol. Rep.*, **49**, 2847–2856
5. **Juma, K.M.**, Inoue, E., Asada, K., Fukuda, W., Morimoto, K., Yamagata, M., Takita, T., Kojima, K., Suzuki, K., Nakura, Y., Yanagihara, I., Fujiwara, S., and Yasukawa,

K. (2023) Recombinase polymerase amplification using novel thermostable strand-displacing DNA polymerases from *Aeribacillus pallidus* and *Geobacillus zalihae*. *J. Biosci. Bioeng*., **135**, 282–290

6. **Juma, K.M.**, Morimoto, K., Sharma, V., Sharma, K., Biyani, R., Biyani, M., Takita, T., and Yasukawa, K. (2023) Detection of SARS-CoV-2 spike protein D614G mutation using μTGGE. *Mol. Biol. Rep.*, in press

Related papers

1. Biyani, R., Sharma, K., Kojima, K., Biyani, M., Sharma, V., Kumawat, T., **Juma, K.M.**, Yanagihara, I., Fujiwara, S., Kodama, E., Takamura, Y., Takagi, M., Yasukawa, K., and Biyani, M. (2021) Development of robust isothermal RNA amplification assay for lab-free testing of RNA viruses. *Sci. Rep.*, **11**, 15997

2. Kojima, K., Morimoto, M., **Juma, K.M.**, Takita, T., Saito, K., Yanagihara, I., Fujiwara, S., and Yasukawa, K. (2023) Application of recombinant human pyruvate kinase in recombinase polymerase amplification. *J. Biosci. Bioeng.*, **136**, 341–346